TRANSPORT PROCESSES IN THE TROPICAL LOWER STRATOSPHERE AND THEIR ROLE IN THE VARIABILITY OF TRACE GASES

by

Olga V. Tweedy

A dissertation submitted to Johns Hopkins University in conformity with the requirements for the degree of Doctor of Philosophy

Baltimore, MD

June 2018

Abstract

The chemical composition of the tropical lower stratosphere (TLS) plays a key role in the climate system through changes in radiative forcing. Variability of long-lived chemical trace gases (e.g. O_3, H_2O, and N_2O) in the TLS is mainly due to transport processes, which are dominated by the vertical component of the residual mean circulation and two-way isentropic mixing by eddies. The strength of these transport processes controls a rate of vertical and horizontal mass exchange. Here, I perform an analysis of the transport processes in the TLS and their role in the variability of trace gases from seasonal to interannual timescales using a combination of data, meteorological reanalysis, and global chemistry climate models (CCMs).

First, an analysis of the transport processes affecting the seasonality of tracers in the TLS was performed using simulations from a collection of CCMs. The majority of the CCMs produce the observed feature of a larger annual cycle in ozone and other trace gases in the northern tropics (NT) than in the southern tropics (ST). Transformed Eulerian-mean (TEM) analysis reveals a major role of quasi-horizontal mixing and vertical advection in determining the NT and ST ozone seasonality respectively. Increase in summertime mixing in the NT is attributed to the Asian summer monsoon anticyclone.

Next, ozone variations over interannual time scales are explored to determine the impact of El-Niño Southern Oscillation (ENSO) on TLS composition. The model simulations and observations show large differences in ozone anomalies between NT and ST during boreal summer, but small differences in winter. The interannual variability in NT ozone is primarily due to meridional transport, connected with the Asian summer monsoon anticyclone. During boreal summer

cold (La Niña) events there is a stronger monsoon anticyclone and more transport of ozone from lower stratosphere extratropics into the NT, with the reverse for boreal summer warm (El Niño) events.

Finally, changes in circulation and trace gases in response to an unprecedented disruption in the quasi-biennial oscillation (QBO) during late-2015 through 2016 period are examined. It is shown that the QBO disruption led to increases in equatorial O_3 and HCl and a substantial decrease in total column ozone in the extratropics. Cold temperature anomalies near the tropical tropopause resulted in a global decrease in stratospheric water vapor during the fall 2016.

Faculty Advisor and First Reader: Professor Darryn Waugh
Earth and Planetary Science Department, Johns Hopkins University
Second Reader: Professor Richard Stolarski
Earth and Planetary Science Department, Johns Hopkins University

Acknowledgements

Firstly, I would like to express my sincere gratitude to my advisor Dr. Darryn Waugh for continuous support of my Ph.D study and related work, for his patience, motivation, and immense knowledge. His guidance helped me during research and writing of this thesis. I could not have imagined having a better advisor and mentor for my Ph.D study.

I am profoundly grateful to my undergraduate research advisor and mentor, Dr. Varavut Limpasuvan, without whom my graduate school experience would not be possible in the first place, and whose leadership and example has helped me grow into my potential. Thank you for opening my eyes to new stages of opportunity and strength during my first steps in becoming a scientist. I will forever be grateful for his guidance and kindness.

Besides my graduate and undergraduate advisors, I would like to thank the second reader of my thesis, Dr. Richard Stolarski. His hard questions and insightful suggestions inspired me to widen my research from various perspectives, showed me how to stand my ground, and have the kind of career that I can be proud of. I am so lucky to get to work with someone who inspires me every day.

Heartfelt thanks go to my Ph.D committee members, Dr. Darrell Strobel and Dr. Anand Gnanadesikan, for their insightful comments and encouragement, but also for their patience and support in overcoming numerous obstacles I have been facing throughout my research.

My sincere thanks also goes to our collaborators from NASA Goddard Space Flight Center (Dr. Luke Oman, Dr. Paul Newman, Dr. Natalya Kramarova, Dr. Susan Strahan, and others) and from National Center for Atmospheric Research (Dr. William Randel, Dr. Marta Abalos (now at UCM, Spain), and Dr. Mijeong Park), who provided me with an opportunity to join their teams and gave me access to the laboratory and research facilities. Without their support it would not be possible to conduct this research.

I am very grateful for the financial support from the National Science Foundation Graduate Research Fellowship Program, the department of Earth and Planetary Sciences at Johns Hopkins University, the NASA ACMAP program, and NCAR Advance Study Program (ASP) Graduate Student Visitor Program Fellowship.

I would like also to thank all my fellow doctoral students, EPS faculty and staff for their feedback, cooperation and for being a part of my graduate school experience.

Last but not the least, I would like to thank my husband and family in US and Russia for supporting me spiritually throughout my studies and my life in general.

Contents

List of Tables

List of Figures

List of acronyms and abbreviations

ASM Asian summer monsoon
BDC Brewer-Dobson circulation
CCM Chemistry climate model
CCMVal-2 Chemistry-Climate Model Validation activity phase 2
CMIP5 Coupled Model Intercomparison Project Phase 5
DU Dobson Unit
ENSO El Niño Southern Oscillation
EOF Empirical Orthogonal Function
GEOSCCM Goddard Earth Observing System Chemistry Climate Model
GHG Green house gases
HadISST Hadley Centre Sea Ice and Sea Surface Temperature
MERRA-2 The Modern-Era Retrospective analysis for Research and Applications, Version 2
MLS Microwave Limb Sounder
MOD Merged Ozone Dataset
NCAR National Center for Atmospheric Research
NH Northern Hemisphere
NT Northern Tropics
ODSs Ozone-Depleting Substances
OMPS Ozone Mapping and Profile Suite
SAGE II The Stratospheric Aerosol and Gas Experiment II
SBUV the Solar Backscatter Ultraviolet
SST Sea Surface Temperature
ST Southern Tropics
T Temperature
TEM Transformed Eulerian Mean
TLS Tropical Lower Stratosphere
UTLS Upper Troposphere and Lower Stratosphere
UV Ultraviolet
QBO Quasi-biennial Oscillation
WACCM Whole-Atmosphere Community Climate Model

CHAPTER 1

Introduction

1.1 Motivation

The chemical composition of the Tropical Lower Stratosphere (TLS) plays a key role in the climate system. Even small changes in the concentration and distribution of radiatively active gases such as ozone (O_3), nitrous oxide (N_2O) and water vapor (H_2O) in the TLS significantly impact radiative forcing and thus global climate. Fluctuations in stratospheric ozone affect surface ultraviolet radiation, while stratosphere-troposphere exchange of ozone impacts near-surface composition and climate.

Strong spatial and temporal variability of trace gases in the lower stratosphere are mainly due to transport processes, including the mean residual circulation (with air rising in the tropics and sinking in the polar and middle latitudes) and two-way isentropic mixing by eddies (Figure 1.1). Their respective strengths control how fast air masses are exchanged between troposphere and stratosphere, and between tropics and extratropics. Upper Troposphere/Lower Stratosphere (UTLS) transport determines the rate of the ozone hole recovery through defining lifetimes of ozone, ozone depleting substances and other green house gases (GHG). In spite of the great importance of UTLS composition on climate, which mechanisms

control UTLS variability are not fully understood and future change remains uncertain.

Most uncertainties in the UTLS composition result from uncertainties in mechanisms that would cause trace gas variability from seasonal to interannual timescales. For instence, the relative importance of different processes in determining seasonality and year-to-year variability in the tropics remains uncertain. Even more uncertain are controlling factors of longitudinal variations in TLS gases. Interannual variability of the TLS composition is dominated by Quasi-biennial Oscillation (QBO) and El Niño Southern Oscillation (ENSO) modes which modify mean residual circulation [*Calvo et al.*, 2010] as well as dynamical eddies [*Abalos et al.*, 2016a]. However, there still a lot of questions remain unanswered regarding mechanisms involved. Thus, the impact of QBO and ENSO on UTLS transport and tracer distributions merits further study.

1.2 Science background

1.2.1 UTLS transport and seasonal variability of trace gases

Transport in the TLS plays a key role in determining the stratospheric spatial and temporal distribution of ozone, water vapor, methane, and other trace constituents, and the coupling between the stratosphere and climate [*Fueglistaler et al.*, 2009; *Riese et al.*, 2012]. It is therefore important to understand and quantify this transport, and how it may change in the future.

Transport of chemical tracers is often decomposed into vertical and quasi-horizontal components. The vertical transport in the tropics is dominated by the large-scale ascent by the Brewer-Dobson circulation (BDC) while the quasi-horizontal transport (we will refer to it as simply “horizontal transport”) is associated with the eddy mixing (Figure 1.1). The effect of these two transport processes on chemical constituents whose dynamical timescales are longer than timescales for chemical sources and sinks ("long-lived tracers") are to increase and decrease latitudinal gradients in the case of vertical and horizontal transport

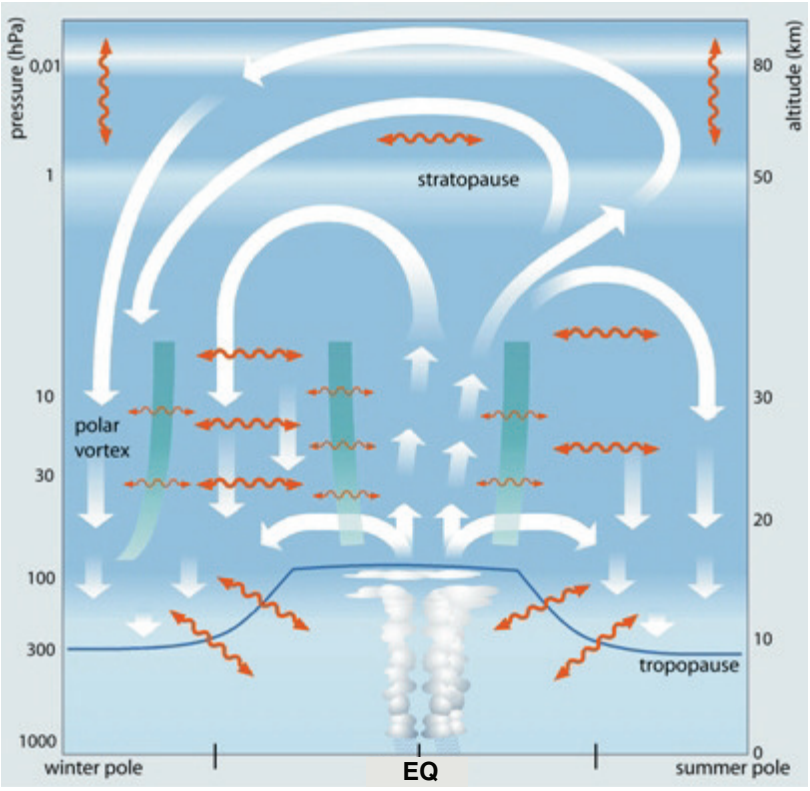

FIGURE 1.1: Schematic representation of the Brewer-Dobson circulation and Middle Atmosphere Transport. Tropospheric air masses enter the stratosphere via the tropical tropopause, from where they are distributed via different pathways in the stratosphere. White arrows represent large scale residual circulation while red arrows are two-way isentropic mixing by eddies. Transport barriers that separate tropics from extratropics and midlatitudes from polar regions are shown in light green. From `http://www.goethe-university-frankfurt.de/69128060/Atmospheric-Transport`.

respectively [e.g., *Andrews et al.,* 1987, chapter 9]. For example, Figure 1.2 shows a tropical upward bulge of methane due to tropical upwelling by the BDC and sharp horizontal gradients where strong mixing occurs.

The temporal variability of O_3 and other long-lived tracers in the TLS is strongly influenced by the transport processes described above as well as by photochemical production and loss. However, the relative importance of different processes in the tropics remains uncertain. Earlier studies considered tropics being "well-mixed" and exchange of air masses with extratropics (eddy mixing) very weak [*Plumb*, 1996]. Using the assumption of weak mixing, [*Randel et al.*, 2007] explained the large seasonal cycle in the lower stratospheric ozone as a response to seasonal changes in upwelling. This would result in upwelling by the

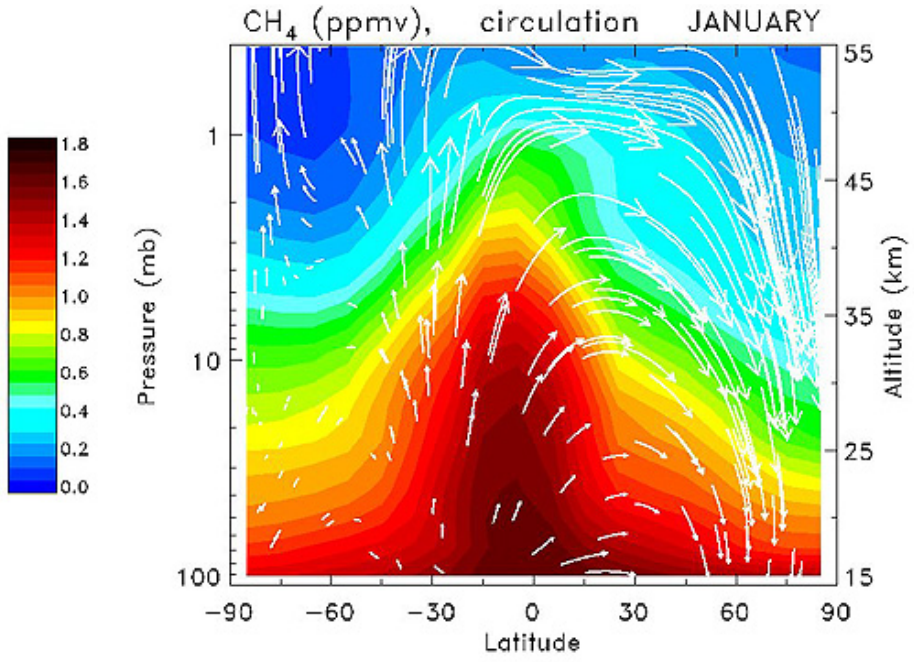

FIGURE 1.2: Latitude - height concentrations (in ppmv) of zonally averaged methane (contours) and the Brewer-Dobson circulation (white arrows) for January. From `http://www.ccpo.odu.edu/SEES/ozone/class/Chap_6/`

BDC and local chemical sources and sinks to dominate tracer budget in the tropics. However, effective diffusivity calculations of *Haynes and Shuckburgh* [2000] showed mixing into the TLS, and a number of more recent studies have shown that horizontal mixing within the extratropics plays an important role [e.g. *Konopka et al.*, 2009, 2010; *Abalos et al.*, 2012, 2013a,b; *Ploeger et al.*, 2012]. For example, *Konopka et al.* [2009] reported that mixing by eddies contributes to about 40% of O_3 during boreal summer in the lower stratosphere, while *Abalos et al.* [2013b] demonstrated the dominant role of horizontal transport near the tropical tropopause and increasing role of vertical advection above 70 hPa. Horizontal mixing is primarily driven by the large anticyclonic circulations above Asia and North America in the UTLS (Asian and North American Monsoons). The studies described above emphasized the important role of horizontal and vertical transport in the TLS from different perspectives [*Abalos et al.*, 2013a]; however, the exact balance between upwelling by the residual circulation and eddy-mixing (and how this balance varies with altitude) remains a topic of debate.

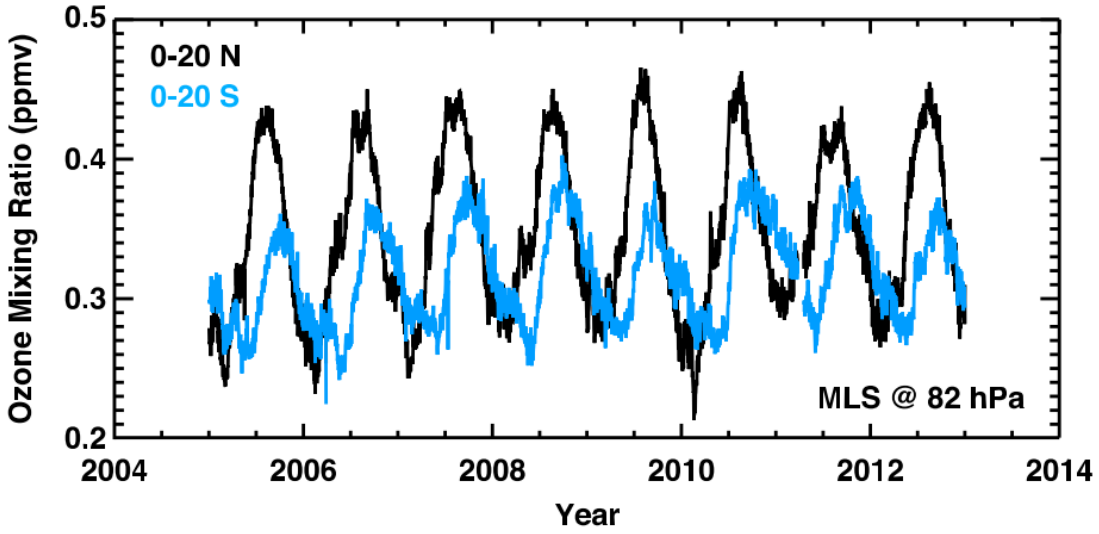

FIGURE 1.3: Evolution of MLS ozone at 82 hPa averaged over the Northern Tropics (EQ-20° N; black) and Southern Tropics (EQ-20° S; blue). From Stolarski et al. [2014].

An additional complication for understanding the annual cycle in O_3 is the feedback between ozone and upwelling by the residual circulation ($\overline{w}*$) [*Andrews et al.*, 1987]. Changes in O_3 lead to changes in heating rates that impact the upwelling, and then O_3 [*Ming et al.*, 2016b]. Furthermore, changes in ozone heating rates would impact $\overline{w}*$ indirectly through changes in wave-induced forcing [*Ming et al.*, 2016a]. This is, however, not an issue for nitrous oxide (N_2O) and other long-lived tracers which do not have a significant radiative impact in the tropical lower stratosphere.

A further uncertainty comes from the fact that the above studies have focused primarily on the variations in the tropical-wide average (20° N-20° S) of tracers, i.e. have considered "well-mixed" tropics. Recently, *Stolarski et al.* [2014] showed significant differences in the observed seasonality of O_3 and other tracers between the northern and southern tropics (NT and ST, respectively). In particular, they showed that the amplitude of the seasonal cycle in O_3 from the Microwave Limb Sounder (MLS) at 82 hPa in the NT is larger than in the ST, and that the maximum in O_3 mixing ratio in the NT occurs in July-August while in the ST it occurs 1-2 months later (Figure 1.3). Further, they concluded from an analysis of $\overline{w}*$ that

seasonal variations in upwelling alone could not explain the hemispheric contrast in annual cycle of tracers, and there must be other processes that affect the seasonality of tracers in the tropical lower stratosphere.

1.2.2 ENSO induced variability of TLS trace gases

Near the tropical tropopause ENSO dominates ozone interannual variability[*Randel et al.*, 2009; *Calvo et al.*, 2010; *Oman et al.*, 2013]. Previous studies showed that ENSO modulates both advective transport by the BDC and mixing by eddies in the tropics, which have impact on ozone distribution. As an example of ozone variability due to ENSO-related changes in the BDC, O_3 composites for El Niño and La Niña events during December- April in WACCM are shown in Figure 1.4a and 1.4b respectively. Increase (decrease) in the tropical ozone during La Niña (El Niño) events are explained by changes in the strength of BDC (i.e., increase in tropical upwelling during El Niño and decrease during La Niña) [*Calvo et al.*, 2010; *Oman et al.*, 2013].

So far, observational investigations of ENSO-related variability in mixing, focusing on a range of different altitudes, have shown somewhat differing results. Based on the effective diffusivity calculations and ERA-15 reanalysis,*Scott et al.* [2003] observed weaker mixing at 350 K during strong El Niño years but their results showed a strong sensitivity to the change of the reanalysis dataset. *Garny et al.* [2007] examined the interannual variability of mixing based on NCEP/NCAR reanalyses over the period 1979-2005 on three isentropic levels (450, 550 and 650 K) in the stratosphere and found no significant effect of ENSO. *Abalos et al.* [2016a] showed that ENSO modifies isentropic dynamical eddies, which could impact transport of tracers and contribute to NT/ST differences. Recently, *Yan et al.* [2018] analysed the ENSO influence on the ASM anticyclone with major focus on how the ENSO winter signal propagates into the following seasons. Using satellite (MLS), in-situ (SHADOZ) observations and model simulations (CLaMS) of ozone they showed less in-mixed ozone from the stratosphere into the tropical tropopause layer during and after strong El Niño events

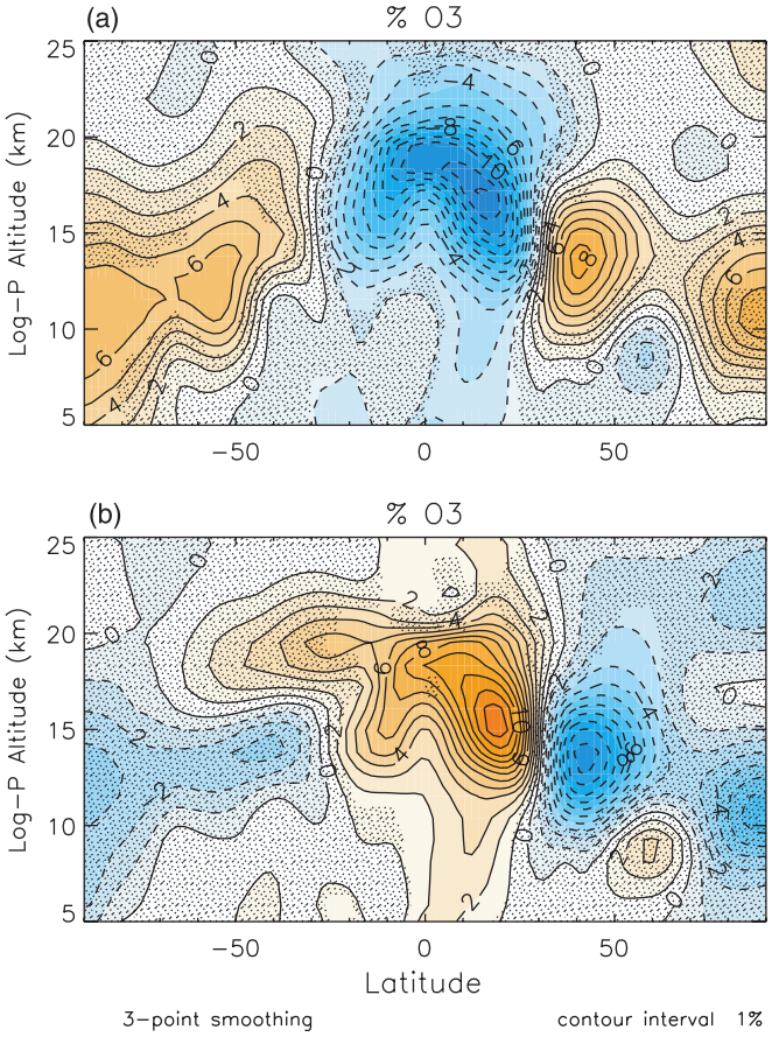

FIGURE 1.4: (Height vs latitude cross section of the percentage change in ozone anomalies with respect to the DJFMA value for (a) El Niño and (b) La Niña events. Contours are drawn every 1%. Red denotes positive values and blue denotes negative values. From *Calvo et al.* [2010]

due to earlier onset of ASM anticyclone, but the difference between El Niño and La Niña composites becomes very small in the summer.

The above studies focused on NH cold-season (DJF) SST anomalies in the equatorial Pacific because ENSO usually peaks during boreal winters. However, there are also ENSO events that are strong or moderately strong during boreal spring and summer (e.g., 2015/2016 El Niño) and some peak in warm seasons (e.g., the 1987/1988 El Niño). As we will show later in Chapter 4, analysis of model simulation shows a strong correlation of ozone with SSTs

leading ozone anomalies just by 1 month. This demands evaluation of the role of ENSO events during warm seasons (late boreal spring and summer) on interannual variability of ozone in the TLS, an issue that has received little attention in literature.

1.2.3 QBO induced variability of TLS trace gases

QBO is a quasiperiodic alternation between easterly and westerly zonal winds in the tropical stratosphere that is driven by a broad spectrum of vertically propagating Kelvin and mixed Rossby-gravity waves along with smaller-scale gravity waves[*Lindzen and Holton*, 1968; *Holton and Lindzen*, 1972; *Dunkerton*, 1997]. As shown in Figure 1.5, the alternating wind regimes (i.e., the easterly and westerly phases) propagate downward from the middle stratosphere to the tropopause with a period that varies from 24 to 32 months (~28 months on average).

There is also a QBO in ozone (O_3), which was first observed by *Funk and Garnham* [1962] in Australian midlatitude total-column O_3 observations. *Ramanathan* [1963] showed the connection between the QBO in total O_3 and the QBO in equatorial zonal winds using a series of ground stations spanning both hemispheres but most importantly noted the "out-of-phase" relationship between ozone in midlatitudes and the equator. *Angell and Korshover* [1964] found a QBO signal in Shanghai (31.2° N) total O_3 observations in the 1932-1942 period. *Zawodny and McCormick* [1991] used satellite O_3 profile observations to show the ozone QBO vertical structure from 20 to 50 km and 50° S-50° N. *Randel and Wu* [1996] used numerical techniques to filter the QBO ozone structure showing the equatorial and midlatitude out-of-phase relationship and revealing the seasonal synchronization between the equatorial QBO and the large-amplitude winter-to-spring extratropical O_3 anomalies that appear in both winter hemispheres.

Because most O_3 is found in the lower stratosphere where its lifetime is more than 1 year, the tropical O_3 distribution is strongly controlled by the tropical lower-stratosphere

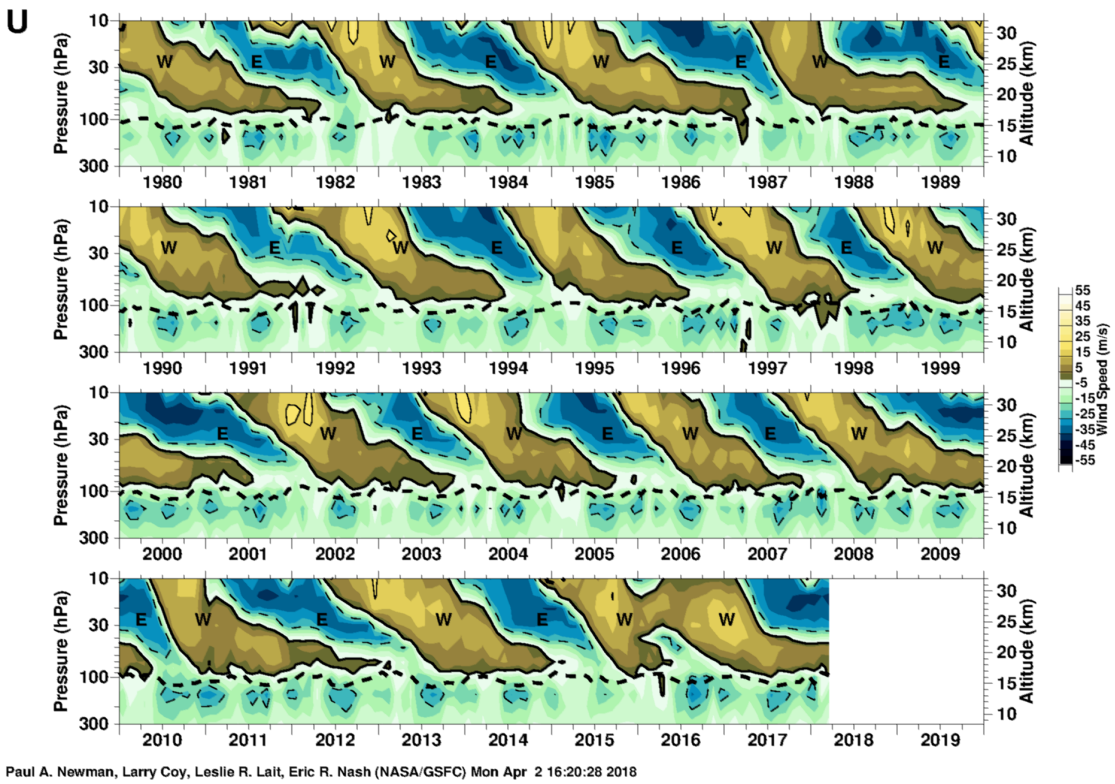

FIGURE 1.5: Monthly mean zonal wind (m s^{-1}) derived from Singapore radiosondes (1° N, 104° E) between 70 and 10 hPa for 1981 through October 2017. Easterlies are shown in cyan blue, while westerlies are in green brown. Contours are every 20 m s^{-1}, with easterlies dashed and westerlies solid, and a thick black zero wind. From `https://acd-ext.gsfc.nasa.gov/Data_services/met/qbo/qbo.html`.

transport [*Ling and London*, 1986]. *Gray and Pyle* [1989] used a two-dimensional (latitude vs. altitude) model to simulate the relationship between winds, temperatures, and the O_3 distributions. Those modeled relationships were confirmed by the observations of *Zawodny and McCormick* [1991]. The *Gray and Pyle* [1989] simulation revealed that the wave-induced QBO drove a secondary meridional circulation which modulated the O_3 distribution. Assimilated meteorological data and modern transport models confirm these early results, and satellite instruments such as MLS have shown additional QBO impacts on water (H_2O), hydrochloric acid (HCl), nitrous oxide (N_2O), and carbon monoxide (CO) [*Schoeberl et al.*, 2008].

The QBO meridional circulation develops between the tropics and subtropics (from the equator to ~30° N and 30° S) to maintain the thermal wind balance between the de-

scending QBO wind shear and its temperature anomaly. At the equator, westerly shear (westerlies aloft and easterlies below) is in balance with a downward-propagating, adiabatically warmed perturbation, while easterly shear (easterlies aloft and westerlies below) produces an upward, adiabatically cooled perturbation. The enhanced upwelling during easterly shear and reduced upwelling during westerly shear in the tropics are mass balanced by the changes in the subtropical descent. The circulation is "completed" by the equatorial divergence/convergence of air at the levels of maximum easterly/westerly winds [*Choi et al.*, 2002]. The QBO-induced meridional circulation acts on local trace gas gradients to modify their distributions [*Gray and Chipperfield*, 1990]. O_3 responds with increased/decreased values in the tropics and decreased/increased values in the extratropics during descending westerly/easterly shear.

QBO effects on composition are found throughout the extratropics. QBO-driven column O_3 anomalies originating in the southern subtropics in early winter reach 60° S by the early spring [*Gray and Ruth*, 1993; *Randel and Wu*, 1996; *Kinnersley and Tung*, 1998].*Strahan et al.* [2015] also showed a transport pathway by which the midlatitude middle-stratosphere QBO signal affects polar O_3 depletion by modulating Antarctic inorganic chlorine.

The QBO has been widely analyzed because it is a major source of stratospheric O_3 interannual variability [*Baldwin et al.*, 2001], and the QBO in total-column O_3 is a dominant factor controlling interannual variations in surface ultraviolet levels [*Udelhofen et al.*, 1999]. Further, the detection and attribution of long-term O_3 changes caused by ozone-depleting substances (ODSs) requires accurate statistical models that include QBO regression terms in order to remove the QBO-driven natural O_3 variability and thereby reveal the residual ODS-forced ozone depletion [e.g. *Stolarski et al.*, 1991]. Hence, investigating the QBO driven variability is fundamental to understanding O_3 levels and trends and the resulting changes to surface ultraviolet (UV) radiation.

During the Northern Hemisphere (NH) winter of 2015-2016, radiosonde observations

revealed that the normal downward propagation of the QBO westerly phase was disrupted by the upward propagation of westerlies from ~30 hPa up to 15 hPa and the sudden appearance of easterlies at 40 hPa [*Newman et al.*, 2016; *Osprey et al.*, 2016]; also see Figure 1.5. This disruption began in November 2015, and the easterlies were fully developed by March 2016. Such a disruption is unprecedented in the equatorial wind observational record from 1953-present. *Osprey et al.* [2016] showed that this anomalous event was linked to the transport of easterly momentum from the northern extratropics into the equatorial region, and *Coy et al.* [2017], using meteorological analysis fields beginning in 1980, showed that the 2015-2016 tropical easterly momentum flux had the largest values in December-February. None of these studies examined the changes in O_3 or other trace gases during 2015-2016.

1.3 Objectives and thesis overview

This thesis has multiple objectives. The first one is to evaluate the ability of chemistry climate models to reproduce observed hemispheric difference in the seasonality of the ozone and other long-lived trace gases in the TLS and to determine the causes of these differences. The second objective is to explore trace gas variations in the lower stratosphere over interannual time scales. In particular, we aim to analyze the impact of boreal summer ENSO events on TLS ozone and quantify the changes in circulation and trace gases in response to an unprecedented disruption in the QBO during late-2015 through 2016 period.

In other words we would like to answer the following three questions:

1. Do chemistry climate models capture larger ozone annual cycle amplitude in the NT than ST? If yes, what is the cause of these differences?

2. What is impact of boreal summer ENSO events on circulation and ozone transport near the tropical tropopause layer?

3. How changes in the circulation due to 2015-2016 QBO disruption impacted trace gases

distribution in the lower stratosphere?

The thesis is structured in 5 chapters describing the work done. This chapter outlines the motivation (1.1), the scientific background (1.2) and objective that we want to reach (1.3). In Chapter 2, we examine hemispheric differences in annual cycle amplitude and transport processes causing these variations. The third chapter explores ozone variability related to the boreal summer ENSO events and its connections to the Asian summer monsoon. In Chapter 4 we analyze changes in the stratospheric circulation and composition related to the unprecedented QBO disruption. The conclusions, outstanding issues and future work are given in the Chapter 5.

CHAPTER 2

Hemispheric differences in the annual cycle of tropical lower stratosphere transport and tracers

The work contained in this chapter is based upon *Tweedy et al.* [2017a] published in *Journal of Geophysical Research - Atmosphere*.

2.1 Introduction

In this chapter, we examine the NT-ST difference in annual cycle of tracers (O_3, N_2O, and HCl) using CCM simulations. We first evaluate the ability of the suite of CCMs from the Chemistry-Climate Model Validation activity phase 2 (CCMVal-2) [*Eyring et al.*, 2008] to reproduce the observed tracer annual cycles. We then examine the relative role of different transport processes and chemical production and loss in producing the O_3 and N_2O annual cycles in the ST and NT. This analysis includes an examination of the differences in O_3/N_2O and $\overline{w}^*$ among the CCMVal-2 simulations, as well as a more detailed Transformed Eulerian Mean (TEM) analysis of two of the CCMs within CCMVal-2.

The observations and models used and method of analysis are described in the next section. In Section 2.3 we evaluate the ability of the CCMVal-2 models to reproduce the

observed tracer annual cycles, while in Section 2.4 we perform a more detailed analysis of two of the CCMs.

2.2 Models, observational data, and methods

2.2.1 Chemistry Climate Models

TABLE 2.1: CCMVal-2 models with references and half Peak-to-Peak Annual Cycle Amplitude in O_3 and w*. The models are listed in numerical order as they appear in Figure 2.3

Number	Models	Reference	ST O3 (%)	NT O3 (%)	ST w* (mm/s)	NT w* (mm/s)
1	AMTRAC3	Austin and Wilson [2006]	20.4	30.4	N/A	N/A
2	CAM3.5	Lamarque et al. [2008]	16.6	39.06	0.181	0.164
3	CCSRNIES	Akiyoshi et al. [2009]	30.0	18.4	0.278	0.113
4	CMAM	Scinocca et al. [2008]	27.6	29	0.367	0.223
5	CNRM	Teyssédre et al. [2007], Déqué [2007]	27.7	42.5	0.387	0.500
6	E39CA	Garny et al. [2009]	21.4	19.5	0.241	0.138
7	EMAC	Joöckel et al. [2006]	24.4	29.0	0.195	0.217
8	GEOSCCM	Pawson et al. [2008]	15.8	37.0	0.113	0.086
9	LMDZrepro	Jourdain et al. [2008]	22.9	36.9	0.157	0.125
10	MRI	Shibata and Deushi [2008]	23.4	15.9	0.204	0.104
11	Niwa-SOCOL	Schraner et al. [2008]	10.6	16.1	0.270	0.238
12	SOCOL	Schraner et al. [2008]	8.7	14.7	0.233	0.136
13	ULAQ	Pitari et al. [2002]	39.7	14.0	0.476	0.454
14	UMETRAC	Austin and Butchart [2003]	19.3	26.0	N/A	N/A
15	UMSLIMCAT	Tian and Chipperfield [2005]	18.9	25.0	N/A	N/A
16	UMUKCA-METO	Morgenstern et al. [2009, 2010]	15.9	16.8	N/A	N/A
17	UMUKCA-UCAM	Morgenstern et al. [2009, 2010]	10.7	22.0	0.102	0.057
18	WACCM	Garcia et al. [2007,2008]	24.1	44.7	0.174	0.157

We examine simulations from CCMs that participated in the second CCM Validation (CCMVal-2) project [*Eyring et al.*, 2008]. CCMVal-2 was an international project, organized under the auspices of WCRPs (World Climate Research Programme) SPARC (Stratosphere Processes and their Role in Climate) project [*CCMVal SPARC*, 2010], designed to compare and evaluate stratospheric CCMs. The CCMs considered here are listed in Table2.1. All of these models include stratospheric chemistry that is radiatively coupled to the dynamics, i.e. the distributions of radiatively active gasses (e.g., CO_2, H_2O, N_2O, CFCs, O_3) influence the radiative heating rates and thus dynamics. We use the "historical" REF-B1 simulation that covers the period 1960 - 2006. These simulations include natural and anthropogenic forcings based on observed changes in the abundance of trace gases, and were designed to provide the best possible representation of the stratospheric climate and variability over this period. A more extensive description of these models and simulations is provided in *Morgenstern et al.*

[2010] and references in Table2.1.

We first examine the ability of all CCMs listed in Table2.1 to reproduce the observed hemispheric differences in annual cycles of tropical ozone and other trace gases, and then focus in more detail on simulations from the Goddard Earth Observing System Chemistry Climate Model (GEOSCCM) and the Whole-Atmosphere Community Climate Model (WACCM). We have access to fields not in the CCMVal-2 data archive from these two models that enable a more detailed analysis of the transport in the tropical lower stratosphere.

GEOSCCM couples the Goddard Earth Observing System (GEOS) general circulation model with a comprehensive stratospheric chemistry module. The GEOSCCM simulations in CCMVal-2 used version 5 of GEOS (GEOS-5), described in *Pawson et al.* [2008]. The GEOSCCM simulations analyzed have horizontal resolution of 2° latitude by 2.5° longitude and include 72 vertical levels from the surface up to 0.01 hPa (80 km). GEOSCCM performed well in evaluations of both chemical- and transport-related processes [*CCMVal SPARC,* 2010; *Strahan et al.,* 2011; *Douglass et al.*, 2012]. The required output for a full TEM budget analysis was not archived from the CCMVal-2 simulations, but are available for simulations from an updated version of GEOSCCM, described in *Oman and Douglass* [2014]. The annual cycle of ozone and other tracers in the TLS is very similar between the two GEOSCCM simulations.

WACCM is the atmospheric component of the coupled climate system model CESM1 (Community Earth System Model, Version 1), and is described in *Garcia et al.* [2007]. It has horizontal resolution of 2.5° latitude and 1.9° longitude, and extends vertically from the ground up to the lower thermosphere (180 km) with 66 vertical levels. Vertical resolution in the upper troposphere and lower stratosphere is 1.1-1.4 km. As with GEOSCCM, the required fields for the TEM analysis were not archived for the CCMVal-2 REF-B1 historical simulation, but are available from a later WACCM simulation. The later simulation is described in *Abalos et al.* [2013b], where it is shown that the simulated annual cycle

in ozone and temperature agrees well with satellite observations. As with the GEOSCCM simulations, there is good agreement in the ozone distributions between the two WACCM simulations considered here.

2.2.2 Observational data

The ability of CCMs to realistically represent ozone and its seasonality in the TLS is evaluated against measurements from several satellite instruments. *Stolarski et al.* [2014] examined the seasonality of TLS ozone from the Stratospheric Aerosol and Gas Experiment II (SAGE II) [*Wang et al.*, 2002] and version 3 of the Aura MLS (MLS-v3) [*Livesey et al.*, 2008] instruments. We consider these data sets together with a new version of MLS (MLS-v4), which incorporates some modifications that improve ozone vertical profiles [*Livesey et al.*, 2015], and measurements from the Ozone Mapping and Profile Suite (OMPS) on board NASA/NOAA Suomi-NPP satellite [*Kramarova et al.*, 2014].

SAGE II data are available from 1984 to 2005, MLS from September 2004 to present, and OMPS from 2012 to present. We use MLS and OMPS data up to 2015 in our analysis. The MLS and OMPS data have sufficient horizontal and temporal coverage to enable examination of the ozone annual cycle for each year. MLS has a vertical resolution around 3 km, whereas OMPS has higher vertical resolution of around 1.5 - 2 km. SAGE II also has higher vertical resolution than MLS (~1km), but has sparser spatial and temporal coverage, and the long (21 year) data set is needed to create a climatology with a good horizontal and temporal coverage.

The observational data sets described above are publicly available. MLS data are available from the NASA Goddard Space Flight Center Earth Sciences (GES) Data and Information Services Center (DISC). OMPS satellite ozone data have been obtained from the NASA Goddard Space Flight Center Website (`https://jointmission.gsfc.nasa.gov/omps.html`) and SAGE II ozone data have been obtained from the Langley Data Center

(https://eosweb.larc.nasa.gov).

2.2.3 *Calculations of the climatological annual cycle.*

We focus on the climatological annual cycle of tracers and $\overline{w}^*$, i.e. we examine seasonal changes in the climatological monthly-mean values. The climatological means from the CCMs are formed by averaging output from 1990 to 2005, while the periods used for the observations vary among data sets (see above). The amplitudes of the tracers and $\overline{w}^*$ annual cycle are calculated as half the difference between the maximum and minimum in monthly climatologies. This yields results similar to fitting annual sines and cosines to the full monthly-mean ozone timeseries (as done in *Stolarski et al.* [2014]).

The results of our analysis are not sensitive to the time interval used to create the climatology. Ozone annual cycle amplitudes computed using three different time intervals (1960-2005, 1980-2005 and 1990-2005) give very similar results (differences in annual amplitude are less than 3 %, not shown). While there is some interannual variability in the details of stratospheric ozone and $\overline{w}^*$ seasonality, our results are representative of typical seasonal cycle variability within the considered time period.

2.3 Evaluation of CCMVal-2 models

We first evaluate the ability of the CCMs to reproduce the observed annual cycle of tropical ozone. Figure 2.1 shows the seasonal evolution of climatological monthly-mean O_3 at 80 hPa from the CCMs (colored curves) and satellite observations (black symbols), for averages over the (a) northern tropics (NT; EQ-20° N) and (b) southern tropics (ST; EQ-20° S). The observations show, as discussed in *Stolarski et al.* [2014], a larger amplitude in the NT than in the ST, and a 1-2 month lag in the timing of the peak between the ST and NT. There are some differences among the data sets (see further discussion below), but these differences are much smaller than the spread in the simulated ozone annual cycle among the models.

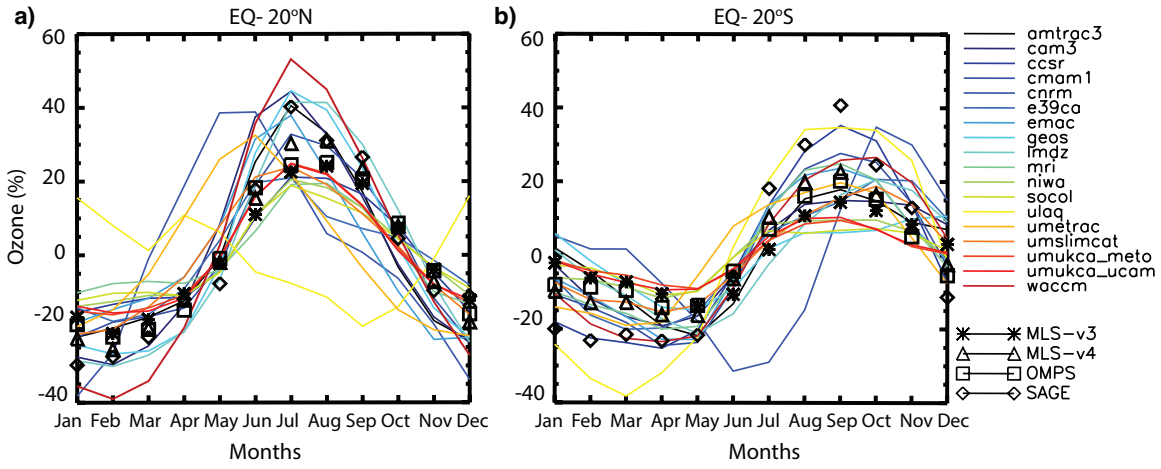

FIGURE 2.1: Seasonal evolution of lower stratospheric (~80 hPa) ozone deviations averaged over (a) NT and (b) ST, from observations (black symbols) and CCMVal-2 models (colored lines). Values are shown as percent difference of climalogical monthly averaged ozone from its climatological annual mean.

While some models produce an annual cycle with similar amplitude and phase, there are models with amplitude much smaller or much larger than observed, and some models have the incorrect phase. To examine the differences among the models, and among the data sets, we show the latitude-pressure variation in the amplitude of the ozone annual cycle in Figure 2.2. As discussed above, the observational data sets (top row) all show larger amplitude in northern than southern tropics in the lower stratosphere. They also all show that this NT-ST difference goes away in the middle and upper stratosphere. There are, however, differences among the data in the vertical variations in the lower stratosphere, including where the maximum amplitude occurs (with SAGE II showing the peak at a higher altitude than MLS or OMPS) and whether there is a two-peak structure in the vertical. As discussed in *Stolarski et al.* [2014], SAGE II measurements show only a single peak in the annual cycle amplitude in the lower stratosphere, while MLS (-v3) shows a double peak with local maximum at 100 and 68 hPa. This two-peak structure is not found in the ozonesondes (not shown) and the newer version of MLS (-v4) but occurs in OMPS. The cause of these differences between the different observational data sets is unknown, and is the subject of ongoing research.

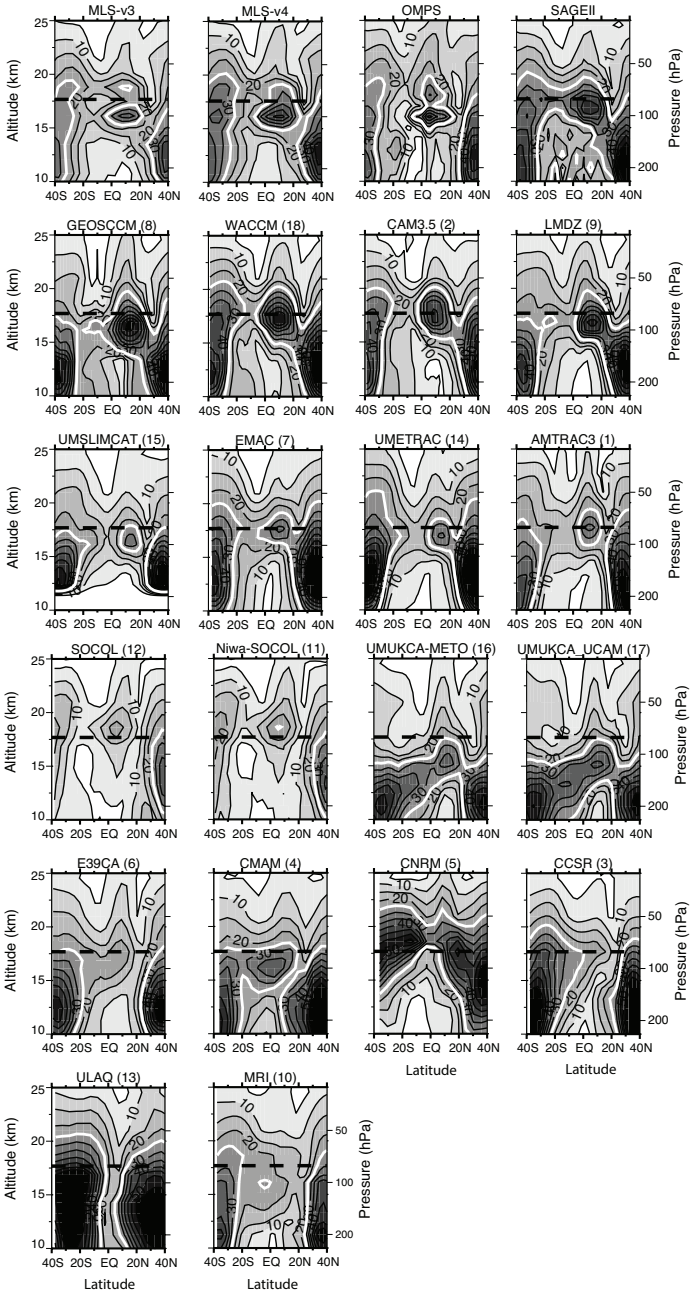

FIGURE 2.2: Latitude-altitude dependence of the magnitude of the annual cycle in ozone, in percent of the annual-mean value, from 4 observational datasets (MLS-v3, MLS-v4, OMPS, and SAGE II) and 18 CCMVal-2 models (see table 1). Contour interval is every 5% percent with thick white contour corresponding to 25%. 80 hPa vertical level is indicated by dashed line.

Consistent with the observations, the majority of the CCMs show a larger amplitude in the NT than in the ST. This suggests that these CCMs include the key processes (transport and chemical production and loss) that cause the hemispheric differences in tropical ozone

seasonality. However, none of the models produce a double peak structure as found in MLS-v3 and OMPS. Also, there are differences in the magnitude of the peak and its location among the CCMs, indicating quantitative differences in the transport among the models. Furthermore, there are several CCMs that don't show a significant hemispheric difference in the annual amplitude (CMAM, CNRM, 39CA) or even show a larger amplitude in the ST than the NT (ULAQ, CCSR, MRI), suggesting some problems in the representation of this aspect of transport in the tropical lower stratosphere.

To quantify the differences among models, we calculate the amplitude of the annual cycle of 80 hPa ozone averaged over the NT and ST. The 80 hPa vertical level is highlighted as dashed black horizontal line in Figure 2.2. Figure 2.3a shows the relationship between the NT-averaged and ST-averaged amplitude for the CCMs (black diamonds) and for the observations (blue stars). The amplitudes at 80 hPa for each CCM are also listed in Table 1. As discussed above, the majority of the CCMs reproduce the observed feature of larger amplitude in the NT than the ST (i.e. the symbols for the majority of the models lie above the 1-1 line in Figure 2.3a). However, for some models the NT and ST amplitudes have similar values or the ST amplitude is larger than the NT amplitude. There is also a large spread in the amplitude of the ST and NT annual cycles among the models. Some of the spread is due to the variations in altitude of the peak in annual cycle amplitude. For example, the NT peak in ozone amplitude from UMUKCA-METO and UMUKCA-UCAM is located below 80 hPa reaching a maximum near 100 hPa (see Figure 2.2). Note that given the differences between the annual cycle in different observational data sets we are limited on how precise we can be in determining the reality of the simulated annual cycle. However, even with this uncertainty there are models that are well outside the observational estimates.

A similar analysis of the NT-averaged and ST-averaged amplitude of annual cycle in other long-lived tracers (e.g. N_2O, HCl and mean age) shows very similar results, with a wide spread in amplitudes among the CCMs and CCMs with larger (smaller) O_3 amplitude in the NT than ST also have a larger (smaller) NT amplitude for the other tracers (not

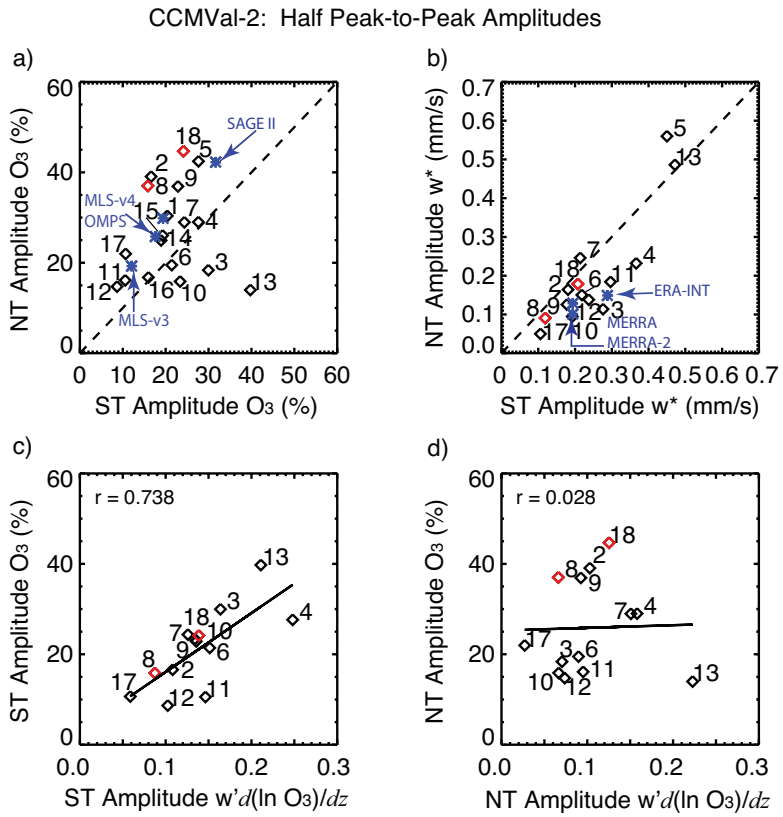

FIGURE 2.3: (a) The magnitude of ozone seasonality at 80 hPa averaged over the NT (EQ-20° N) vs the magnitude averaged over the ST (EQ- 20° S) for 18 models (black diamonds) from the CCMVal-2 intercomparison project. The symbols in red show model simulations from (8) GEOSCCM and (18) WACCM. The blue stars correspond to four data sources MLS-v3, MLS-v4, OMPS and SAGE II. (b) The same as in (a) except for magnitude of the annual cycle in $\overline{w}^*$ at 100 hPa for 14 models from the CCMVal-2 intercomparison project (in black) with blue stars representing three reanalysis products (MERRA, MERRA-2, and ERA-INT). (c,d) Relationship between ozone amplitude and vertical transport ($w' \frac{\partial(\ln \overline{O_3})}{\partial z}$) for the CCMs, for (c) ST and (d) NT. The linear regression between ozone and vertical advection is shown in (c) and (d), with Pearson linear correlation coefficient (r) in the left right corner.

shown). This suggests that the NT-ST contrast in annual amplitude is driven by transport and not chemistry.

What could be causing the differences in the annual cycle in NT and ST ozone among the CCMs? One potential cause is differences in the simulated annual cycle of tropical vertical residual circulation ($\overline{w}^*$). Figure 2.3b shows the relationship between amplitude of NT and ST $\overline{w*}$ at 100 hPa for the CCMs (where $\overline{w*}$ is available) and several meteorological reanalyses. Most models show the same qualitative differences between the amplitude of ST and NT $\overline{w*}$ as in the reanalyses (i.e., larger annual cycle in the ST than in the NT), but

with some large quantitative differences among the models. However, there are two models ((5) CNRM and (13) ULAQ) with $\overline{w}^*$ amplitudes in the ST and NT considerably larger than in other models, indicating serious problems with simulated $\overline{w}^*$. Furthermore, the differences in $\overline{w}^*$ among CCMs may only explain some portion of the spread in the O_3 annual cycle amplitude and they do not explain all the differences. For example, models 16 and 17 (UMUKCA-METO and UMUKCA-UCAM) have the smallest amplitudes of $\overline{w}^*$ annual cycle but the O_3 amplitudes are comparable or larger than observed. This indicates that differences in the $\overline{w}^*$ annual cycle are not the only differences in the transport among the models. The fact that other processes are playing a role can also be seen, as discussed in *Stolarski et al.* [2014], by comparing the relative NT-ST amplitudes of $\overline{w}^*$ and O_3: A larger annual cycle of $\overline{w}^*$ in the ST than the NT will, if no other hemispheric differences, produce a larger ST cycle in ozone. This is not observed or simulated in most models, indicating other processes play a role.

To explore this further we examine the relationship between the amplitude of the annual cycle in O_3 and vertical transport by the residual circulation. The local change in tracer concentration due to transport processes and chemical sources and sinks can be quantified by the zonal mean continuity equation [Eq 9.4.13 *Andrews et al.*, 1987]:

$$\bar{\chi}_t = -\bar{v}^* \bar{\chi}_y - \bar{w}^* \bar{\chi}_z + e^{z/H} \nabla \cdot \mathbf{M} + P - L \tag{2.1}$$

where ($\bar{v}^*$,$\bar{w}^*$) is the residual circulation, $P - L$ is the chemical production minus loss rate and M is the eddy transport vector. The first two terms on the right-hand side correspond to horizontal and vertical advection, while the third term is the combined horizontal and vertical eddy transport term. The components of the divergence of eddy transport vector are:

$$M_y = -e^{z/H}(\overline{v'\chi'} - \frac{\overline{v'T'}}{S}\overline{\chi}_z) \tag{2.2}$$

$$M_z = -e^{z/H}(\overline{w'\chi'} - \frac{\overline{v'T'}}{S}\overline{\chi_y}) \tag{2.3}$$

Assuming the annual cycle in tracers is determined only by vertical advection (i.e., seasonality of horizontal advection, $P-L$, and eddy transport are small), *Randel et al.* [2007] showed the relationship between annual variations in tracer and vertical transport in the tropics:

$$i\sigma\frac{\chi'}{\langle\overline{\chi}\rangle} = w'\frac{\partial(\ln\overline{\chi})}{\partial z} \tag{2.4}$$

where $\frac{\chi'}{\langle\overline{\chi}\rangle}$ is the fractional annual amplitude of tracer (i.e. annual amplitude divided by annual-mean value), w' is annual amplitude of upwelling by the residual circulation, and $\sigma = 2\pi/(365$ days). Figure 2.3c,d shows the relationship between fractional annual amplitude of ozone and $w'\frac{\partial(\ln\overline{\chi})}{\partial z}$ for (c) ST and (d) NT averages. If the annual cycle in vertical transport is a major driver in the annual cycle of ozone then we may expect a linear relationship between these two terms.

Figure 2.3c shows that this is generally true for the ST amplitude, as CCMs with larger annual cycles in ST vertical transport also have a larger O_3 amplitude. The steep slope of the regression line and large linear Pearson correlation coefficient (r = 0.73) strongly suggest that variations in the amplitude of the ST annual cycle in vertical transport explain variations in the ST ozone annual cycle. This is not the case for the NT annual cycles, where there is no relationship (r = 0.03 and nearly zero slope of the linear fit) between the amplitude of ozone and $\overline{w}$* (Figure 2.3d). This is consistent with the conclusions from*Stolarski et al.* [2014] that upwelling is not the determining factor in the NT ozone annual cycle and that other processes (such as horizontal mixing and/or chemistry) play a larger role.

Previous studies have also evaluated the transport in suite CCMVal-2 models, and it is interesting to compare their evaluations with our analysis of the CCMs ability to simulate the NT and ST annual cycles. In particular, *Strahan et al.* [2011] evaluated the CCMs considered here based on the model's ability to correctly represent ascent and horizontal mixing based on N_2O and mean age and classified the CCMs into those with "most realistic

stratospheric transport" (CAM3.5, CMAM, GEOSCCM, UMSLIMCAT and WACCM), "slow ascent or too much mixing" (LMDZ, MRI, ULAQ, UMUKCA-METO, UMUKCA-UCAM), or "too fast transport" (AMTRAC3, UMETRAC, CNRM, NIWA-SOCOL, SOCOL). Their results also showed that the five models with the best representation of circulation and mixing show closer agreement with MLS O_3 than most models, and the spread among them is smaller. The six models - AMTRAC3, CCSRNIES, LMDZ, Niwa-COCOL, SOCOL, and UMETRAC - with less serious transport deficiencies compare well with observations in the tropical lower stratosphere as do the models with realistic transport, while models with significant transport problems (such as ULAQ, CNRM and MRI) show large deviations in simulated tropical ozone. Our multi-model analysis shows that four out of the five models with most realistic transport also do well in reproducing the NT - ST differences in ozone annual cycle (CMAM is the exception as it has a similar amplitude in the NT and ST), while the CCMs with too slow or fast transport or too much mixing generally also have unrealistic aspects of their tropical lower stratospheric ozone annual cycle. AMTRAC, LMDZ, and UMETRAC (models with less serious problems) are exceptions, as the amplitudes of NT and ST annual cycles in these models are close to observed. It is unclear why CMAM reproduces N_2O and mean age well but not the ST-NT contrast in the ozone annual cycle and why AMTRAC and LMDZ get the ozone annual cycle but not N_2O and mean age. We are limited in our ability to answer these questions because of lack of required data in the CCMVal-2 archive, e.g. $\overline{w}^*$ is not archived for some models and even fewer models have available outputs to perform detailed TEM or related analysis.

2.4 Detailed analysis of GEOSCCM and WACCM

We now use GEOSCCM and WACCM simulations to examine the transport processes and annual cycle of ozone and other tracers in more detail. As described in Section 2.2 we have access to fields that are not in the CCMVal-2 archive from these models.

The analysis above shows that simulations from these two CCMs capture the observed larger amplitude of the seasonal cycle in lower stratospheric ozone in the NT than in the ST (Figure 2.2). Latitudinal variations in seasonality of lower stratospheric ozone are also very similar between these two models and observations, as illustrated in Figure 2.4a (pattern correlation coefficient is above 0.95). There are strong meridional gradients (i.e., contours

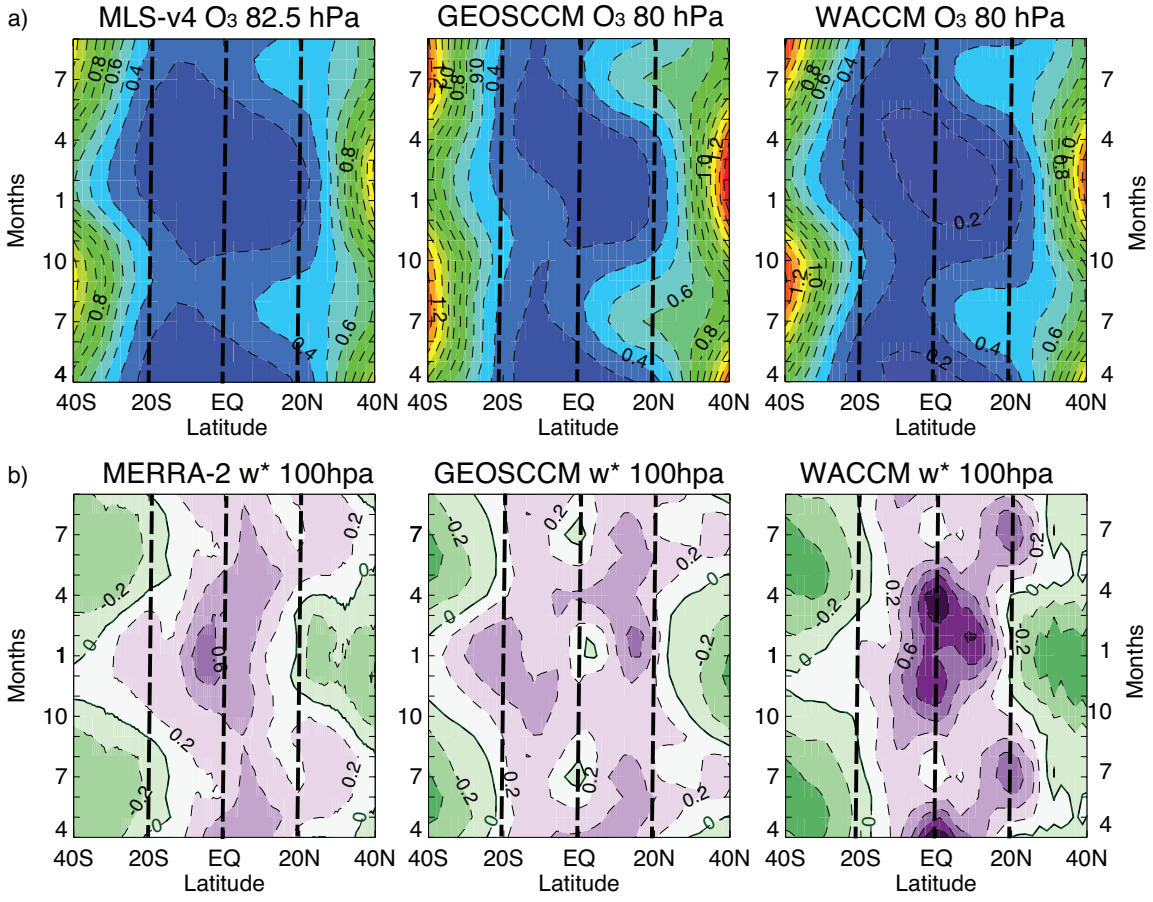

FIGURE 2.4: Latitudinal variations of seasonality in (a) ozone and (b) residual vertical velocity, $\overline{w}^*$, in the tropical lower stratosphere in MLS-v4/MERRA-2, WACCM and GEOSCCM. Ozone is averaged between 80-90 hPa (82 hPa for MLS), while $\overline{w}^*$ is shown at 100 hPa. Thick dashed lines indicate the boundaries of the NT and ST. Contour interval are every 0.1 ppmv for ozone and 0.2 mm/s for $\overline{w}^*$.

are close together) in mid-latitudes but much weaker gradients (contours further apart) in the tropics. In the southern subtropics, there is only weak seasonality in ozone, with slightly higher values around October. In contrast, there is large seasonality in the northern tropics with a large increase in June to August, where the spreading of the contours indicates transport of high ozone values from the midlatitudes into the tropics. This northern-southern

contrast explains the large difference in annual amplitude between the NT and ST. While WACCM and GEOSCCM produce ozone structure similar to that observed, there are differences in the magnitude of the meridional gradients and extent to which high ozone values intrude into the tropics during northern summer.

The annual cycle of the upwelling at 100 hPa also looks qualitatively similar (pattern correlation coefficient around 0.80) among these two models and reanalysis (MERRA-2), see Figure 2.4b. As in the reanalysis, both models capture the oscillating behavior of $\overline{w}^*$ between summer hemispheres with seasonal migration of the edge of the tropical upwelling toward the pole in spring and then back toward the equator in autumn. Although $\overline{w}^*$ is larger in WACCM than in GEOSCCM and MERRA-2, there is a good agreement with reanalysis on overall structure of the tropical upwelling in the lower stratosphere.

While we focus mostly on the seasonality of O_3 in the TLS, other long-lived tracers such as HCl and N_2O also show differences in the annual cycle between the NT and ST [*Stolarski et al.,* 2014]. These NT-ST differences also occur in GEOSCCM and WACCM simulations; see Figure 2.5. HCl, like O_3 is produced in the stratosphere and its volume mixing ratios increase rapidly with height and poleward from the equator in the lower stratosphere (see Figure 6 in *Stolarski et al.* [2014]), and the seasonal cycles in HCl and O_3 are very similar. In particular, for both tracers the amplitude of the annual cycle is larger and the peak occurs around 2 months earlier in the NT than ST. There is also a NT-ST difference for the N_2O annual cycle. The magnitude of seasonal changes in N_2O are much smaller than in O_3 and HCl due to smaller vertical and horizontal gradients of N_2O in the lower stratosphere. As N_2O is produced in the troposphere, its spatial gradients are opposite of O_3 and HCl: rather than a summer maximum in NT there is a summer minimum. In GEOSCCM and WACCM the amplitude of the annual cycle in N_2O is larger in the NT than ST (consistent with other tracers), while for MLS the differences between NT and ST amplitudes are small. Figure 5 shows N_2O mixing ratios from an older version of MLS (v3), since N_2O from MLS-v4 shows unrealistically high values at 68hPa level [*Livesey et al.*, 2015].

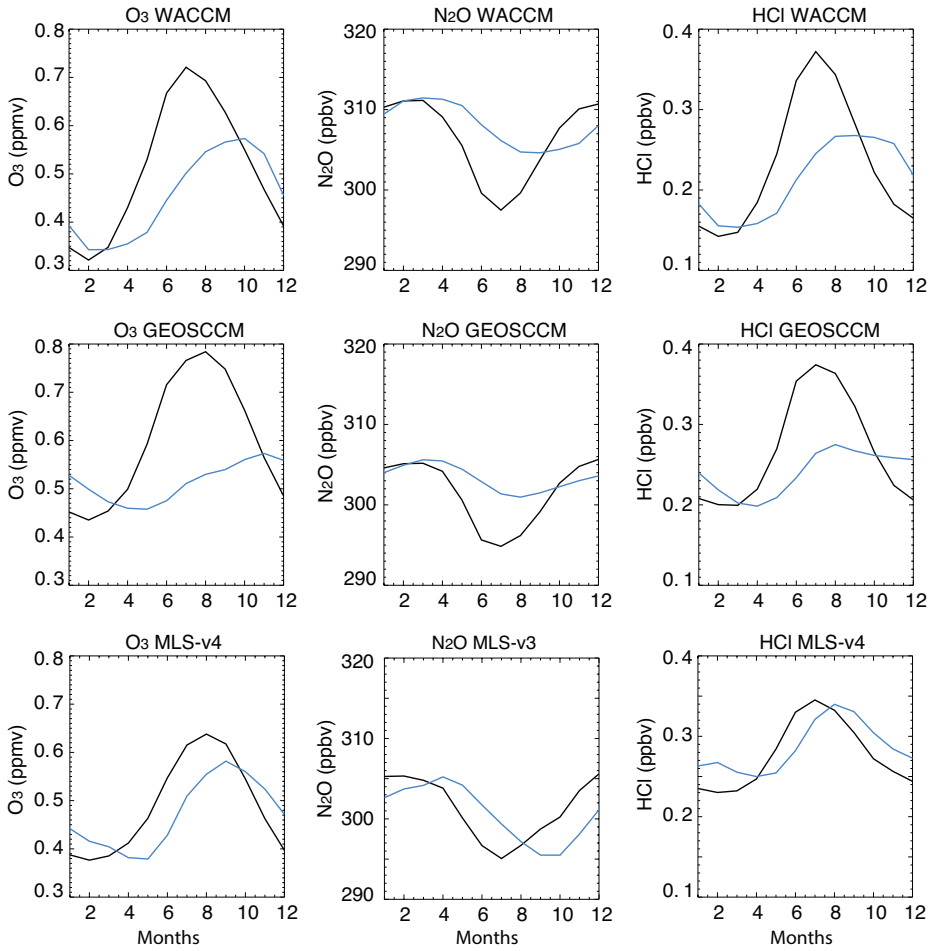

FIGURE 2.5: Climatological annual cycle in O_3, N_2O and HCl from WACCM (top), GEOSCCM (middle) and MLS (bottom) at 70 hPa averaged over northern (black) and southern (blue) tropics. MLS-v3 is used for N_2O because of high N_2O bias in MLS-v4 at this level.

The above analysis demonstrates that GEOSCCM and WACCM simulations capture the hemispheric differences of the observed annual cycle phase and amplitude. The amplitudes in the NT are too large compared to observations, but as the models capture the observed vertical and horizontal structure of the annual cycle amplitude they can be used to further examine the transport processes producing these structures. We first use the TEM formalism to separate the relative importance of transport processes and chemistry on the seasonality of zonal-mean O_3 and N_2O, and then examine the longitudinal variations in ozone.

2.4.1 TEM analysis

The TEM continuity equation for zonal mean tracer concentration (Equation 2.1) can be used to compute tracer budgets based on the role of transport processes and chemical sources and sinks. Equation 2.1, therefore, can be rearranged:

$$\bar{\chi}_t = [-\bar{v}^* \bar{\chi}_y + e^{z/H}(cos\phi)^{(-1)}(M_y cos\phi)_y] + [-\bar{w}^* \bar{\chi}_z + e^{z/H}(M_z)_z] + P - L \tag{2.5}$$

to separate horizontal (terms in the first brackets) and vertical (terms in the second brackets) transport contributions to tracer tendency.

A complete TEM budget analysis based on observations is not possible as the eddy components cannot be calculated from available observations, but all terms can be calculated from model output. *Abalos et al.* [2013b] examined the tropical O_3 and CO TEM budgets in the WACCM and concluded that the seasonality in vertical transport makes an important contribution to the seasonality of ozone in the tropical lower stratosphere, and horizontal in-mixing is most important at the tropopause level (which is 86 hPa in WACCM). However, they only considered tropical-wide averages of the tracer concentrations and residual velocities. We extend this analysis to consider the budgets in the ST and NT separately, for both WACCM and GEOSCCM simulations. Figure 2.6 shows the seasonality of the terms in Equation 2.5 for ST, NT and tropics-wide ozone at 85 hPa from WACCM and GEOSCCM. In both models there is, consistent with the above analysis, a larger annual cycle in ozone tendency (black curves) in the NT than in the ST. In the ST, the annual cycle in the vertical transport (red curves) is larger than that in horizontal transport (green curves), and the timing of maximum/minimum in ozone tendency (black line) roughly coincides with the timing of ozone tendency due to vertical transport (red curve), which peaks during the northern winter (most negative) and decreases during the summer. Examination of individual terms in Equation 2.5 indicates that vertical transport is dominated by vertical advection and that eddy mixing dominates the horizontal transport (as found in the tropical average in *Abalos et al.* [2013b]). Thus, consistent with the above analysis, the seasonality in vertical advection

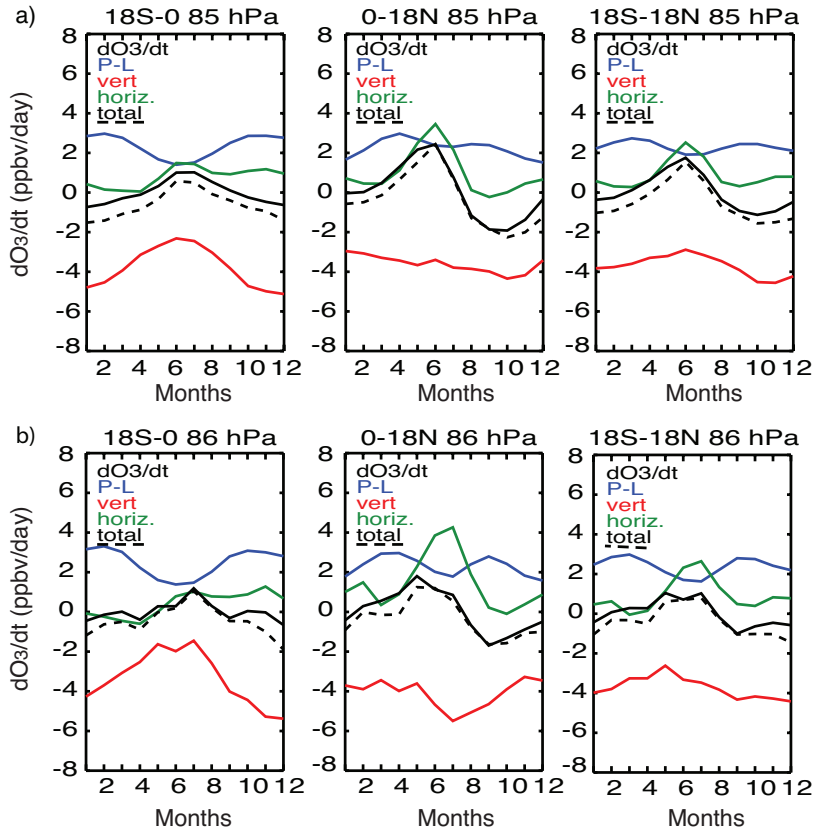

FIGURE 2.6: Mean seasonal cycles (monthly means) of terms in the ozone TEM continuity equation at 85 hPa in (a) GEOSCCM and at 86 hPa in (b) WACCM averaged over (left to right) EQ-18° S, EQ-18° N and 18° S-18° N. Black solid line shows ozone tendency, computed directly from monthly mean zonal mean ozone, while colored lines are the contributions to ozone tendency due to horizontal transport (green), vertical transport(red), and chemical production and loss (blue). The sum of all terms in the continuity equation (total tendency) is shown as black dashed line.

plays a major role in driving the seasonality in ST ozone.

The balance in the NT is different from that in the ST. The seasonality in tendency due to horizontal transport is larger than that due to vertical transport, and the tendency due to horizontal transport (mixing) and the total tendency both peak during June-August. This indicates that seasonality in horizontal mixing plays the major role in the NT ozone annual cycle.

While the seasonality of the different terms is similar between WACCM and GEOSCCM, there are some quantitative differences. The ozone seasonality due to vertical transport is larger in WACCM than in GEOSCCM, as is the seasonality due to horizontal transport. This

is consistent with Figure 2.4, which shows larger annual amplitude for $\overline{w}^*$ and larger summer to winter ozone gradient in WACCM.

We have focused above on the seasonality in transport, but Figure 2.6 shows that there is seasonality in chemical production and loss ($P-L$) that is of comparable magnitude to the transport terms, and this seasonality also differs between the NT and ST. In the NT, ozone tendency due to $P-L$ has two minima during solstices and two maxima during equinoxes. In the ST, there are also two minima and maxima in ozone tendency due to $P-L$. However, the ST minimum during the boreal summer (June-August) is larger than during the boreal winter. Furthermore, the summer/winter minimum in the ST is stronger/weaker than that in the NT. The annual cycle in $P-L$ is mainly due to ozone production (photolysis rate), which depends on solar zenith angle and overhead column ozone. The seasonality of solar zenith angle is the same for NT and ST, but overhead column ozone has a stronger seasonal cycle in the NT leading to a small annual cycle in $P-L$.

The described above TEM budget analysis is complicated by the presence of seasonality in photochemical production and loss. This is much less a factor for N_2O where there is no production and very weak loss in the tropical lower stratosphere. Therefore TEM analysis of N_2O can provide valuable information about the transport and its role in the NT and ST. Figure 2.7 shows N_2O TEM budgets at 86 hPa in GEOSCCM that look very similar to that shown for ozone with dominant role of vertical transport in the ST and horizontal mixing in the NT. Note that N_2O transport terms (green and red lines) are of opposite signs to those for ozone due to reversed horizontal and vertical gradients. There is also a good agreement between O_3 and N_2O TEM transport terms above and below 85 hPa (not shown). The seasonal magnitude of transport at 100 hPa in the ST is much smaller than in the NT with peak in upwelling during the winter rather than during the summer. The NT horizontal and vertical transport is of nearly equal amplitude and opposite sign. At higher levels (near 70 hPa) the magnitude of annual cycle due to horizontal transport in the NT is smaller than at 85 hPa, and the NT contribution due to vertical transport is shifted in phase compared to

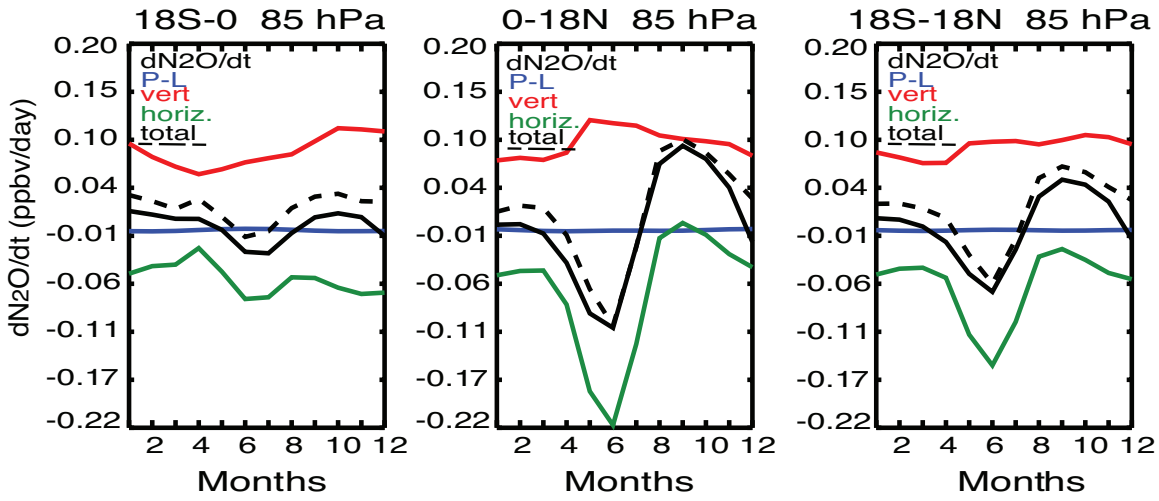

FIGURE 2.7: Mean seasonal cycles (monthly means) of terms in the N_2O TEM continuity equation at 85 hPa in GEOSCCM averaged over (left to right) EQ-18° S, EQ-18° N and 18° S-18° N.

85 hPa with weaker upwelling during the summer. The N_2O tendencies due to vertical and horizontal transport are then in phase, and the annual cycle in tracers is affected by both upwelling and horizontal mixing.

The TEM analysis of WACCM and GEOSCCM supports the hypothesis that the balance between vertical advection and horizontal mixing differs between the ST and NT lower stratosphere. Agreement in TEM transport terms between O_3 and N_2O provides further evidence that hemispheric differences in the annual cycle amplitude are driven by the transport rather than chemical processes. TEM analysis shows that seasonality of ST O_3 and N_2O is primarily due to seasonality in the upwelling whereas the strong seasonality of NT ozone is due to a large increase of horizontal mixing during northern summer.

2.4.2 Longitudinal variations

Thus far, the analysis has focused on zonal-mean tracer concentrations and does not provide any information on longitudinal variations in ozone or the processes causing variations in ozone and other long-lived tracers such as N_2O and HCl. We now examine the zonal variations in ST and NT O_3 in the GEOSCCM and WACCM simulations and MLS-v4 measurements and relate these to variations in mixing and upwelling discussed above. We first exam-

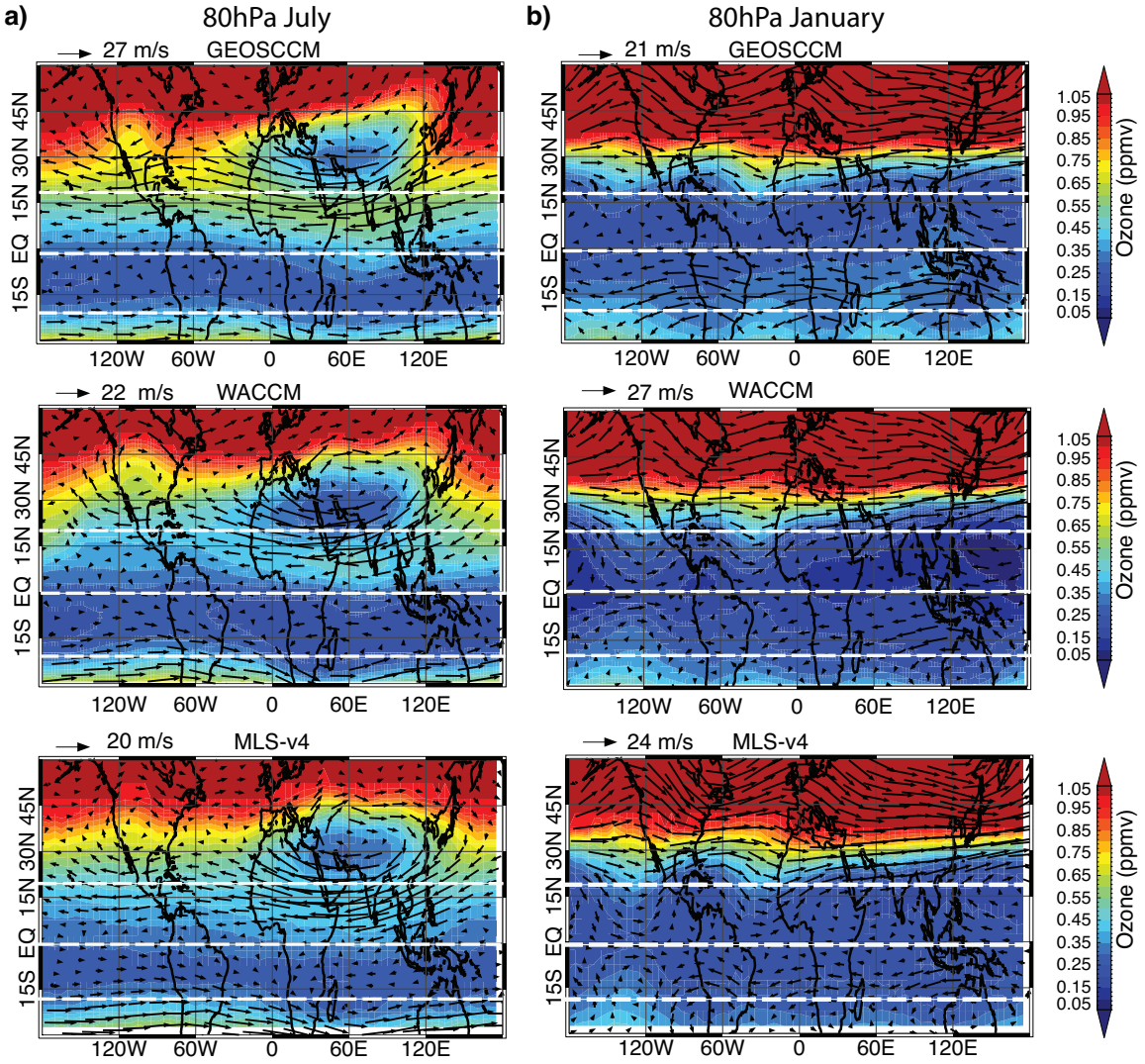

FIGURE 2.8: Maps of climatological ozone and horizontal winds (black vectors) in (a) July and (b) January from GEOSCCM (top), WACCM (middle) and MLS-v4/MERRA-2 (bottom). Ozone and horizontal winds from GEOSCCM and WACCM are shown at 80 hPa, while MERRA-2 winds are averaged over 70 and 100 hPa pressure levels and plotted over 82.5 hPa ozone from MLS. Dashed white lines indicate the boundaries of the northern (EQ-20° N) and southern (EQ-20° S) tropics. Ozone values larger than 1.05 ppmv are shaded in dark red.

ine maps of climatological monthly-mean 80 hPa ozone mixing ratios and horizontal winds for July and January (Figure 2.8). These correspond to the months when the NT-averaged ozone is at its maximum and minimum values, respectively (the ST ozone maximum and minimum occur 1-2 months later). During July, the most distinct non-zonal feature is a region of low ozone centered around 30° N over the Indian subcontinent. Southeast of this, there is a band of higher ozone that penetrates from the extratropical Pacific into the NT (around 60° E). As discussed in previous studies and also shown in Figure 8 by wind vectors from GEOSCCM and WACCM simulations, the low ozone over the Indian sub-continent and mixing of high ozone into the tropics are connected to the ASM anticyclone. [e.g., *Konopka et al.*, 2010; *Randel et al.*, 2007; *Park et al.*, 2007]. There is also transport of ozone rich air to the tropics above North America, identified as weaker than above the Asia anticyclonic circulation (North American monsoon anticyclone). The penetration of ozone rich air by the Asian monsoon anticyclone is larger in GEOSCCM compared to MLS and WACCM and reaches across the equator into the ST.

The strength of these features varies with height. There is lower ozone over the Indian sub-continent and stronger penetration of high ozone into the tropics at 100 hPa in MLS and both simulations, whereas the features are weaker at 70 hPa (not shown). As the influence of monsoons and other disturbances of the tropospheric origin decreases at higher altitudes, so do the zonal differences in ozone seasonal cycle. This is consistent with TEM analysis and the results for the tropical mean balance in *Abalos et al.* [2013b] that showed the decrease with height in the seasonality of ozone tendency due to horizontal mixing.

Monsoon-generated zonal features described above, are also found in other trace gases, such as HCl, N_2O, and CO (not shown). This suggests a large impact of eddy-mixing on the tracer seasonality in NT. The strength of in-mixing and its relative role, however, vary among the tracers and strongly depend on the lower-stratospheric latitudinal gradient of the considered tracer [*Ploeger et al.*, 2012]. For example, water vapor is almost unaffected by the horizontal transport near the tropical tropopause due to the very weak difference in mixing

ratios between tropical and extratropical regions.

In January (Figure 2.8b), there are lower mixing ratios and weaker latitudinal gradients in the tropical ozone than in July for both NT and ST. Furthermore, the zonal variations are also weaker. There are regions of slightly lower equatorial ozone above the central Pacific Ocean (near 170° E) and the continents of South America and Africa (regions of enhanced deep convection). These smaller ozone values coincide with anticyclone circulation within the NT, which isolates the air inside the regions of the anticyclones. There is also penetration of higher ozone into the NT over the eastern Pacific (120° W) and Atlantic (30° W) oceans. Low ozone is likely connected with tropical upwelling over regions of tropical convection, while penetration of high ozone over ocean could be connected with subtropical wave breaking. The strong subtropical jet in winter acts as a barrier for horizontal transport except over the Pacific and Atlantic Oceans where Rossby wave breaking is common [*Waugh and Polvani*, 2000], resulting in high ozone being mixed into the tropics. The differences between the models and observations could be linked to differences in the jet structure and/or in the Rossby waves.

The zonal variations in January and July NT ozone have the potential to cause zonal variations in the annual amplitude. To examine this, we plot in Figure 2.9 the longitudinal variations in the amplitude of the annual cycle (solid curve) together with the variations in the annual minimum (lower dashed) and maximum (upper dashed) values for ozone at 80 hPa from GEOSCCM, WACCM and MLS. As discussed above, the NT seasonal maximum roughly corresponds to the boreal summer and minimum to the boreal winter, while the ST seasonal maximum and minimum are 1-2 months later than in the NT. There are small zonal variations in the annual amplitude in ST ozone (especially in MLS and GEOSCCM), consistent with small zonal variations in ST in Figure 2.8. There are, however, substantial variations in the NT, with the largest annual amplitude occurring around 90-120° E and a secondary maximum around 80° W. There are differences in the magnitude of zonal variations and locations of the peaks between the models and between models and observations,

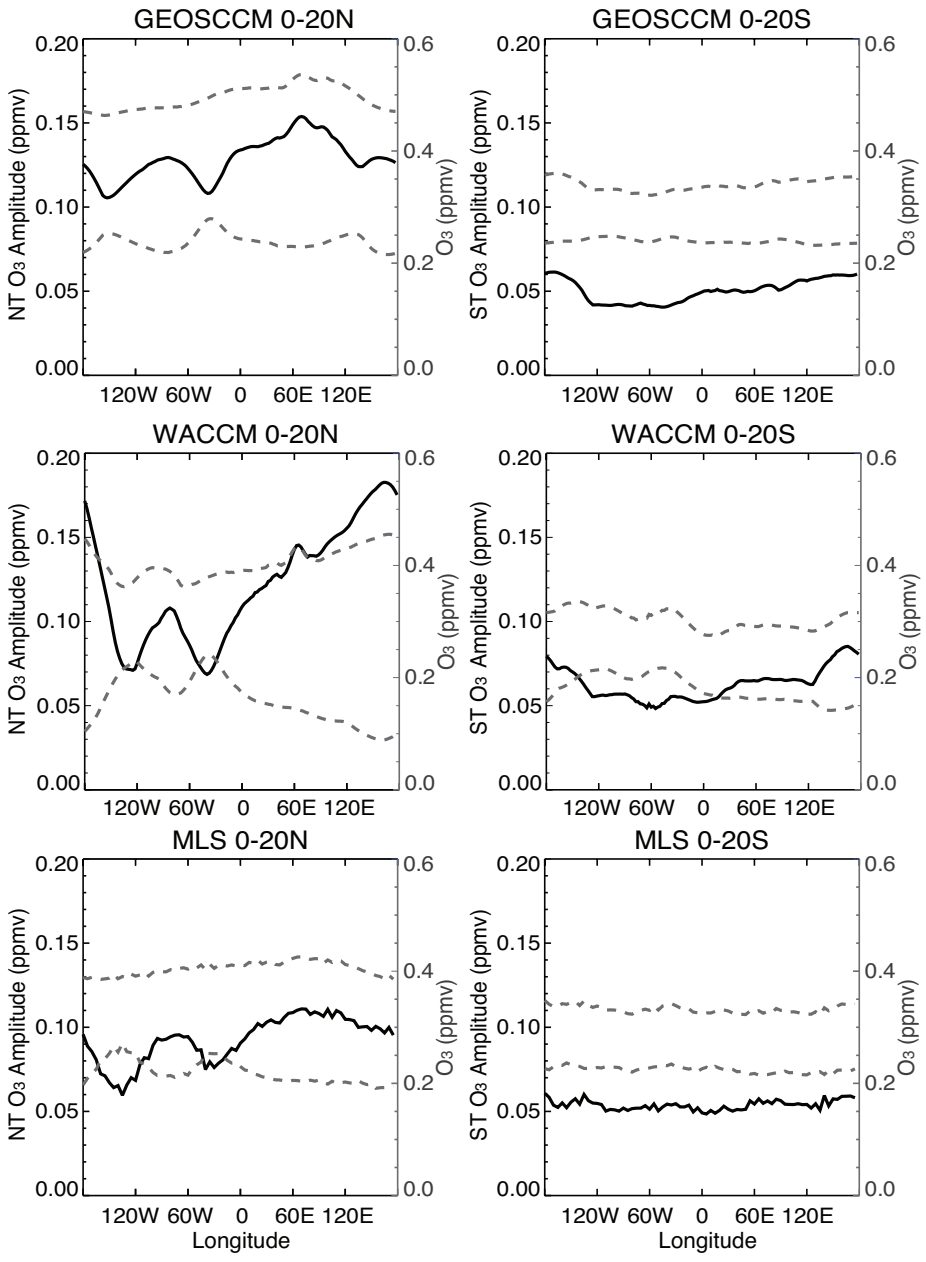

FIGURE 2.9: Zonal variations in the NT (left) and ST (right) annual cycle magnitude (solid black curve) and in maximum (upper dashed gray curve) and minimum (lower dashed gray curve) ozone mixing ratio during the climatological year from GEOSCCM (top), WACCM (middle) and MLS (bottom).

but the same qualitative variation occurs in all three. The maximum around 90-120° E is due primarily to an increase in the NT ozone during annual maximum within this longitude range, and is associated with mixing-in of mid-latitude ozone into the NT due to the Asian summer monsoon anticyclone discussed above (Figure 2.8 left panels). In contrast, the local maximum in the amplitude around 80° W is primarily due to variations in the annual minimum, with larger annual-minimum ozone around 30° W and 150° W. These variations are due to the penetration of higher ozone in NT over the Atlantic and eastern Pacific oceans during NH winter (see above, Figure 2.8 right panels). This wintertime penetration of ozone is stronger in WACCM than in GEOSCCM or MLS.

In summary, the amplitude of the seasonal cycle in ozone varies with longitude, and these variations are due to increased eddy mixing around 90-120° E during summer associated with the Asian monsoon and increased mixing over the Pacific and Atlantic during NH winter. The signal of wintertime mixing is only seen in WACCM TEM analysis in Figure 2.6 as a small increase in ozone tendency due to horizontal transport during winter months (most likely due to stronger wintertime penetration of ozone over the Atlantic and eastern Pacific oceans in WACCM than in GEOSCCM).

2.5 Conclusions

Stolarski et al. [2014] showed that there is a hemispheric difference in the annual cycle of tropical lower stratospheric ozone, with larger amplitude in the NT than in the ST. In this study, we have examined the ability of CCM simulations from CCMVal-2 to reproduce this hemispheric difference and used two of the CCMs to examine the cause. Testing whether CCMs produce the correct spatial structure of tracers' annual cycle is a valuable tool for evaluating the models' performance in the tropical lower stratosphere, as it indicates the correct balance between transport and chemical processes.

Examination of the CCM simulations showed a large variability in the annual cycle of

tropical lower stratospheric O_3. The majority of the CCMs produced the observed feature of a larger annual cycle in the NT than ST, but there are several with similar amplitude in the ST and NT or even with a larger amplitude in the ST. Further, even for models with larger amplitudes in the NT there was a large range in size, with several models showing unrealistically small or large amplitudes. As a result, only around a third of the models produce an ozone annual cycle similar to that observed. A similar analysis of the NT-averaged and ST-averaged amplitude of annual cycle in other long-lived tracers (N_2O, HCl and mean age) shows very similar results, suggesting that the NT-ST contrast in annual amplitude is driven by transport and not chemistry. This indicates that the majority (2/3) of the CCMs have problems in representing transport in the tropical lower stratosphere, which is broadly consistent with previous studies of transport in CCMVal-2 models [e.g., *Strahan et al.*, 2011].

Analysis of the relationship between the vertical transport by the residual circulation and ozone among CCMs provided insights to the cause of the hemispheric differences in the ozone annual cycle. For the ST, the spread in the simulated amplitude of the annual cycle in vertical transport explains most of the spread in the simulated amplitude of the ozone annual cycle, i.e. CCMs with larger annual cycle in ST upwelling tend to have a large annual cycle in ST ozone. In contrast, there is no relationship between the amplitudes of the annual cycle of vertical advection and O_3 for the NT. This indicates that seasonality in upwelling is a major driver of seasonality of ozone in the ST, but other processes (presumably mixing) must be dominating in the NT.

A TEM analysis of WACCM and GEOSCCM simulations provided additional insights to the cause of the hemispheric differences in the annual cycle of ozone and other tracers. We confirmed the importance of seasonality in vertical advection in causing the seasonality in the ST and showed that seasonality of horizontal mixing drives the seasonality in NT O_3 and N_2O. The seasonality of ozone is also influenced by the seasonality of photochemical sources and sinks, which differ between NT and ST, but local chemistry does not play a role in ST-NT contrast in N_2O. As discussed in previous studies [*Konopka et al.*, 2010; **?**; *Park*

et al., 2007], enhanced horizontal mixing during boreal summer is primarily associated with the ASM anticyclone causing an increase in NT ozone (and a decrease in NT N_2O).

CHAPTER 3

The impact of boreal summer ENSO events on interannual variability of tropical lower stratospheric ozone

The work contained in this chapter is based upon *Tweedy et al.* (2018), submitted to *Journal of Geophysical Research*.

3.1 Introduction

In Chapter 2 we focused on seasonal climatological composition and transport, but the TLS ozone also varies on interannual scales and near the tropical tropopause ENSO dominates this variability [*Randel et al.*, 2009; *Calvo et al.*, 2010; *Oman et al.*, 2013]. As an example, the interannual variability of MLS O_3 at 100 hPa (a level that is near the tropical tropopause) is shown in Figure 3.1a for NT and ST separately. The high correlation of NT and ST ozone anomalies strongly suggests that observed variations are driven by the uniform changes in upwelling, linked to variations in SSTs in the equatorial Pacific (ENSO events) [*Calvo et al.*, 2010; *Oman et al.*, 2013] (See Section 1.2). However, this mechanism does not explain differences between NT and ST O_3 during 2015 boreal summer (the only strong El Niño

event during northern summer in the MLS record (2004 -present)). The short record of MLS ozone does not allow determining if these differences in NT and ST ozone are due to random noise, instrument errors or some real physical mechanisms. However, longer time series of ozone are available from model simulations, and these show similar ozone anomalies that, as in 2015, occur during boreal summers with strong positive SST anomalies in the equatorial Pacific (Figure 3.1b).

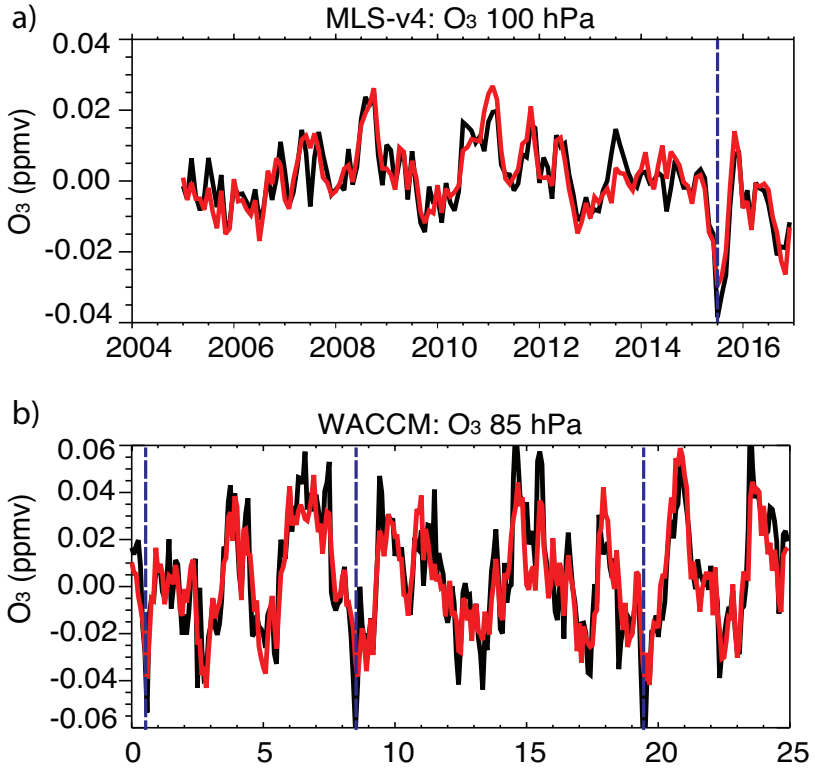

FIGURE 3.1: Deseasonalized monthly anomalies of O_3 (a) at 100 hPa from MLS and (b) at 85 hPa from WACCM simulation with coupled oceans (only 25 years are shown), averaged over the northern tropics (EQ-18° N, black) and southern tropics (EQ-18° S, red). Blue dashed lines indicate strong El Niño events during boreal summers.

In this chapter, we examine O_3 transport from model simulations over interannual time scales and compare them to data and reanalysis. In particular, we explore how SSTs in the tropical Pacific modify transport processes and thus distribution of ozone in this region. In the next section we briefly describe the model, data and methodology. ENSO related interannual variability and the influence of ENSO on ozone seasonality are examined in

section 3.3.1. In sections 3.3.2 and 3.3.3, we evaluate ozone transport and explore the causes of ozone variability in the TLS. Discussion of results and conclusions are in section 3.4.

3.2 Model, data and methodology

3.2.1 Model simulations and data

In this study we examine the response of the TLS ozone to boreal summer ENSO in version 4 of the Whole Atmosphere Community Climate Model (WACCM) [*Garcia et al.*, 2007; *Marsh et al.*, 2013; *Garcia et al.*, 2016]. WACCM includes an interactive atmospheric chemistry package and is coupled to the ocean, land, and sea ice components of the Community Earth System Model version 1. We use version of the model that self-consistently develop SST anomalies (as opposed to WACCM simulations with prescribed historical SSTs), teleconnections between ocean and atmosphere and allows us to examine the stratospheric response to a larger number of ENSO events than have occurred in the historical record. The WACCM simulation has horizontal resolution of 1.9° latitude by 2.5° longitude, 66 vertical levels (from surface to near 140 km) and vertical resolution around 1.2-1.4 km near the tropopause and in the lower stratosphere. We analyze a simulation from 1960 to 2100 where GHGs, tropospheric ozone precursors and aerosol emissions follow the Representative Concentration Pathway (RCP) 6.0 and ozone depleting substances follow the World Meteorological Organization (WMO) A1 scenario [*Meinshausen et al.,* 2011]. *Abalos et al.* [2013b] showed that the simulated annual cycle in ozone and temperature in WACCM agrees well with satellite observations in the TLS. Furthermore, *Tweedy et al.* [2017a] showed that WACCM simulations capture the observed larger amplitude of the seasonal cycle in the lower stratospheric ozone in the NT than in the ST, which indicates that it also captures the inter-hemispheric differences in TLS transport processes.

The ozone of the coupled model simulation is compared with measurements from the Microwave Limb Sounder (MLS) on board the Aura satellite. The MLS data provide hori-

zontal, vertical and temporal coverage suitable for examining seasonal changes in O_3, while the continuous record over 13 years allows characterizing interannual variations. We use Version 4.2 MLS level 2 data at 100 hPa to construct a monthly mean data set for January 2005 through 2017. The data is binned into 2.5° latitude by 5° longitude grid, using the recommended quality and convergence thresholds [*Livesey et al.*, 2015].

Meteorological fields are from Modern-Era Retrospective analysis for Research and Applications (MERRA-2). MERRA-2 is the latest atmospheric reanalysis of the modern satellite era produced by NASA's Global Modeling and Assimilation Office (GMAO) and is available for 37 years (1980 - present) [*Bosilovich et al.*, 2015]. A detailed overview of MERRA-2, including a description of the data assimilation system and various measures of performance can be found in *Gelaro et al.* [2017].

SST data is from the Met Office Hadley Centre's sea ice and Sea Surface Temperature data set, HadISST. The HadISST dataset combines monthly-mean fields of SST and sea ice concentration on a 1-degree latitude-longitude grid from 1850 to date. In this study we use SST fields from 1980 to 2017. For a detailed description of the dataset and its production process, see *Rayner et al.* [2003].

3.2.2 Methodology

In this study we primarily focus on ozone that is near the cold point tropopause. At this level the ASM impact on ozone distribution during boreal summer is expected to be the strongest. As the tropopause is higher in WACCM than in observations (shown in *Abalos et al.* [2013b], we examine ozone at 85 hPa in the model and at 100 hPa in observations. For both WACCM and observations we calculate NT and ST ozone as area averages between EQ - 18° N and EQ - 18° S.

ENSO events in observations are identified based on SST anomalies averaged over the Niño34 region (5°N to 5°S, from 170°W to 120°W) that are above a specified threshold. SST

fields are not available for WACCM simulation, and surface air temperatures (SATs) are used instead to calculate the ENSO index. Although SATs and SSTs are not exactly the same, their variability is very similar (i.e., the explained variance between SSTs and SATs from WACCM simulations with prescribed SSTs is 99% (not shown)). SST and SAT anomalies are calculated by removing long-term linear trend and seasonal cycle. Our main focus is on warm-season ENSO events, and strong El Niño and La Niña events in WACCM are identified when May-June (MJ) SAT anomalies in the Niño34 region exceed +1K and -1K respectively.

In Section 3.2 a Transformed Eulerian Mean (TEM) tracer budget analysis (Eq. 9.4.13 in *Andrews et al.* [1987] is used to quantify the relative role of different transport processes and chemical production and loss in causing changes in ozone, i.e.

$$\frac{\partial \overline{O_3}}{\partial t} = -\overline{v^*}\frac{\partial \overline{O_3}}{\partial y} - \overline{w^*}\frac{\partial \overline{O_3}}{\partial z} + \frac{1}{Cos\phi}e^{z/H}\frac{\partial (M_y Cos\phi)}{\partial y} + P - L \tag{3.1}$$

where $(\overline{v^*},\overline{w^*})$ are the meridional and vertical components of the residual circulation, $P-L$ is the chemical production minus loss rate, and M_y is the horizontal component of eddy transport vector, calculated as $M_y \equiv -e^{-z/H}(\overline{v'O_3'} - \frac{\partial \overline{O_3}}{\partial z}\overline{v'T'}/S)$. The small vertical eddy term is neglected because not all fields were available as daily outputs for these runs. The first two terms on the right-hand side correspond to vertical and horizontal advection, which reduce trace gas concentration in the tropics when the residual circulation and ozone gradients are both positive. In other words, increased upwelling transports ozone-poor air from the tropopause to the TLS while poleward (positive in the NH) meridional transport moves low in ozone tropical air into the northern subtropics.

3.3 Results

3.3.1 *Hemispheric asymmetries in the tropical ozone interannual variability*

Previous studies by *Stolarski et al.* [2014] and *Tweedy et al.* [2017a] showed that annual cycle amplitude in ozone is different between NT and ST due to hemispheric differences in transport processes; however, interannual variability in the NT and ST ozone in the TLS was not examined. To explore this interannual variability we examine deseasonalized ozone anomalies from WACCM simulation for NT and ST separately and also distinguish between boreal summer (JJA) and winter (DJF) months. Figure 3.2 shows that the NT ozone anomalies during JJA are larger than corresponding anomalies averaged over the ST as well as both NT and ST ozone anomalies during DJF. This is suggestive of different mechanisms controlling NH summertime ozone variability in the NT.

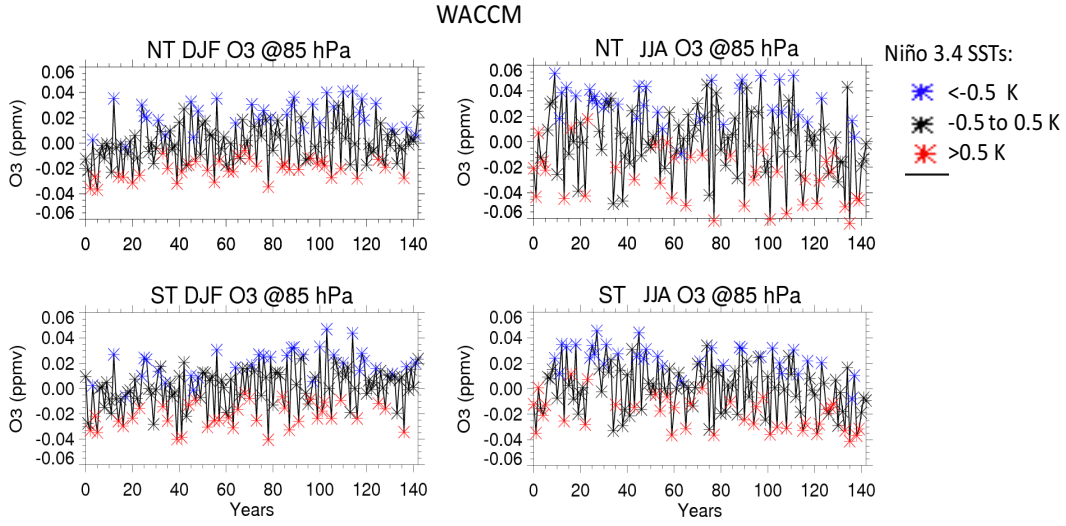

FIGURE 3.2: Deseasonalized ozone anomalies at 85hPa from the WACCM simulation averaged over the NT(top) and ST (bottom) and over the winter (DJF) and summer (JJA) months. Colored symbols are Niño34 SST anomalies larger/smaller than +0.5 K/-0.5 K (red and blue respectively) 1-month prior to ozone values.

The ozone anomalies shown in Figure 3.2 have a strong relationship with SATs in

the equatorial Pacific (Niño34 region in particular). Years when the SAT anomalies in the Niño34 region are larger (smaller) than +0.5K (-0.5K) (El Niño and La Niña events respectively) are shown by red (blue) stars. There is a distinct separation of colors for both NT and ST ozone and during both seasons. Blue stars (cold La Niña events) are collocated with high O_3 anomalies and red stars (warm El Niño events) with low O_3 anomalies, demonstrating a strong negative correlation between ozone and Niño34 index.

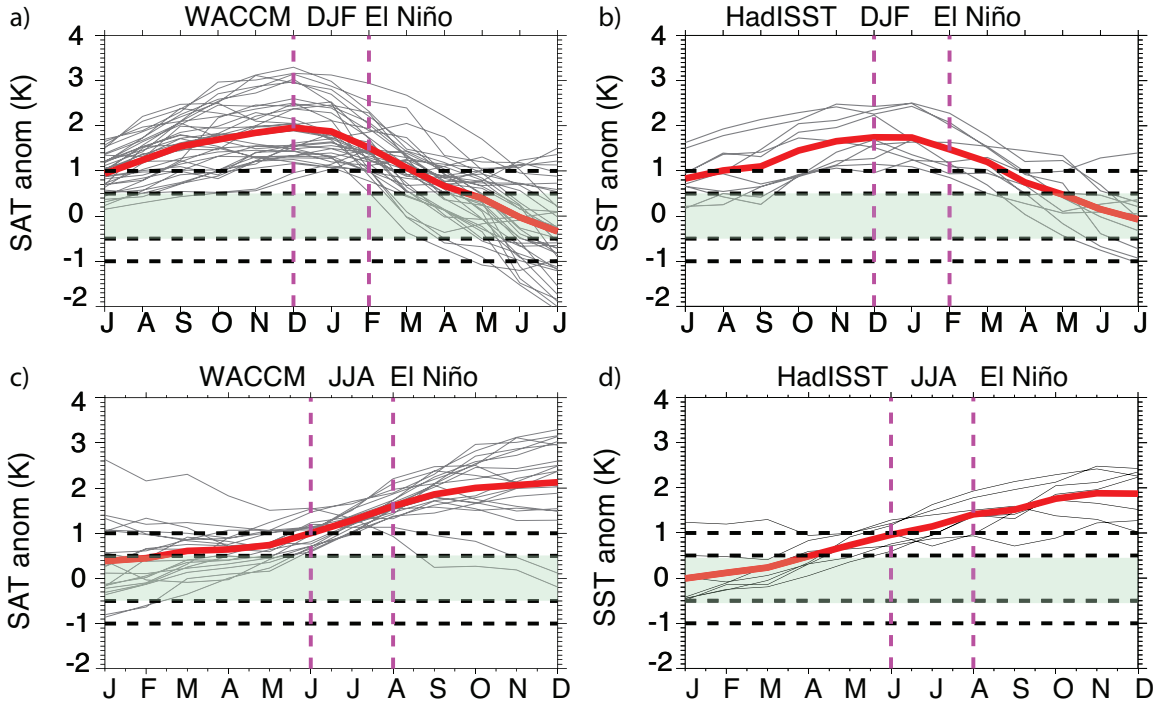

FIGURE 3.3: Seasonal evolution of detrended and deseasonalized SAT and SST anomalies over the Niño34 region (5° N-5° S; 120° W- 170° W) from the WACCM simulation and HadISST dataset averaged, for (a, b) DJF El Niño events and (c, d) JJA El Niño events. Black curves show all years in WACCM or observations when (a, b) the DJF SAT/SST anomalies are greater than +1 K or (c,d) when JJA anomalies are greater than +1 K for WACCM or +0.8 K for HadISST. Thick red contour is an average of all events. Green shading highlights ENSO neutral conditions (between −0.5 and +0.5 K) with horizontal dashed lines indicating boundaries of weak and strong ENSO events (+/− 0.5 and +/− 1 K).

To evaluate how realistic ENSO events are in the model, we compare seasonal evolution (i.e., build up and decay) of El Niño events from WACCM and the HadISST dataset, for DJF (Figure 3.3a and 3.3b) and JJA events (Figure 3.3c and 3.3d). This shows that WACCM generates realistic DJF and JJA El Niño events, with seasonal evolution in a good agreement with observations. In both the model and observations, the DJF El Niño events start to

develop during late-spring and early-summer, peak during boreal winter and rapidly decay after DJF with SST anomalies becoming neutral during late boreal spring and summer. In contrast, the majority of JJA ENSO events are developing El Niño that will become mature during following winter. While El Niño events during the boreal summer are weaker and less frequent than during boreal winter, in both WACCM and observations, there is still a large number of years with summer SST anomalies exceeding +1 K. Similar results but opposite in magnitude hold for La Niña events (not shown).

Other studies have also showed that WACCM reproduces the key features of SST anomalies associated with ENSO [*Jian and Rong-Cai*, 2014; *Kim and Yu*, 2012; *Yang and Giese*, 2013]. *Marsh et al.* [2013] showed that WACCM reproduces well the periodicity in the Nino34 index but overestimates the amplitude of ENSO events, as can also be seen in Figure 3.3a-b. *Jian and Rong-Cai* [2014] evaluated statistical characteristics of ENSO events from 24 Coupled Model Intercomparison Project Phase 5 (CMIP5) models and showed that WACCM can successfully reproduce the relatively higher frequency of cold-season-matured ENSO events (peak phase in the boreal winter, DJF) than warm-season-matured events (peak phase in the boreal summer, JJA). In their study, the composite intensity of El Niño and La Niña for WACCM is comparable to ERSST dataset and overall WACCM performs above average compared to other CMIP5 models.

As the observed ENSO tends to be strongest during boreal winters, previous studies have focused primarily on cold-season-matured ENSO events and their influence on TLS composition during boreal winter and spring. However, Figure 3.2 shows that simulated ozone anomalies in the NT are largest during boreal summer. To isolate ozone variability during summer and the strength of the relationship of this variability with SSTs, we examine the regression and correlation coefficients of JJA ozone anomalies with the Niño34 index for different months, see Figures 3.4a-b. This shows large (negative) regression and correlation coefficients in tropical ozone with summer SAT anomalies (i.e., correlations less than -0.6 for May - June) but low values for SAT anomalies from the preceding winter (correlations near

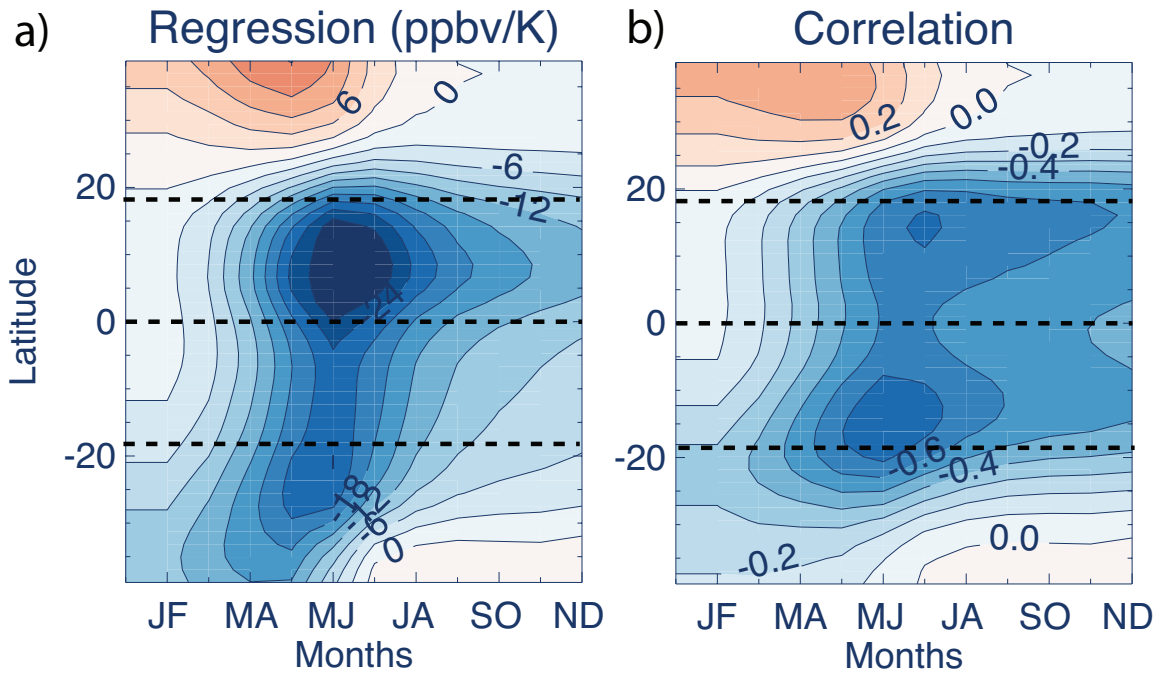

FIGURE 3.4: (a) Regression (in ppbv/K) and (b) correlation of JJA deseasonalized ozone anomalies from the WACCM simulation at 85hPa with 2-month running average of Niño34 index. Dashed horizontal lines indicate 18°N, equator and 18°S

0 for months January - February). Thus, ozone anomalies during JJA have the strongest sensitivity to the SST changes during MJ, and the sensitivity rapidly decreases towards the winter indicating weak influence of boreal winter ENSO on summertime ozone.

The decrease in tropical ozone during boreal summer El Niño events has a large impact on ozone annual cycle amplitude. Figure 3.5a and 3.5e shows El Niño and La Niña composites of ozone seasonality based on Niño34 index during MJ, for NT and ST respectively. The annual cycle amplitude in ozone is larger during La Niña (green) than El Niño (purple). Furthermore, in agreement with *Stolarski et al.* [2014] and *Tweedy et al.* [2017a], ozone seasonality is larger in the NT than in the ST for both ENSO composites. The differences between ENSO composites are largest during JJ in the NT and JA in the ST.

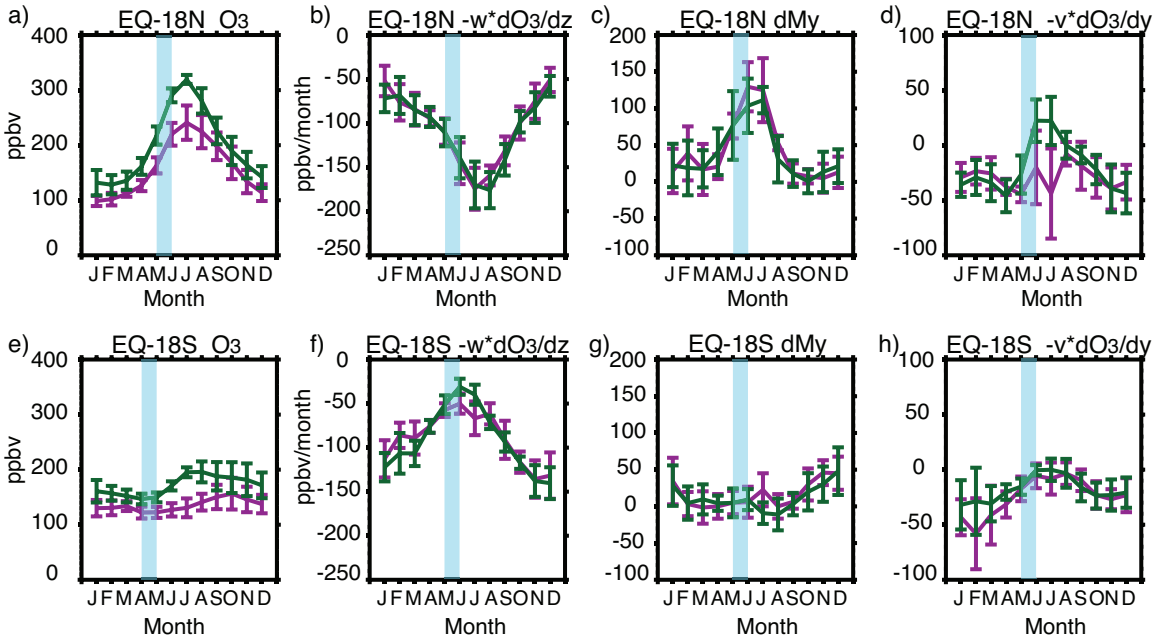

FIGURE 3.5: El Niño (purple) and La Niño (green) composites of a) ozone annual cycle, b) vertical advection, c) horizontal mixing, and d) horizontal advection averaged over the NT (EQ-18°N, top) and ST (EQ-18°S, bottom) from the WACCM simulation. Composites are based on Niño34 index during May and June indicated by blue shading. Units are ppbv/month

3.3.2 ENSO related variability in transport.

The local change in ozone concentration due to transport processes and chemical sources and sinks are quantified by the TEM continuity equation (Equation 3.1). ENSO composites of the ozone seasonal cycle and its major transport terms (upwelling, horizontal mixing and meridional advection), are shown in Figure 3.5 for the NT (Panels b - d) and ST (Panels f-h). In the NT, there is a clear difference for ozone in El Niño and La Niña composites during summer, primarily attributable to differences in horizontal advection during JJ. During this period there is a positive tendency during La Niña but a negative tendency during El Niño. In the ST, the differences in the JA ozone are mostly due to differences in upwelling during JJ with 1-sigma uncertainty bars only slightly overlapping between two composites. Note that enhanced mixing during boreal summer in the NT is a major contributor to larger climatological seasonal cycle amplitude in the NT than ST ozone; however, interannual variability of the NT summertime ozone is dominated by variations in meridional advection.

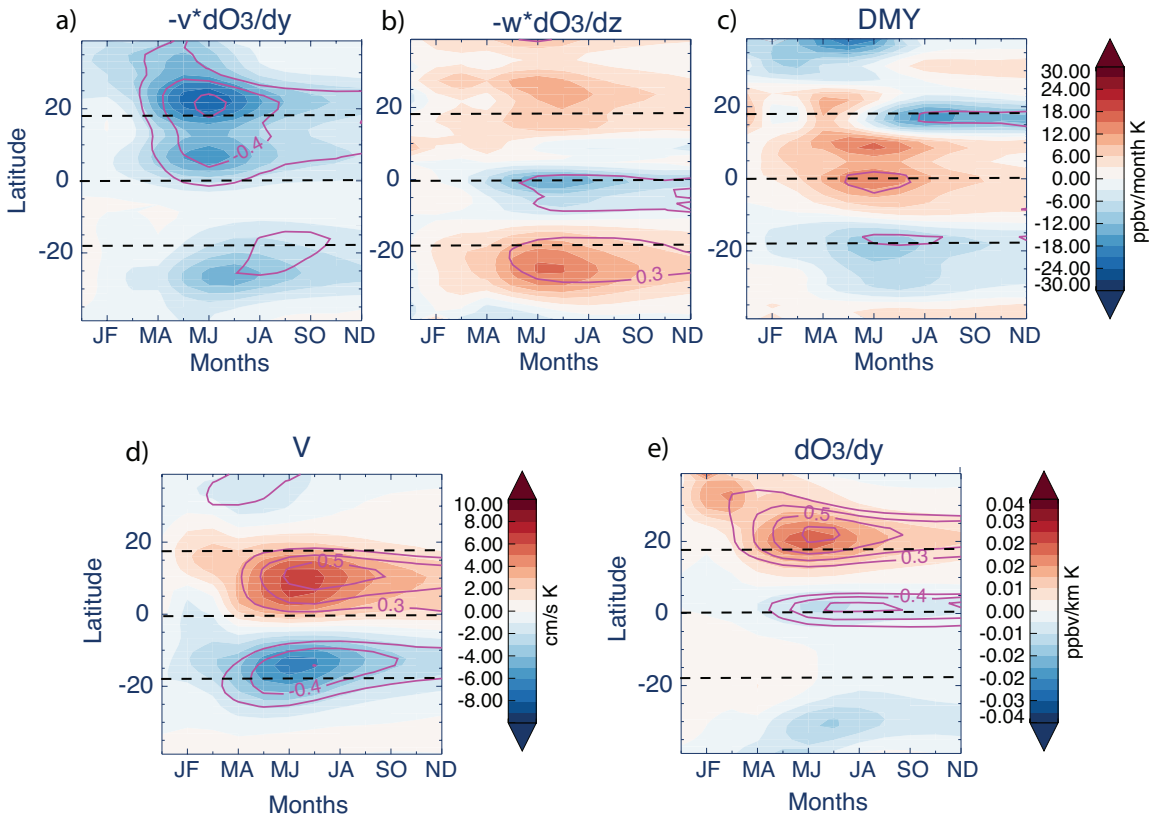

FIGURE 3.6: Regression (filled contours) and correlation (magenta) of a) meridional advection, b) upwelling, c) horizontal mixing and (d-e) meridional velocity and horizontal ozone gradients during JJA at 85hPa with 2-mo running average of Niño34 SAT anomalies.

The above conclusions are also supported by regression and correlation analysis of JJA TEM transport terms at 85 hPa with the ENSO index (Figure 3.6a-c). In agreement with Figure 3.5, horizontal advection is a dominant term in the NT, with enhanced negative sensitivity and correlation (coefficients are smaller than -0.4) with Niño34 index during late spring and early summer. Vertical advection and horizontal mixing have weak negative and positive sensitivities in the NT with Niño34 index respectively, with the magnitude of their correlation coefficients less than 0.3 almost everywhere. In the ST, the upwelling term has the strongest sensitivity to the changes in SAT anomalies during the summer with correlation coefficients below -0.3. These results are consistent with larger annual cycle amplitude during MJ La Niña than El Niño. Thus, interannual variability in the NT summertime ozone is dominated by changes in horizontal advection, while ENSO-related changes in the

upwelling dominate the ST ozone variability.

The pronounced negative peak in the horizontal advection in the NT is due to two factors. First, meridional velocities (v^* and also v in general) are more positive during boreal summer El Niño than La Niña events Figure 3.6d), indicating weaker inflow of subtropical air into the NT during El Niño. Second, the maximum in ozone meridional gradient during boreal summer is located further northward in the NT during El Niño (Figure 3.6e). Both factors contribute to the reduction (increase) in the NT ozone during warm -season El Niño (La Niña) and, therefore, a smaller (larger) annual cycle amplitude.

Not all terms in the TEM continuity equation are shown in Figure 3.5 and Figure 3.6. The net P-L is nearly identical between El Niño and La Niña cases and therefore not shown. Vertical eddy mixing terms are not available for this simulation but assumed to be a smaller contribution in the TLS [*Abalos et al.*, 2013b; *Tweedy et al.*, 2017a]. Given the relatively small differences in ozone between El Niño and La Niña cases, absence of this term provides additional uncertainty in our calculations. Additional errors also could be due to use of daily data instead of smaller time steps (6-houly or 4-hourly) to calculate horizontal eddy term. Nevertheless, the TEM analysis provides valuable insights into the nature of processes that cause ozone changes in the TLS. The boreal summer ENSO alters the meridional advection in the northern tropics and subtropics leading to larger variability in the NT summertime ozone, while in the ST the ozone variability is dominated by changes in upwelling related to ENSO.

3.3.3 Zonal variations: role of the Asian summer monsoon anticyclone

The analysis in the previous sections has focused on zonally averaged characteristics of ozone and transport. However, the NH summertime ozone transport in the TLS has large zonal variations that need to be considered. A major cause of these zonal variations is the ASM anticyclone. We now examine ENSO-related differences in the horizontal structure of ozone

and winds.

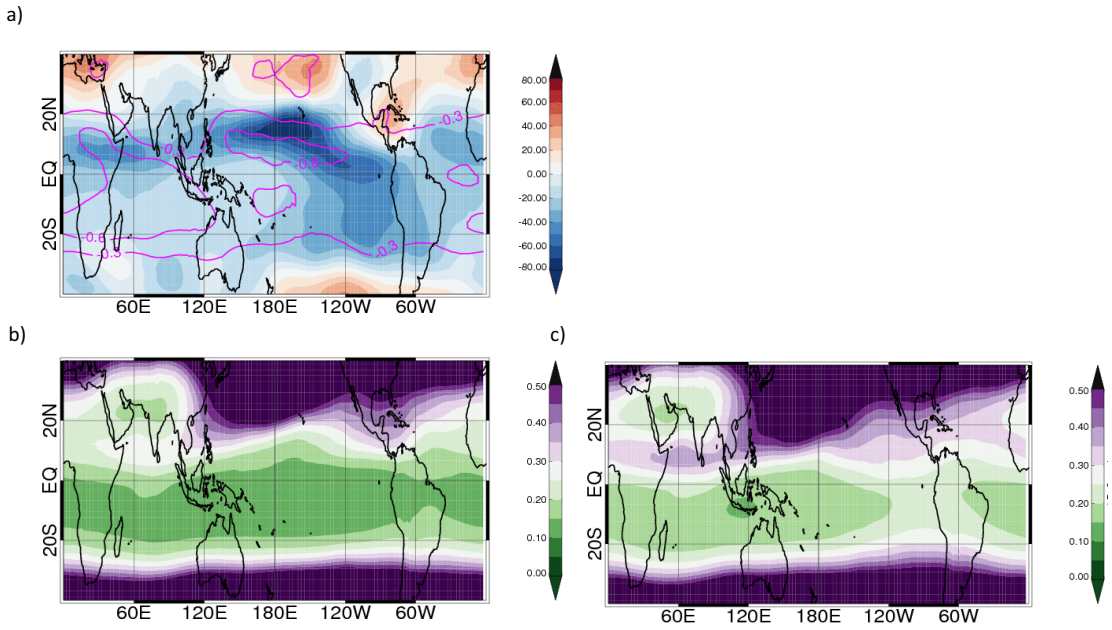

FIGURE 3.7: (a) Regression (color) and correlation (magenta) of JJA deseasonalized ozone anomalies with MJ Niño34 index from the WACCM simulation. Correlation coefficients that are between -0.3 and 0.3 are not shown. (b) El Niño and (c) La Niño composites of ozone during JJA based on Niño34 index in MJ. Units are ppbv/K in (a) and ppm in (b) and (c)

Figure 3.7a shows a map of the regression (shaded) and correlation (contours) coefficient of JJA ozone anomalies at 85 hPa with MJ Niño34 SAT anomalies. A strong negative correlation with the Niño34 index throughout the tropics (18° N-18° S) indicates that overall ozone is smaller following El Niño than La Niña (consistent with Figure 5a and 5e). However, the regression coefficients are larger (more negative) in the NT than in the ST with the largest magnitude above the tropical Pacific Ocean (120° E-120° W) and Africa - northern Indian Ocean sector (20° E-70° E).

Analysis of ENSO composites for JJA ozone shows a stronger inflow of ozone rich air deep into the NT during La Niña than El Niño events (compare Figure 3.7b and Figure 3.7c). This is in contrast with *Yan et al.* [2018] who showed almost no difference in ozone fields during boreal summer (JJA) when compositing on wintertime (DJF) ENSO index (see their Figure 7). See Section 4.4 for further comparisons with *Yan et al.* [2018].

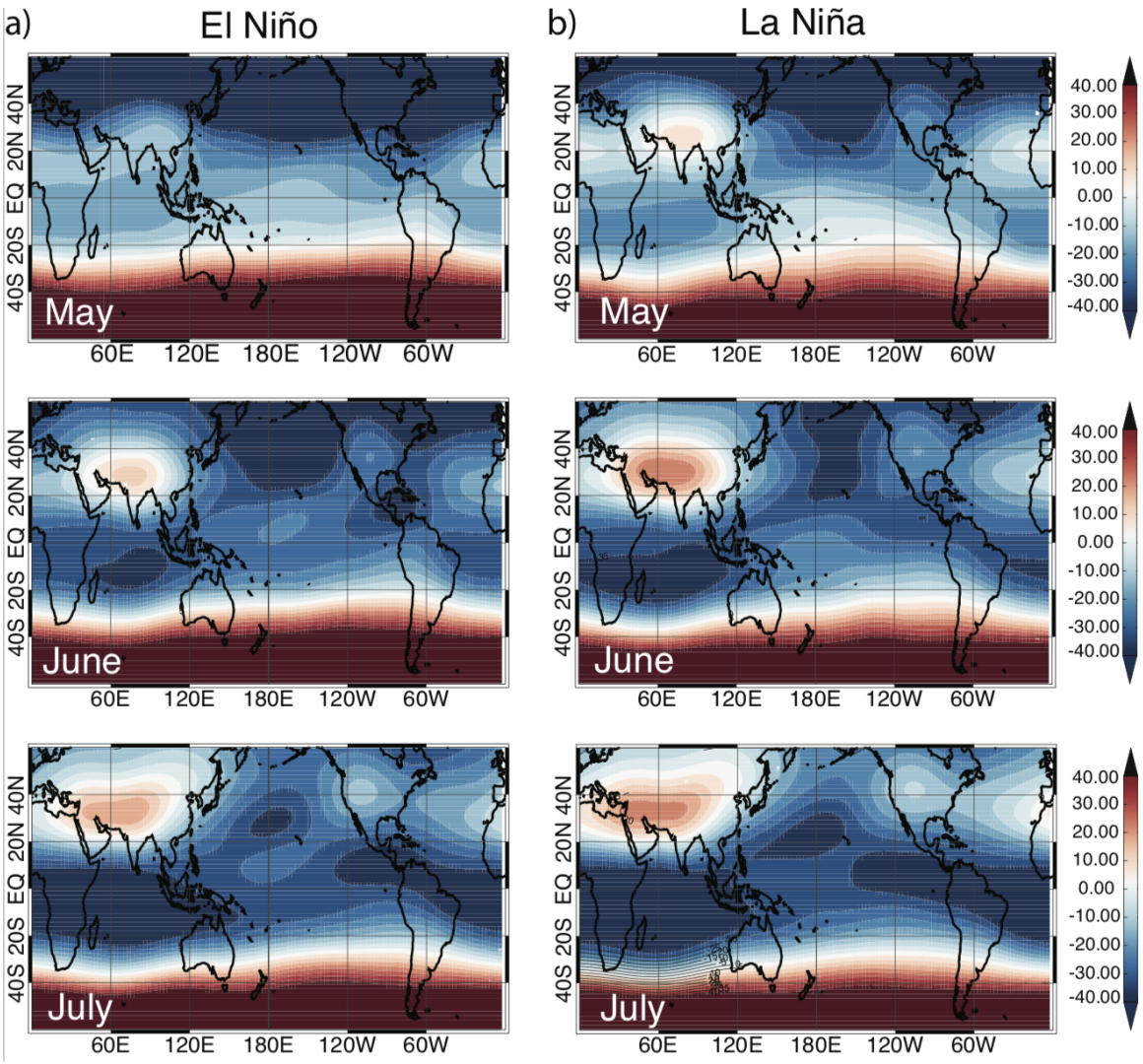

FIGURE 3.8: a) El Niño and b) La Niña composites of stream function at 85 hPa from WACCM based on Niño34 index (+/- 1K) for the same month during May (top), June (middle) and July (bottom). Unites are 10^6 $m^2 s^{-1}$

The geographical distribution of ENSO-related anomalies in ozone fields strongly suggests an important role of the ASM anticyclone in ozone transport. As stated in the Introduction, the ASM can impact transport of chemical constituents by either horizontal advection or isentropic mixing. The TEM analysis indicates that horizontal advection is the dominant cause of differences in ozone in the NT between El Niño and La Niña cases during boreal summer. To examine this further we analyze composites of the stream function for warm-season El Niño (Figure 3.8a) and La Niña (Figure 3.8b) events. We composite 85 hPa stream function based on Niño34 index for May, June and July separately. In May, the ASM anti-

cyclone during El Niño is not fully developed but during La Niña the anticyclone is already formed as indicated by circular enclosed contours and positive values of stream function above Asia. The anticyclone is fully formed in June but remains much weaker during El Niño than La Niña years. In July, the ASM is still weaker during El Niño but the difference between two composites is smaller. These results are in agreement with previous studies that examined the impact of warm-season ENSO on the onset date and strength of the ASM [*Webster and Yang*, 1992; *Ju and Slingo*, 1995]. *Webster and Yang* [1992] shows a variation of 25 days between the weak, late monsoon of 1987 (strong El Niño conditions) compared with the strong, early monsoon of 1986 and also suggested that the biggest differences in the strength of the monsoon flow occur during the onset (May and early June) and the mature stages of the monsoon development (June and July).

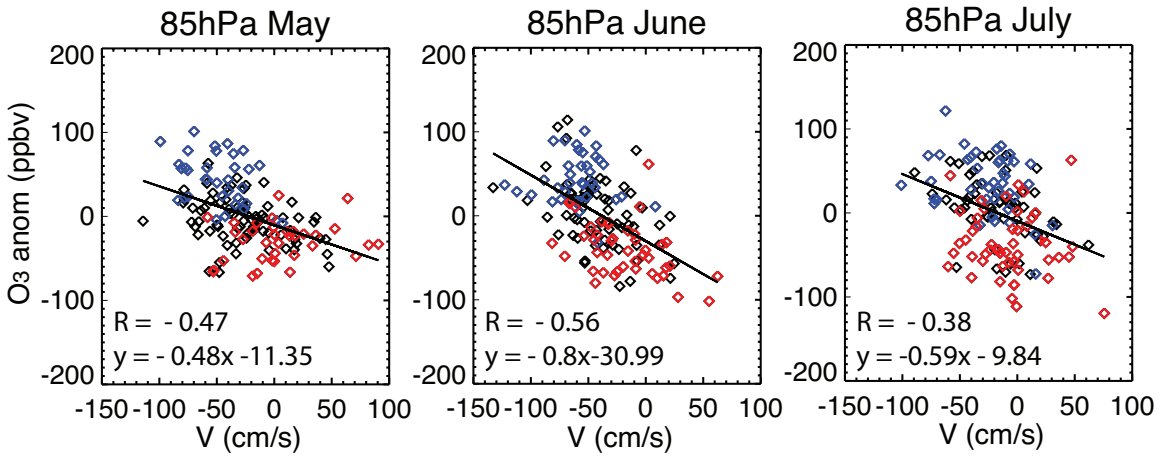

FIGURE 3.9: Relationship between 85 hPa ozone anomalies and meridional velocity (v) for 144 years in WACCM simulation in (a) May, (b) June, and (c) July. O_3 and v are averaged over the northern Pacific Ocean (EQ -18° N and 120° E- 120° W). Years with SST anomalies greater (smaller) than +0.5 K (-0.5 K) in Niño34 region are shown in red (blue). Black line shows the linear regression between ozone and v, with Pearson linear correlation coefficient (R) and equation of linear regression line in the bottom left corner of each panel

The equatorward meridional winds in the NT Pacific (120°E - 120°W) are weaker (stronger) during El Niño (La Niña) in May and June leading to lower (higher) ozone in this region (also seen as stronger negative regression between 120°E and 120°W in Figure 3.7a). This negative relationship between the simulated v and O_3 anomalies at 85 hPa is demonstrated in Figure 3.9 from May to July, showing more O_3 when equatorward flow is stronger. This re-

lationship is strongest during June. During La Niña years (blue symbols), ozone anomalies and v are overall larger than during El Niño years (red symbols). This is consistent with zonal-mean TEM analysis showing stronger meridional advective transport of ozone into the NT during La Niña than El Niño.

Table 1. Nino3.4 index larger and smaller than +/-0.8 K since 1980 for May to August from HadISST dataset. Warm SST anomalies (El Niño events) are in red, cold anomalies are in blue (La Niña events) and values that are between -0.8 and 0.8 K are in black. Last raw indicates total number of El Niño (EL) and La Niña (LA) for corresponding month

Year	May	June	July	August
1982	0.65	0.92	0.64	0.93
1983	1.12	0.62	-0.11	-0.13
1984	-0.60	-0.90	-0.40	-0.44
1985	-0.90	-0.76	-0.61	-0.49
1987	0.91	1.24	1.34	1.48
1988	-1.05	-1.46	-1.54	-1.44
1989	-0.80	-0.64	-0.47	-0.58
1992	1.27	0.53	0.27	-0.15
1993	0.93	0.64	0.33	0.16
1997	0.87	1.15	1.60	1.94
1998	0.68	-0.39	-0.73	-0.83
1999	-0.87	-0.95	-0.84	-0.98
2000	-0.80	-0.75	-0.57	-0.36
2010	-0.15	-0.62	-0.89	-1.33
2015	1.04	1.28	1.56	1.87
#EL/LA	6/5	4/3	3/3	4/4

Testing the above results in observations is difficult given the short data record for MERRA-2. The number of strong El Niño (La Niña) events that are larger (smaller) than +0.8 K (-0.8 K) since 1980 in MERRA-2 reanalysis is 6 (5) in May, 4 (3) in June and only 3 (3) in July, see Table 1. However, despite the limited number of cases with strong ENSO events during late boreal spring and summer, the El Niño and La Niña composites of the stream function calculated from MERRA-2 winds at 100 hPa Figure 3.10) agree well with WACCM results (Figure 3.8) and conclusions made above. The ASM anticyclone in MERRA-2 forms

later and is weaker during boreal summer El Niño events.

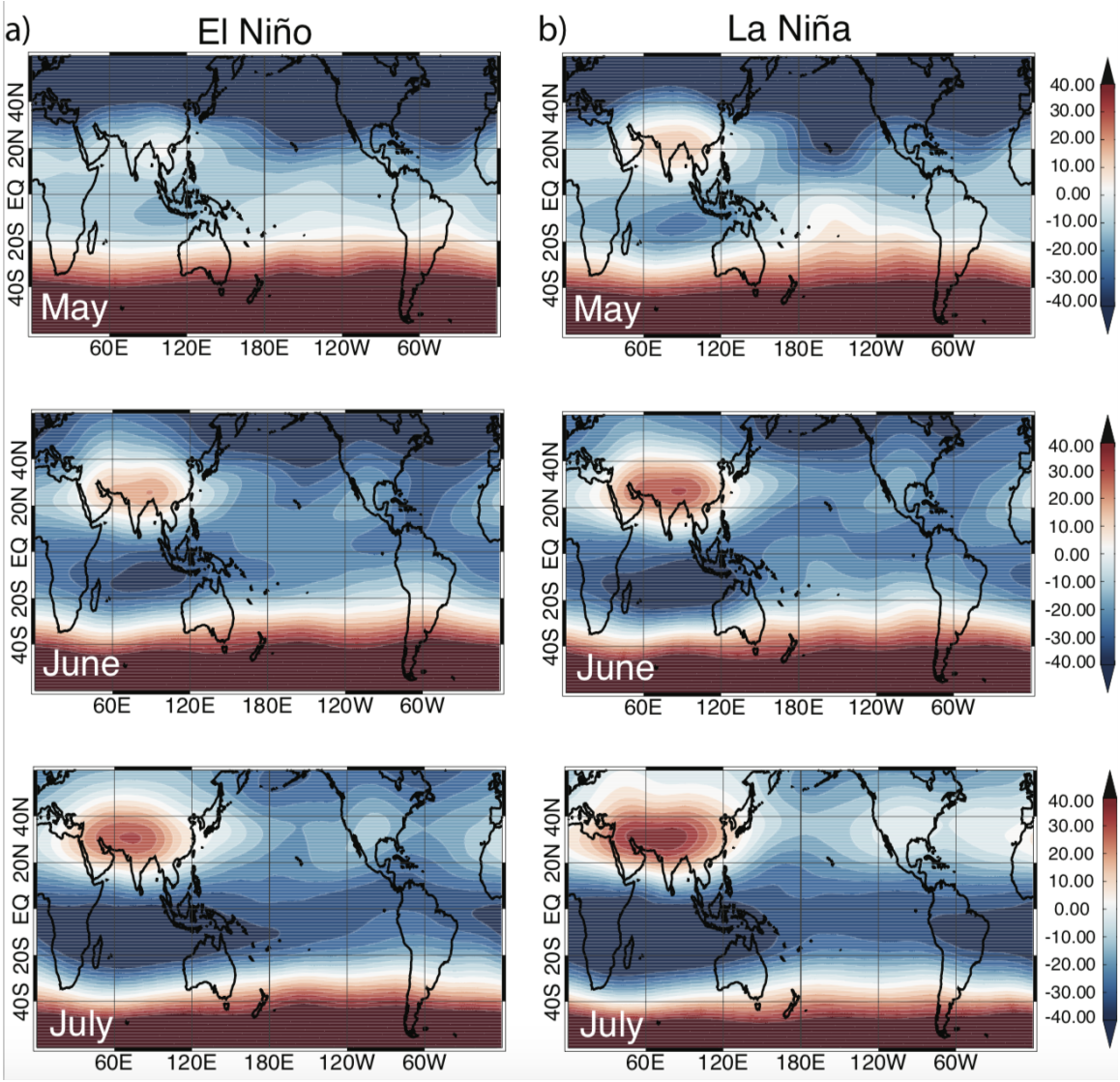

FIGURE 3.10: The same as in Figure 10 only from MERRA-2 at 100 hPa. Composites are based on Niño34 index (+/- 0.8K) for the same month. Number of cases in the composites are 6 in May, 4 in June and 3 in July

Examination of the interannual variability in ozone and ozone transport using observations is even more complicated as there is an even shorter MLS data record. There has been only one strong El Niño (2015) and one La Niña (2010) event occurring during boreal summer since 2004. In 2015, the Niño34 SST anomalies were already above +1 K during late spring and they reached +1.8 K by August. In 2010, Niño34 SST anomalies were -0.6 K

in June, -0.9 K in July and -1.3 K in August. Therefore, in Figure 3.11a and 3.11b we show June-August averaged ozone from MLS at 100 hPa during 2015 (El Niño) and 2010 (La Niña) respectively. Ozone values in 2015 are smaller on average than in 2010 throughout most of the tropics. There is also stronger ozone inflow into the NT during 2010 at the Eastern flank of the anticyclone. Differences in the NT ozone between El Niño and La Niña cases are in good agreement with the strength of the monsoon anticyclone (e.g., in 2010 monsoonal flow is stronger than in 2015, see Figure 3.11c-d)

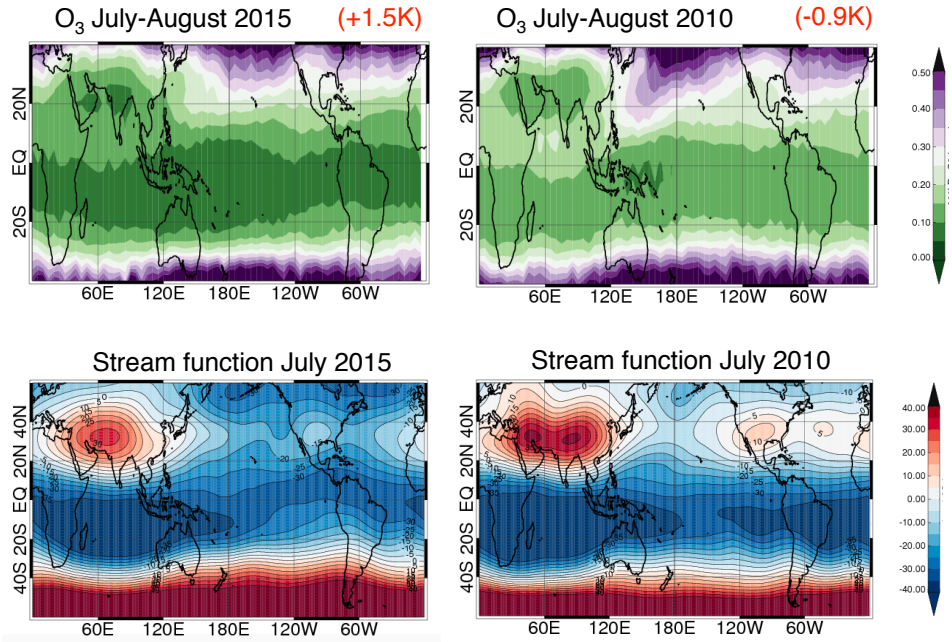

FIGURE 3.11: (Top) 2015 (El Niño) and 2010 (La Niña) ozone from MLS during July-August (in ppmv) and (bottom) stream function from MERRA-2 (in $10^6 m^2 s^{-1}$) during July. Niño34 index for July-August in 2015 and 2010 are shown in red.

3.4 Discussion and conclusions

In this study a coupled ocean chemistry climate model and observations have been used to investigate the influence of boreal summer ENSO events on the ozone in the TLS. We have shown that ozone interannual variability is larger in magnitude in the NT during the boreal

summer than during the winter and also larger than in the ST during both seasons. JJA ozone anomalies are strongly correlated with SSTs in the central equatorial Pacific (Niño34 region) and correlation is strongest when O_3 anomalies lag Niño34 index by 1 month.

A TEM budget analysis of the CCM allowed us to assess the role of different transport processes on the ozone distribution. The seasonal cycle amplitude in ozone is larger in the NT than in the ST for all years (El Niño, La Niña and ENSO neutral years) due to enhanced summertime mixing in the NT associated with ASM anticyclone [*Tweedy et al.*, 2017a]. However, boreal summer ENSO events alter the meridional advection in the northern subtropics leading to larger variability in the NT summertime ozone, while in the ST ozone variability is dominated by changes in upwelling related to ENSO (just like during the winter [*Calvo et al.*, 2010]). These lead to larger annual cycle amplitude during boreal summer La Niña and smaller amplitude during boreal summer El Niño events in both ST and NT.

The changes in the meridional advection during boreal summer ENSO are related to changes in the onset date and strength of the ASM anticyclone. The anticyclone develops earlier and tends to be stronger throughout the NH summer during La Niña than El Niño. This results in the stronger meridional inflow of ozone-rich air into the NT during La Niña.

Recently, *Yan et al.* [2018] also showed a later onset of the ASM anticyclone after boreal winter El Niño events, but in contrast to our study they showed almost no difference in the atmospheric circulation and ozone fields during boreal summer when compositing on wintertime ENSO index. This is mainly because the majority of boreal winter ENSO events rapidly decay towards next summer and Niño34 SST anomalies become neutral during JJA. Thus, the analysis of *Yan et al.* [2018] does not include the influence of boreal summer ENSO events on the monsoon anticyclone and ozone transport.

Although we only show results from WACCM simulation with coupled oceans, similar results are found for a version of WACCM with prescribed SSTs and a Goddard Earth Observing System Chemistry-Climate Model (GEOSCCM) simulation with coupled ocean. This

provides us with additional confidence in results and conclusions made in this study.

The main focus of this study is to understand ozone variability in the tropics and ENSO-related ozone variability outside of the tropics was not examined. However, Figure 3.4 indicates an increase (decrease) in JJA ozone near 40°N during AMJ El Niño (La Niña) events. A similar ENSO signal in midlatitude ozone during the boreal winter and early spring was previously shown in *Calvo et al.* [2010], where the higher ozone during El Niño was related to enhanced downwelling branch of the BDC, which transports ozone from the tropics and higher altitudes into midlatitudes and polar regions. Our initial analysis of ozone transport in WACCM (not shown) also indicates strong sensitivity of midlatitude vertical advection in JJA to Niño34 SST anomalies during boreal spring, suggesting that enhanced tropical upwelling and downwelling in the NH midlatitudes is a likely cause of higher ozone in northern midlatitudes during El Niño. However, more work has to be done to quantify ozone changes in the midlatitudes and polar regions and their relationships to boreal summer ENSO events. These investigations will be the subject of future research.

CHAPTER 4

Response of trace gases to the disrupted 2015-2016 QBO

The work contained in this chapter is based upon *Tweedy et al.* (2017b), submitted to *Journal of Atmospheric Chemistry and Physics*.

4.1 Introduction

As discussed in Chapter 1 (section 1.2.3) QBO is another major source of interannual variability in the lower stratosphere. In this chapter we investigate the response of stratospheric trace gases to the unprecedented 2015-2016 QBO disruption event. We quantify the impact of the disruption on O_3 and other trace gases and further compare their observed changes to the expected behavior due to the QBO in the absence of the disruption. Furthermore, we examine the interannual variations in total ozone and water vapor.

4.2 Methods and data

We use Aura MLS version 4.2 level 2 measurements of temperature (T), O_3, and HCl from January 2005 to February 2017 between 10 and 100 hPa. O_3 and T are reported on a fixed

vertical grid with 12 surfaces per decade change in pressure between 1000 hPa and 1 hPa; HCl is reported on 6 pressures per decade. O_3 and HCl have a vertical resolution of ~3 km in the pressure range used in this analysis while the vertical resolution of T is ~4 km. Although O_3 and T are reported on the same pressure grids, their vertical resolution is not the same because the number of independent measurements that the instrument makes varies between MLS T and O_3 [*Livesey et al.*, 2015]. O_3 accuracy varies from 50 to 300 ppb between 100 and 10 hPa while HCl accuracy is estimated at ~10%. MLS temperatures have a -1 K bias in the stratosphere with respect to correlative measurements. Details on MLS measurements, data quality, and improvements on previous versions can be found in the MLS v4.2 data quality document [*Livesey et al.*, 2015].

We examine total-column O_3 during the anomalous QBO event using total O_3 observations from the Solar Backscatter Ultraviolet (SBUV) Merged Ozone Data Set (MOD). The MOD is constructed from monthly zonal mean ozone profiles by individual SBUV instruments, providing the longest available satellite-based time series of profile and total O_3 from a single instrument type [*Frith et al.*, 2014]. The MOD used here includes observations from January 1980 to the present to evaluate the temporal and spatial distribution of total O_3.

We use monthly averaged analyses of meteorological data on constant pressure levels from the Modern-Era Retrospective analysis for Research and Applications- Version 2, (MERRA-2) [*Bosilovich et al.*, 2015] to determine the vertical wind shear and QBO phase. The MERRA-2 analysis begins in January 1980. *Coy et al.* [2016] showed that MERRA-2 produces a realistic QBO from 1980 to 2016, a period encompassing 15 QBO cycles. We show changes in the meridional circulation due to the disrupted QBO using the vertical component of the MERRA-2 residual mean meridional circulation, $\overline{w}^*$ [*Andrews et al.*, 1987], which is calculated using 3-hourly output.

To determine the impact of the 2015-2016 disruption on the distribution of trace gases, we create a QBO composite ("QBO climatology") for each analyzed dynamical variable (T,

TABLE 4.1: the QBO composite dates (month 0)

QBO cycle	1	2	3	4	5	6	7	8
Month 0	1982-06	1984-10	1987-06	1989-12	1992-06	1994-09	1996-11	1998-09
QBO cycle	9	10	11	12	13	14	15	
Month 0	2001-10	2003-12	2006-02	2008-01	2010-06	2012-12	2015-05	

zonal winds ($\overline{u}$), and upwelling by the residual circulation ($\overline{w}^*$)) and trace species (O_3, HCl, and total O_3). These QBO composites include all available data except for 2015-2016. The composite is based on the month of change from zonal mean easterly (negative) to westerly (positive) vertical wind shear at 40 hPa. This is identified by month "0" in the figures. Compositing based on this criterion emphasizes that chemical trace gases are most closely related to the changes in the wind shear ($\frac{\partial \overline{u}}{\partial z}$ or $\overline{u}_z$), not the zonal wind ($\overline{u}$) [*Baldwin et al.*, 2001]. Compositing dates (month 0) for each QBO cycle are listed in Table4.1. Prior to compositing, we use monthly $\overline{u}$ data to compute $\overline{u}_z$ as a first vertical derivative of an unevenly-spaced array of $\overline{u}$ using three-point (quadratic) Lagrangian interpolation. The annual cycle was removed from T, $\overline{w}^*$, and trace gases to better isolate QBO variations, and values are shown in percent difference relative to the monthly climatology, except for the total-column O_3, which is shown as an absolute difference in Dobson units (DU). Anomalies due to the 2015-2016 event are calculated as the difference between '2015-2016' and the composite, with values larger than 2 standard deviations considered "significant".

Empirical orthogonal function (EOF) analysis has been applied to specify the instantaneous state of the QBO [*Wallace et al.*, 1993]. The two leading EOFs (EOF1 and EOF2) were derived from the deseasonalized monthly mean zonal wind data from Singapore radiosondes.

Interannual changes in global stratospheric water vapor and cold-point tropical tropopause temperatures were analyzed by forming time series from multiple observational data sets. Data were deseasonalized to isolate anomalies due to the QBO. Time series of stratospheric water vapor anomalies were derived from combined HALOE (Halogen Occultation Experiment; 1991-2005) and Aura MLS (2004- 2016) satellite measurements. These data represent

near-global (~60° N - 60° S) averages in the lower stratosphere (83 hPa). HALOE and MLS data were combined using the overlap period during 2004-2005. Cold-point temperatures are derived from radiosonde data (1991-2016) and GPS radio occultation data (2001- 2016). More details of the data and analysis are provided by *Randel and Jensen* [2013].

4.3 Results

4.3.1 The response of the equatorial stratosphere to the anomalous QBO event

Prior to 2015, wind observations show the robust features of the QBO's zonal wind pattern of descent in the middle and lower equatorial stratosphere [*Newman et al.*, 2016; *Coy et al.*, 2017]. The $\overline{u}$ composite in Figure 4.1 (top, column a) shows typical descending easterlies (blue) and westerlies (red) with zero wind shear (thick solid black contours). The alternating regime of downward-propagating wind shear leads to a modification of lower-stratospheric tracers. Composites of tropical O_3 and HCl (Figure 4.1, column a) show decreases/increases in mixing ratios, relative to the climatological seasonal values, during negative (easterly)/positive (westerly) wind shear. This O_3 and HCl behavior results from the QBO-induced ("secondary") meridional circulation, acting on local gradients of these chemical tracers [*Gray and Chipperfield*, 1990]. A downward (adiabatically warmed) perturbation (decreased $\overline{w}^*$ and increased T) is associated with descending westerly wind shear (positive $\overline{u}_z$) while an upward (adiabatically cooled) perturbation is associated with easterly shear (negative $\overline{u}_z$). Since the tracer's tendency ($\overline{\chi}_t$) is proportional to $-\overline{w}^*\overline{\chi}_z$ and mixing ratios of both chemical species increase with height in the lower stratosphere (positive vertical gradient, $\overline{\chi}_z$), O_3 and HCl decrease with time when $\overline{w}^*$ increases. The opposite is true for a downward perturbation (decreased $\overline{w}^*$). This is supported by the good agreement between the analyzed $\overline{w}^*$ and observed T, O_3 and HCl composites with vertical wind shear. As discussed in the introduction, horizontal transport completes the circulation and also contributes to some changes in tropical stratospheric composition (not shown).

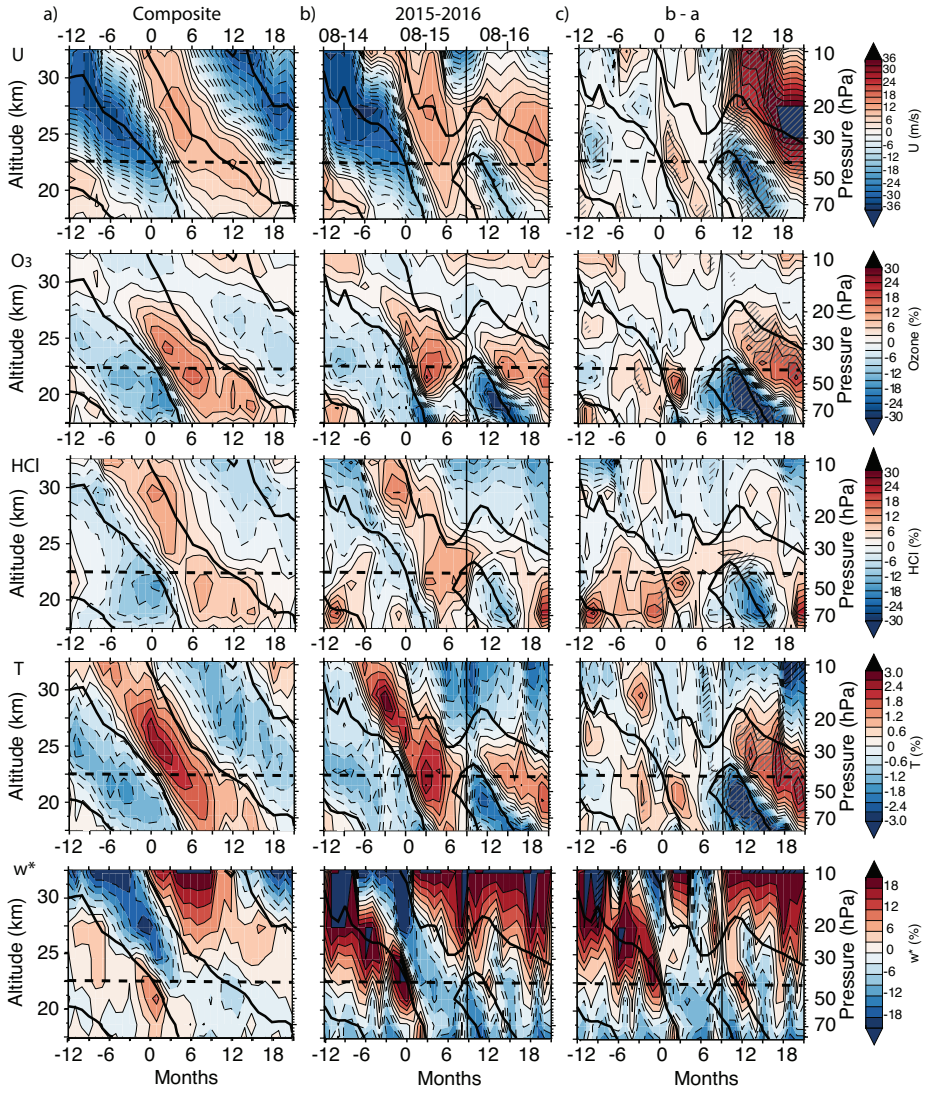

FIGURE 4.1: The rows show the MERRA-2 zonal mean zonal wind component, u (m s^{-1}), deseasonalized MLS O_3, HCl, temperature (T), and vertical component of the MERRA-2 residual circulation (w^*), as a function of time and pressure (in percent change from long-term monthly averages), averaged over 5° S - 5° N. Column (a) shows the composite of the easterly-to-westerly shear transitions based on four shear transitions at 40 hPa. Column (b) shows the 2015-2016 QBO cycle, which includes the data from May 2014 to February 2017, with month 0 in May 2015. Column (c) shows the difference between the 2015-2016 event and the climatology (b−a) with hatching indicating regions with absolute difference (b−a) larger than 2 standard deviations The thick black contours denote zero wind shear. The horizontal dashed line indicates the 40 hPa level, while the vertical line indicates February 2016.

In late 2015 westerlies were displaced upward between 30 and 15 hPa, and anomalous easterlies developed at ~40 hPa in early 2016 [*Newman et al.*, 2016; *Coy et al.*, 2017]; see Figure 4.1b (top). During the northern spring the anomalous ascending westerlies reverted back to a more typical descent, reaching 50 hPa in September 2016 and 70 hPa in February 2017. The vertical residual velocity, $\overline{w}^*$ (Figure 4.1b bottom), responded to the changes in equatorial zonal winds during 2015-2016 with decreased upwelling in association with the westerly shear and increased upwelling below the easterly maximum. A strong positive temperature perturbation developed in the 50-30 hPa layer (westerly shear zone) due to this reduced upwelling, while a strong negative perturbation developed in the easterly shear zone – due to the enhanced upward motion. Although analyzed $\overline{w}^*$ is noisy and involves greater uncertainty because of its highly derived nature, the excellent agreement between the wind shear and temperature changes (Figure 4.1b bottom panels) provides evidence of secondary circulation changes resulting from the anomaly.

The circulation anomalies created by the 2015-2016 event altered stratospheric composition patterns (Figure 4.1b, O_3 and HCl) relative to the composites seen in the left column. Changes in O_3 and HCl are in good agreement with changes in the wind shear and temperature (and thus $\overline{w}^*$). Prior to November 2015, both trace gases were followed similar tendencies to their composites. Beginning February 2016 (black vertical line in Figure 4.1b), O_3, and HCl increased between 50 and 30 hPa (due to the reduced upward motion) and decreased below 50 hPa (due to the enhanced upward motion). When the composites are subtracted from the last QBO cycle (Figure 4.1c), QBO-induced anomalies in T, O_3 and HCl are seen to be colocated with the changes in wind shear during the last QBO cycle and anomalies in u, T, and O_3 are larger than 2 standard deviations (hatched gray lines), indicating that their changes were driven by the 2015-2016 QBO disruption. The unprecedented nature of the 2015-2016 event is demonstrated in Figure 4.2 showing "the orbits of the QBO" in two-dimensional phase space, based on the projections of two leading empirical orthogonal functions (EOF1 and EOF2), following *Wallace et al.* [1993]. QBO orbits are used to

quantify the amplitude and phase propagation among the QBO cycles. Each point in this figure describes the instantaneous state of the QBO, described by the amplitude and phase angle of the vector in polar coordinates and specified in terms of variables (EOF1 and EOF2) that define the vertical structure of the zonal wind. EOF1 reflects the negative correlation between zonal wind fluctuations at 10 and 70 hPa while EOF2 indicates the variability at intermediate levels. Time progression corresponds to counterclockwise transits and each orbit corresponds to an individual QBO cycle.

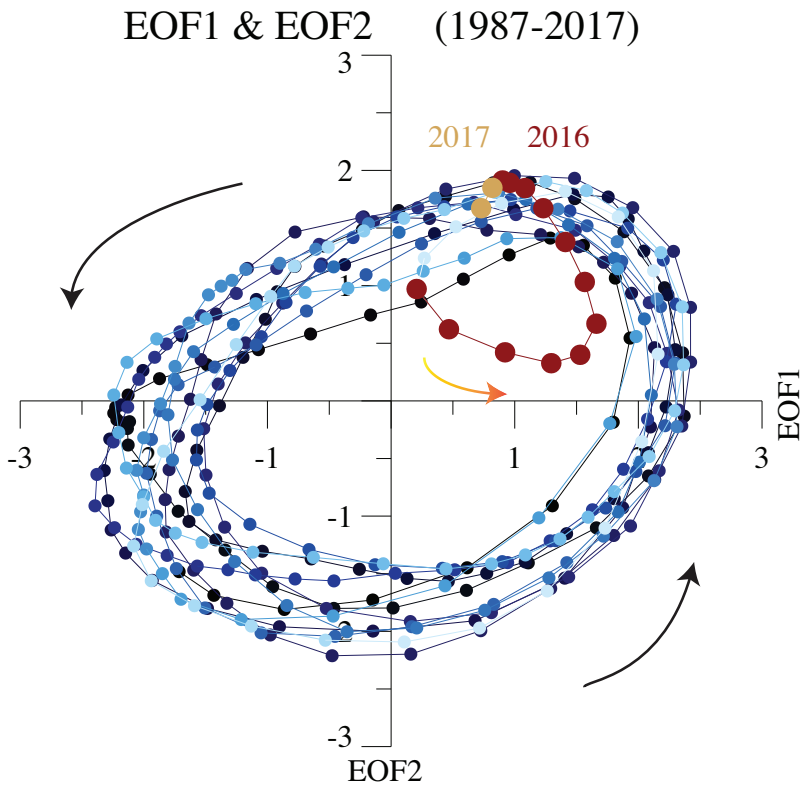

FIGURE 4.2: Phase space diagram of the projection of the monthly equatorial zonal wind anomalies onto spatial structures EOF1 and EOF2. Time progression coincides with counterclockwise orbit transits. Dots represent each month from January 1987 to February 2017. Different shades of blue indicate different years from 1987 to 2015 (from darker to lighter), while red and yellow dots correspond to 2016 and 2017, respectively

Prior to 2016, the QBO orbits (blue dots in Figure 4.2) are roughly circular and data points are distributed uniformly along the orbits, indicating the remarkably uniform structure and nearly constant amplitude of the QBO in this record (1987-2015). During this time, EOF1 and EOF2 combined explain ~95.5% of the variance of the deseasonalized smoothed

time series of zonal winds between 70 and 10 hPa. Based on this stability, EOF1 and EOF2 are commonly used to isolate the variability related to the QBO when deriving ODS-induced changes in long-term ozone records.

The repetitive QBO pattern was disrupted in 2016, as shown by the red points that deviate from the regular circular pattern. The smaller amplitude (closer to the center) of EOF1 and EOF2 in Figure 4.2 during the disruption means the zonal winds either are weaker than the typical QBO or do not fit the EOFs well. Analysis of the variance explained by two leading EOFs shows that the first two EOF patterns do not match the disruption very well, with the lowest percent variance (~71%) explained by the two EOFs in the entire data record occurring during the disruption (not shown). Such disruptions add unpredictable variability to the time series, reducing the accuracy of stratospheric ozone trends determined by multivariate regressions.

4.3.2 Latitudinal changes in ozone

The stratospheric impact of the 2015-2016 event extends into the extratropics. Figure 4.3 shows the evolution of O_3 for the composite (left), 2015-2016 (middle) and their difference (right). Figure 4.3(a, b, and c) show MLS O_3 at 38 hPa, the pressure level of maximum O_3 anomaly during the NH summer of 2016. As shown in the composite (Figure 4.3a), the positive O_3 perturbation during the westerly shear in the tropics and the negative perturbations in the extratropics are replaced by anomalies of opposite signs as the wind shear reverses to easterly 12-14 months later. However, in 2016 (Figure 4.3b) the 40 hPa westerly shear changes to a weak easterly shear for only a short time interval (Jan-Apr) before switching back to westerly shear (note that the wind shear at 30 hPa remains westerly). O_3 responds by decreasing/increasing in mixing ratios during the easterly/westerly shear changes. The O_3 anomalies due to the 2015-2016 event are highlighted in Figure 4.3c, which shows large differences after February 2016 (black line). A strong negative tropical O_3 perturbation developed by early spring 2016, propagating to the extratropics in both hemispheres by the end

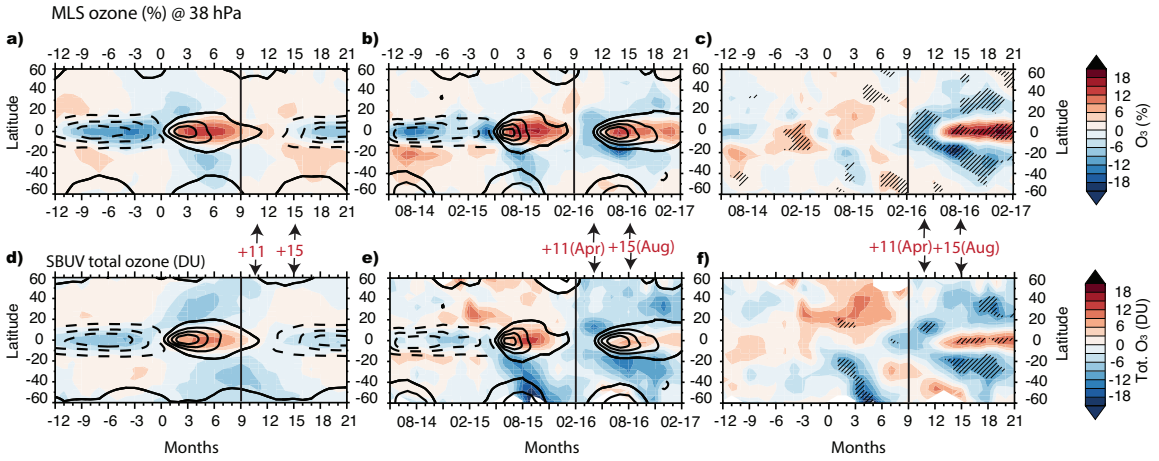

FIGURE 4.3: Latitude and time evolution of MLS ozone at 38 hPa (top row) for (a) the composite, (b) 2015-2016, and (c) their difference (b-a), highlighting the anomalies due to the disruption. MLS ozone values are shown in percent change from long-term monthly averages with contour intervals every 3% (zero contour is omitted). The bottom row shows the deseasonalized SBUV total ozone (in Dobson units, contour intervals every 3 DU) for d) the composite, e) 2015-2016, and f) their difference (e-d). Black thick solid and dashed contours show westerly and easterly vertical wind shear respectively for (a and d) the composites and (b and e) 2015-2016. MLS (SBUV) composites are based on 4(14) transitions from easterly to westerly vertical wind shear at 40 hPa. Vertical black line highlights +9 months after wind shear reversal from negative to positive (month 0), corresponding to February 2016 in (b) and (e) while arrows indicate ozone at +11 and +15 months after month 0, corresponding to April 2016 and August 2016 in (b) and (e). Gray hatching in (c) and (f) indicates regions with absolute difference between 2015-2016 and the composites being larger than 2 standard deviations

of the NH summer. In the equatorial region, a positive perturbation replaced the negative O_3 perturbation as the wind shear switched back to westerly. QBO-induced anomalies after February 2016 are larger than 2 standard deviations.

The 2016 NH summer positive tropical O_3 anomaly at 30-50 hPa - the level of maximum O_3 number density - contributed to substantial changes in the total-column O_3. As in the 38 hPa O_3 from MLS (Figure 4.3, top), the typical QBO behavior of SBUV total O_3 (Figure 4.3d) contrasts with the anomalous 2015-2016 behavior (Figure 4.3e), with their difference (Figure 4.3f) highlighting the 2016 anomalies. The SBUV total O_3 QBO composite is based on 14 transitions of wind shear at 40 hPa (excluding 2015-2016). Total O_3 was deseasonalized and values are shown as absolute difference from the monthly climatology (in Dobson units). This SBUV composite captures the major features of the typical QBO and the O_3 perturbations.

Prior to February 2016, Figure 4.2f shows small total O_3 differences except for the large

midlatitude anomalies from 0 to +6 months in the southern (negative anomaly) and northern (positive anomaly) hemispheres. However, only the negative anomaly in the southern midlatitudes is larger than 2 standard deviations. The cause of these anomalies prior to the 2015-2016 disruption remains unclear and is the subject of ongoing investigation. After February 2016 (black line in Figure 4.3e), there is a large decrease in total ozone in the extratropics and midlatitudes of both hemispheres and the total O_3 differences between composite and last QBO cycle (Figure 4.3f) are very similar to the differences in 38 hPa O_3 from MLS (Figure 4.3c). This strongly suggests that the 2015-2016 event had a significant impact on both tropical and extratropical total O_3.

4.3.3 Temporal and spatial morphology of ozone in April and August 2016

Large negative O_3 anomalies in the lower stratosphere start in April 2016 in the tropics and propagate to the extratropics by August 2016. Note that these two months occur at 11 and 15 months after month 0 on the "composited" time axes and are indicated by arrows in Figure 4.3. Therefore, we compare the latitudinal and vertical extent of the QBO-induced anomalies in T and O_3 during these two months (Figure 4.4b and Figure 4.4d) to the expected behavior based on the composite eleven (+11) and fifteen (+15) months after the wind shear reversal (Figure 4.4a and Figure 4.4c). In agreement with Figure 4.1b, in April 2016 the anomalous easterly shear below 40 hPa (dashed horizontal line in Figure 4.1b) leads to strong negative T and O_3 perturbations in the tropics, while the appearance of ascending westerly shear leads to weak tropical T and O_3 increases between 20 and 40 hPa. By August 2016, the westerly shear strengthens and descends to 30-50 hPa resulting in strong positive T and O_3 perturbations in this layer, while the easterly shear below 50 hPa leads to negative perturbations in the equatorial (10° N-10° S) stratosphere. This is consistent with our understanding of trace gas response to changes in tropical upwelling. The consistency of O_3 and T anomalies during 2015-2016 is evidence of circulation changes. In the subtropics, the

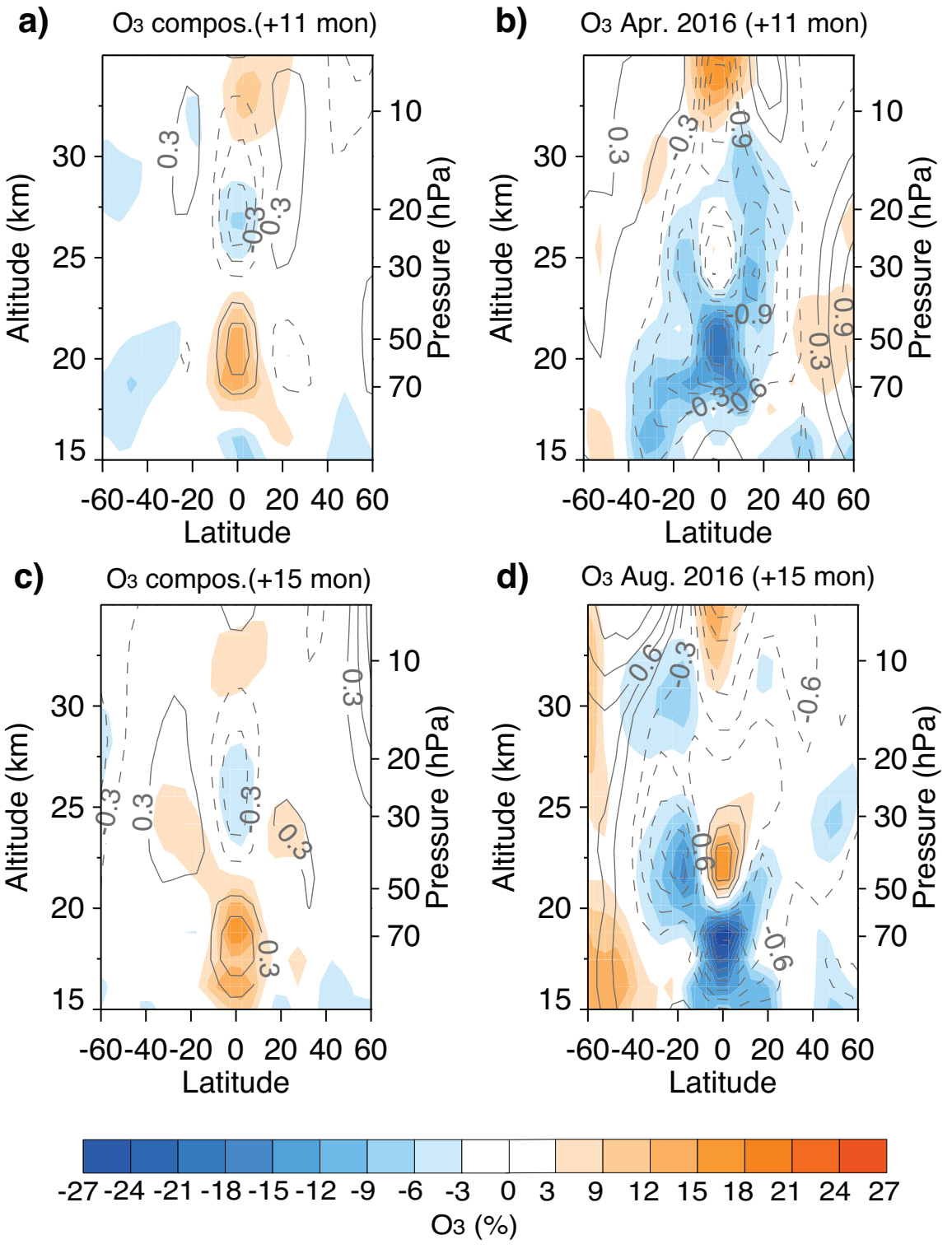

FIGURE 4.4: Latitude-height cross sections of deseasonalized MLS ozone (filled) and temperature (gray contours) in the composite (a) 11 and (c) 15 months after the wind shear reversal based on four QBO cycles and during (b) April (+11 months) and (d) August 2016 (+15 months). Ozone and temperature values are shown in percent change from long-term monthly averages with contour intervals every 3% and 0.3%, respectively (zero contour is omitted).

deseasonalized O_3 QBO signature is out of phase with that at the equator, in agreement with Figure 4.3b. In August 2016, strong negative O_3 perturbations develop during the NH summer on both sides of the equator (although they are much stronger in the winter Southern Hemisphere) as a response to the QBO-induced meridional circulation. In the composites at +11 and +15 months (Figure 4.4a and Figure 4.4c) anomalies in MLS O_3 and T are opposite to those observed in April and August 2016 (Figure 4.4b and Figure 4.4d) due to the descending easterly shear. Thus, O_3 is responding as expected to a QBO-induced meridional circulation but this period is anomalous with respect to a normal QBO progression.

The observed 2015-2016 anomalies are unique in the total O_3 record. Figure 5 compares the latitudinal distribution of deseasonalized total O_3 from April and August 2016 (in red) to the total O_3 composite (the average of the 14 composited QBO cycles) shown in Figure 4.3d at +11 and +15 months respectively (in black). Total O_3 from each individual QBO cycle included in the composite is shown in blue, with light blue shading indicating the range of total O_3 from all QBO cycles (excluding 2015-2016). In the absence of the disruption, we expect total O_3 at +11 (Figure 4.5a) and +15 (Figure 4.5b) months to lie within the blue shaded range of past observations. Instead, in April 2016 total O_3 is lower than during other QBO cycles in the NH tropics (10° N - 20° N). Furthermore, during August 2016 total ozone is higher at the equator and lower/near the edge in the extratropics between 10 and 40° S /30 and 50° N compared to other QBO cycles. Calculations suggest that anomalously low total-column O_3 at 22.5° S in August 2016 increased the monthly zonal mean surface clear-sky UV index by ~8.5 % compared to the 36-yr mean [*Newman and McKenzie*, 2011]. Increased surface UV radiation has a harmful effect on health by damaging cells, DNA, and increasing the risk of developing skin cancer. Increased exposure to UV in plants leads to enhanced plant fragility, growth limitation, and yield reduction affecting our ability to secure food production [*Caldwell et al.*, 1995; *Tevini*, 1993].

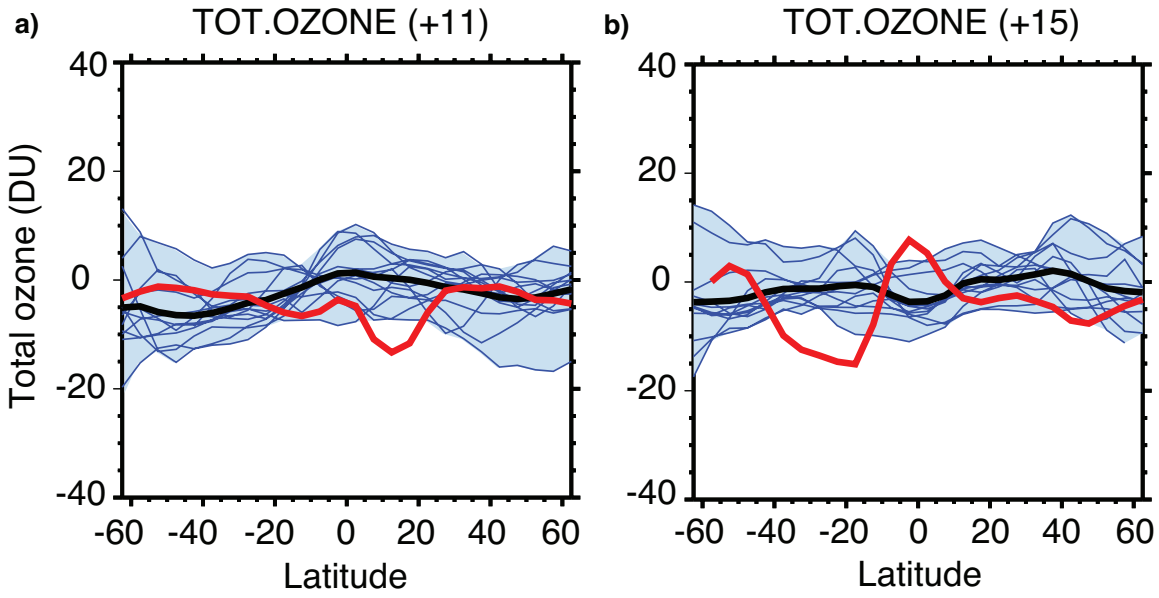

FIGURE 4.5: (a) Deseasonalized SBUV total ozone (in Dobson units) as a function of latitude 11 months after wind shear reversal from easterly to westerly from f14 QBO cycles prior to 2015-2016 (blue lines), the composite (black line) based on 14 QBO cycles, and 2015-2016 (April 2016; red line). (b) The same as (a) only for total ozone at +15 months, corresponding to August 2016. The blue shading shows the observed O_3 range at +11 and +15 months, respectively, for all 14 QBO cycles (excluding the 2015-2016 event).

4.3.4 QBO-driven changes in total ozone and water vapor in the context of long-term time series

Examination of the interannual variations in SBUV monthly and zonal mean total O_3 shows very low total O_3 values in the extratropics during spring and summer of 2016 compared to other years within this observational record. Figure 4.6 displays the time series for April (top panels) and August (bottom panels) total O_3 values in the northern and southern extratropics. The regions shown are locations with large anomalies in Figure 4.3f. The individual 1σ error estimates are shown as the vertical gray bars in Figure 4.6, while the horizontal line is the 2016 value. Each of these plots shows that the 2016 value was the record or near-record low in the more than 40 years of the SBUV data. Near-record low total O_3 in the extratropics during the spring and summer 2016 is due to the 2015-2016 QBO disruption event. As shown in Figure 4.3e, beginning about February 2016 the disruption in the descent of easterly zonal winds led to lower O_3 values in both the northern and southern extratropics and

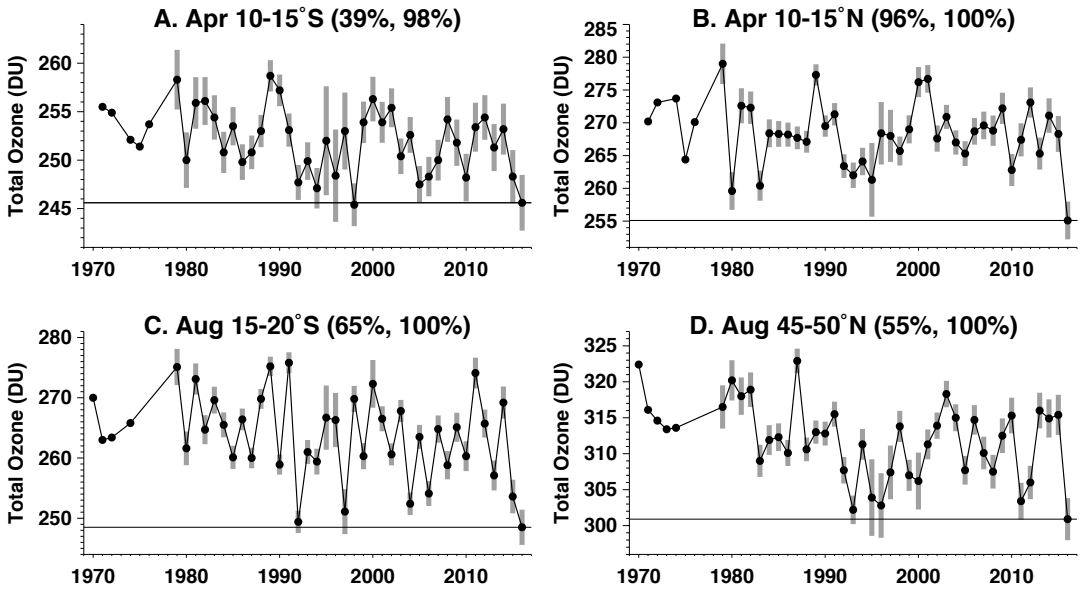

FIGURE 4.6: SBUV total ozone (in Dobson units) time series from 1970 to 2016 for April, averaged over (a) 10° S -15° S and (b) 10° N -15° N, and for August, averaged over (c) 15° S -20° S and (d) 45° N -50° N . Vertical bars show 1σ uncertainties in the measurements. The horizontal line shows the total ozone value in April or August 2016 and the panel captions show the percentage estimates of the 2016 value that are the lowest and amongst the lowest 20% of all values. The probability that the 2016 values were record lows was estimated using 10,000 Monte Carlo simulations of the monthly means in the time series [*Frith et al.*, 2014]

persisted into the fall of 2016. The ozone anomalies, shown in Figure 4.3e, are up to -12 DU at 12.5° N in April 2016 and -15 DU at 17.5° S in August 2016. This strongly contrasts with the expected behavior (Figure 4.3d) that would have been either near zero or small positive anomalies.

The 2015-2016 QBO event also significantly impacted the global amount of stratospheric water vapor in 2016. H_2O enters the stratosphere from the troposphere primarily in the tropics. The amount of H_2O in the stratosphere is controlled by the tropical tropopause temperature ("cold-point tropopause temperatures", or T_{cp}) with colder T_{cp} resulting in less

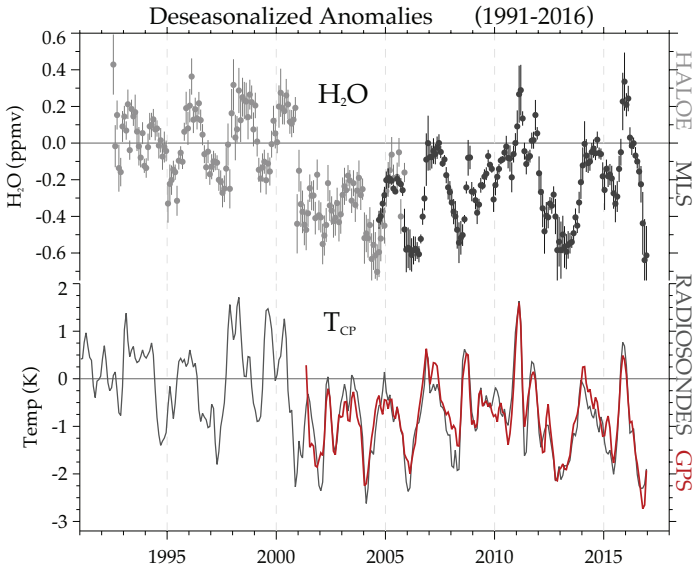

FIGURE 4.7: Observed variations in lower-stratospheric water vapor and tropical cold-point tropopause temperatures from satellite measurements over the period 1992 - 2016. Water vapor data are deseasonalized near-global averages at 83 hPa from combined HALOE and MLS satellite measurements. Each dot represents a monthly average. Temperatures are deseasonalized anomalies derived from radiosonde data (black line) and GPS radio occultation data (red line, for 2001-2016). Vertical bars are 1σ standard deviations of the monthly averages.

H_2O entering the tropical stratosphere from the troposphere. Figure 4.7 demonstrates a very strong correlation of stratospheric water vapor anomalies with T_{cp} (also see [*Randel and Jensen*, 2013]). In 2016, cold tropical tropopause temperatures (in balance with anomalous easterlies) led to a global decrease in the stratospheric H_2O in October-December 2016. Global H_2O in November is amongst the lowest in the record (1992-2016) due to very low T_{cp}. In addition to the QBO disruption, there was a strong El Niño in the 2015-2016 winter [*Hu et al.*, 2016]. While changes in the global water content and stratospheric ozone from late spring to the end of fall 2016 are attributed mostly to the unprecedented QBO event, El Niño could strongly influence the lower stratosphere during the winter of 2016. Previous studies showed cooling of the tropical lower stratosphere and strengthening of the Brewer-Dobson circulation during El Niño [*Randel et al.*, 2009; *Calvo et al.*, 2010] followed by an associated decrease in ozone and increase in H_2O in this region. The impact of ENSO on stratospheric water vapor, however, is nonlinear and often depends on the phase of the QBO [*Liess and Geller*, 2012], time of the year (early or late in the winter) and location (central or eastern

Pacific) where the ENSO maximum occurs [*Garfinkel et al.*, 2013]. The interplay between El Niño and the QBO disruption during the 2015-2016 boreal winter is not well understood and their relative importance on trace gas distribution requires a detailed investigation.

4.4 Conclusions

This study demonstrates that the 2015-2016 QBO disruption had a substantial impact on the composition of the stratosphere. It led to a modified circulation that reduced the equatorial upward circulation in association with the positive (westerly) shear, while the negative shear below the easterly maximum led to enhanced upward motion. Following the appearance of the disruption in February 2016, there were two layers of zonal wind shear in the tropics. Westerly shear in the 30-50 hPa layer was linked to increased temperature and decreased upwelling, resulting in positive perturbations in O_3 and HCl. The easterly shear from the disruption in the 50-100 hPa layer produced negative temperature perturbations in association with increased tropical upwelling, inducing negative perturbations in O_3 and HCl. Cold temperature anomalies extended to the tropopause level in late 2016, resulting in decreases in global stratospheric water vapor. Because the ozone number density maximum is in the 50-30 hPa layer, the QBO disruption increased total O_3 at the equator.

The decrease in tropical ascent during the disruption was balanced by reduced downwelling in the extratropics. This reduced extratropical downward motion decreased O_3 in those regions (although the horizontal component to this circulation contributes as well). In this study we focused mostly on O_3 changes, however, the response of other long-lived tracers such as HCl and N_2O is consistent with the QBO meridional circulation induced by the disrupted QBO. While HCl anomalies are consistent with the O_3 anomalies, the N_2O anomalies have an opposite sign due to the negative vertical gradient of this tracer. The similarities in the responses of temperature and observed changes in chemical trace gases to the QBO disruption show that these composition changes are primarily dynamically driven. Trace

gases show perturbed behavior compared to the past, but their response is consistent with our understanding of the QBO-induced meridional circulation.

At nearly the same time as the QBO disruption, there was one of the strongest El Niño events on record and very strong stratospheric polar vortex in early to midwinter [*Cheung et al.*, 2016; *Hu et al.*, 2016; *Scaife et al.*, 2017]. The interplay of these three events and their potential impact on trace gas distributions remains to be investigated. For instance, we acknowledge the possible influence of 2015-2016 El Niño event on tropical tropopause temperature and therefore global redistribution of stratospheric water vapor. Furthermore, previous studies by *Fioletov and Shepherd* [2003, 2005] showed very strong correlations between polar and midlatitude total ozone. Ozone-depleted air inside cold polar vortex could mix into the Northern Hemisphere midlatitudes contributing to the negative anomalies in total ozone during the 2016 boreal summer. *Strahan et al.* [2016] showed that the impact of Arctic ozone depletion on the midlatitudes in spring after winters with moderate depletion (such as 2016) was about 5 DU (south of 45° N). But they also found that the dynamical impact on O_3 due to a strong polar vortex winter was roughly the opposite of the depletion changes, resulting in very little net impact. Furthermore, the very symmetric nature of negative anomalies around the equator during the boreal summer and fall strongly suggests a dominant role of circulation changes due to the 2015-2016 QBO disruption.

It is unclear if this QBO disruption is an event of great rarity or if similar events will reoccur. Similar disruptions with the same timing could potentially alter ozone and trace gas distributions, affecting the stratospheric climate and making it more difficult to accurately estimate climate trends. For example, a series of disruptions could drive a downward ozone trend and lead to a long-term increase in the surface UV index during the peak of northern summer.

CHAPTER 5

Conclusions

5.1 Summary of results

The focus of this thesis has been on quantifying and understanding the seasonal and inter-annual variability of chemical trace gases (e.g., O_3) in the tropical lower stratosphere. This work is motivated by the essential role of transport processes on composition and structure of UTLS, by the impact of these coupled processes on climate through changes in trace gas distribution, and by desire to critically diagnose and improve model simulations of this region.

Stolarski et al. [2014] showed significant differences in tracers' seasonality between the NT and ST using satellite observations. In Chapter 2, we looked at this issue for the first time in global chemistry climate models. We found that the majority of the CCMs produced the observed feature of a larger annual cycle in the NT than ST. However, only around a third of the models produce an ozone annual cycle similar to that observed. Furthermore, TEM tracer budget analysis from GEOSCCM and WACCM simulations shows that the ST annual cycle is dominated by upwelling, whereas in the NT, horizontal mixing during boreal summer dominates. In agreement with previous studies, we attributed summertime increases in

mixing to the ASM, which mixes in high ozone from NH extratropics into the tropics and seldom penetrating the equator.

In Chapter 3, the interannual variability of TLS ozone and its connections to SSTs in the equatorial Pacific were examined using a combination of CCM simulations, satellite observations, and reanalysis. The model simulations and observations show large differences in the magnitude of interannual variability in ozone between NT and ST during boreal summer, but small differences in winter. The interannual variability during boreal summer is highly correlated with summer SSTs in the eastern and central Pacific Ocean and ENSO events. Larger variability in the NT ozone is primarily due to meridional advection, connected to the changes in the onset date and strength of the ASM anticyclone. The ASM anticyclone forms earlier in a season and tends to be stronger during cold (La Niña) events leading to more transport of TLS ozone into the NT, with the reverse for warm (El Niño) events.

Finally, in Chapter 4, the impact of unprecedented QBO disruption during 2015-2016 on the composition and transport of the lower stratosphere was examined using satellite observations and reanalysis. Results reveal the development of positive anomalies in stratospheric equatorial O_3 and HCl over 50–30 hPa in May–September of 2016 and a substantial decrease in O_3 in the subtropics of both hemispheres. The SBUV observations showed near-record low levels of column ozone in the subtropics in 2016, resulting in an increase in the surface UV index during northern summer. Furthermore, cold temperature anomalies near the tropical tropopause result in a global decrease in stratospheric water vapor.

5.2 Outstanding issues and future investigations

There are several outstanding issues from this thesis. One is the causes of the differences between annual cycles from the different ozone data sets, and which data set is most realistic. Of particular importance is whether the double peak structure in the vertical is real, or an

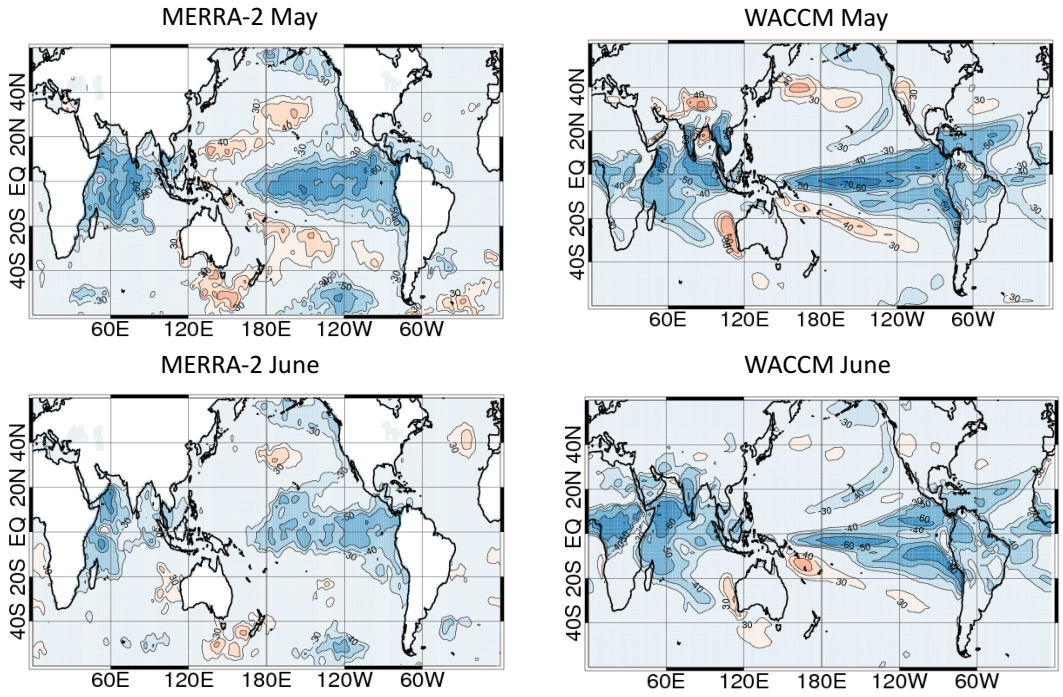

FIGURE 5.1: Correlation of the 100hPa stream function averaged over anticyclone region (May: 10° N-30° N and 60° E-120° E; June: 20° N-40° N and 20° E-100° E) and SST/SAT anomalies from WACCM and MERRA-2 for May and June. Correlation coefficients are multiplied by 100 and values that are between -30 and 30 are not shown.

artifact of the sampling, resolution, or uncertainties of the data. Clarification of this issue is needed for a more detailed analysis of the tropical transport and evaluation of the CCMs (especially as none of the models show the double peak structure).

Similarly, the cause of the spread in ozone annual cycle among the CCMs needs further examination. A process-based analysis, such as the TEM analysis, would be useful if applied to all of the individual models. The CCM simulations examined here are generally not from the latest versions of the CCMs, and it will be of value to repeat this analysis using simulations submitted to the new SPARC/IGAC CCM Initiative [*Eyring et al.*, 2013], and to also compare with other transport diagnostics (such as those considered in *Strahan et al.* [2011]).

An open question from Chapter 3 is the mechanism by which SSTs in the tropical

central-eastern Pacific influences the ASM anticyclone, and associated ozone transport into the tropics. One possibility is that the anomalous SSTs in the Pacific lead to changes in the latitudinal position of the ITCZ over the eastern Indian Ocean and the west Pacific in the preceding spring as well as changes in Walker circulation and Indonesian convection [e.g. *Ju and Slingo*, 1995] that then modify the onset and strength of the monsoon. But it is also possible the mechanism involves changes in Indian Ocean SSTs (via the "atmospheric bridge" and/or the Indian Ocean dipole) that alter the land-sea contrast and thus the summer monsoon [*Lau and Nath*, 2000; *Song et al.*, 2007; *Cherchi et al.*, 2007]. There is a high correlation between tropical SSTs over the central-eastern Pacific and those over the western Indian Ocean, and the strength of the ASM anticyclone is highly correlated with SSTs in both regions (Figure 5.1). Further research, and perhaps dedicated simulations with anomalous Pacific or Indian ocean SSTs [e.g., *Lau and Nath*, 2012], is needed to isolate the processes involved in connecting the Pacific SSTs to the monsoon anticyclone and transport of lower stratosphere ozone into tropics.

As shown in Chapter 3, ENSO-related variability in the strength of the ASM anticyclone impacts the horizontal advection of ozone in the NT. This ENSO-related variability in the ASM anticyclone could also affect other aspects of the atmospheric transport. Stronger monsoonal flow in the lower stratosphere could potentially lead to stronger ozone intrusions into the troposphere and thus have a significant impact on near surface climate and amounts of ozone near the surface. Furthermore, previous studies show the important role of ASM as a vertical transport pathway for tropospheric air entering the lower stratosphere [*Park et al.*, 2007; *Randel et al.*, 2010; *Pan et al.*, 2016]. An important question is whether or not boreal summer ENSO modifies the timescales of this transport pathway and also the confinement of surface pollutants and tropospheric gases within the anticyclone.

Finally, in Chapter 4 we showed that 2015 -2016 disruption in QBO zonal winds had a significant impact on the composition of the lower stratosphere. At present, numerical models are unable to predict such events [*Osprey et al.*, 2016], pointing to an incomplete un-

derstanding of QBO forcing mechanisms. The model failures could result from missing processes, a poor representation of necessary wave forcings, or resolution. *Osprey et al.* [2016] pointed out that only one event similar to that observed during 2016 was identified among the available models that produce an internally generated QBO. Our inability to simulate and/or predict a disrupted QBO will add uncertainty to future predictions of ozone and other chemical constituents from coupled chemistry climate models, as well as limit our ability to resolve statistically significant ODS-related changes in the observed O_3 record. This event, whether unique or the first of many QBO disruptions, emphasizes the crucial need to continue collecting and evaluating high-quality satellite measurements to trace the impact of stratospheric dynamical changes.

Bibliography

Abalos, M., W. J. Randel, and E. Serrano (2012), Variability in upwelling across the tropical tropopause and correlations with tracers in the lower stratosphere, *Atmos.Chem.Phys.*, *12*(23), 11,505–11,517, doi:10.5194/acp-12-11505-2012.

Abalos, M., F. Ploeger, P. Konopka, W. J. Randel, and E. Serrano (2013a), Ozone seasonality above the tropical tropopause: reconciling the eulerian and lagrangian perspectives of transport processes, *Atmos.Chem.Phys.*, *13*(21), 10,787–10,794, doi:10.5194/acp-13-10787-2013.

Abalos, M., W. J. Randel, D. E. Kinnison, and E. Serrano (2013b), Quantifying tracer transport in the tropical lower stratosphere using WACCM, *Atmos.Chem.Phys.*, *13*(21), 10,591–10,607, doi:10.5194/acp-13-10591-2013.

Abalos, M., B. Legras, and E. Shuckburgh (2016a), Interannual variability in effective diffusivity in the upper troposphere/lower stratosphere from reanalysis data, *Q.J.R.Meteorol.Soc.*, *142*(697), 1847–1861, doi:10.1002/qj.2779.

Abalos, M., W. J. Randel, and T. Birner (2016b), Phase-speed spectra of eddy tracer fluxes linked to isentropic stirring and mixing in the upper troposphere and lower stratosphere, *J.Atmos.Sci.*, *73*(12), 4711–4730, doi:10.1175/JAS-D-16-0167.1.

Akiyoshi, H., L. B. Zhou, Y. Yamashita, K. Sakamoto, M. Yoshiki, T. Nagashima, M. Takahashi, J. Kurokawa, M. Takigawa, and T. Imamura (2009), A CCM simulation of the breakup of the antarctic polar vortex in the years 1980-2004 under the CCMVal scenarios, *J.Geophys.Res.Atmos.*, *114*(D3), D03,103, doi:10.1029/2007JD009261.

Andrews, D. G., J. R. Holton, and C. B. Leovy (1987), *Middle atmosphere dynamics*, 40, Academic press.

Angell, J. K., and J. Korshover (1964), Quasi-biennial variations in temperature, total ozone, and tropopause height, *J.Atmos.Sci.*, *21*(5), 479–492.

Austin, J., and N. Butchart (2003), Coupled chemistry-climate model simulations for the period 1980 to 2020: Ozone depletion and the start of ozone recovery, *Q.J.R.Meteorol.Soc.*, *129*(595), 3225–3249, doi:10.1256/qj.02.203.

Austin, J., and R. J. Wilson (2006), Ensemble simulations of the decline and recovery of stratospheric ozone, *J.Geophys.Res.Atmos.*, *111*(D16), D16,314, doi:10.1029/2005JD006907.

Baldwin, M. P., L. J. Gray, T. J. Dunkerton, K. Hamilton, P. H. Haynes, W. J. Randel, J. R. Holton, M. J. Alexander, I. Hirota, T. Horinouchi, D. B. A. Jones, J. S. Kinnersley, C. Marquardt, K. Sato, and M. Takahashi (2001), The quasi-biennial oscillation, *Rev.Geophys.*, *39*(2), 179–229, doi:10.1029/1999RG000073.

Bosilovich, M. G., and W.-Y. Sun (1998), Monthly simulation of surface layer fluxes and soil properties during fife, *J.Atmos.Sci.*, *55*(7), 1170–1183.

Bosilovich, M. G, and Coauthor (2015), MERRA-2: Initial evaluation of the climate. NASA tech. rep. series on global modeling and data assimilation, NASA/TM-2015-104606, vol. 39, NASA, 136 pp., *NASA Tech. Rep. Series on Global Modeling and Data Assimilation*, *39*(NASA/TM-2015-104606), 136.

Caldwell, M. M., A. H. Teramura, M. Tevini, J. F. Bornman, L. O. Björn, and G. Kulandaivelu (1995), Effects of increased solar ultraviolet radiation on terrestrial plants, *Ambio*, *24*(3), 166–173.

Calvo, N., R. R. Garcia, W. J. Randel, and D. R. Marsh (2010), Dynamical mechanism for the increase in tropical upwelling in the lowermost tropical stratosphere during warm ENSO events, *J.Atmos.Sci.*, *67*(7), 2331–2340, doi:10.1175/2010JAS3433.1.

CCMVal, S. (2010), SPARC report on the evaluation of chemistry-climate models.

Climate Change 2014: Synthesis Report. Contribution of Working Groups I, II and III to the Fifth Assessment Report of the Intergovernmental Panel on Climate Change [Core Writing Team, R.K. Pachauri and L.A. Meyer (eds.)]. IPCC, Geneva, Switzerland, 151 pp.

Cherchi, A., S. Gualdi, S. Behera, J. J. Luo, S. Masson, T. Yamagata, and A. Navarra (2007), The influence of tropical Indian ocean SST on the Indian summer monsoon, *J.Clim.*, *20*(13), 3083–3105, doi:10.1175/JCLI4161.1.

Cheung, H. H. N., W. Zhou, M. Y. T. Leung, C. M. Shun, S. M. Lee, and H. W. Tong (2016), A strong phase reversal of the arctic oscillation in midwinter 2015/2016: Role of the stratospheric polar vortex and tropospheric blocking, *J.Geophys.Res.Atmos.*, *121*(22), 13,457, doi:10.1002/2016JD025288.

Choi, W., Lee, H., Grant, W. B., Park, J. H., Holton, J. R., LEE, K., and B. Naujokat (2002), On the secondary meridional circulation associated with the quasi-biennial oscillation, *Tellus B*, 54, 395–406.

Coy, L., K. Wargan, A. M. Molod, W. R. McCarty, and S. Pawson (2016), Structure and dynamics of the quasi-biennial oscillation in MERRA-2, *J.Clim.*, *29*(14), 5339–5354, doi: 10.1175/JCLI-D-15-0809.1.

Coy, L., P. A. Newman, S. Pawson, and L. R. Lait (2017), Dynamics of the disrupted 2015/16 quasi-biennial oscillation, *J.Clim.*, *30*(15), 5661–5674, doi:10.1175/JCLI-D-16-0663.1, doi: 10.1175/JCLI-D-16-0663.1; 16.

Déqué, M. (2007), Frequency of precipitation and temperature extremes over France in an anthropogenic scenario: Model results and statistical correction according to observed values, *Glob.Planet.Change*, *57*(1), 16–26, doi:10.1016/j.gloplacha.2006.11.030.

Douglass, A. R., R. S. Stolarski, S. E. Strahan, and L. D. Oman (2012), Understanding differences in upper stratospheric ozone response to changes in chlorine and temperature as computed using CCMVal-2 models, *J.Geophys.Res.Atmos.*, *117*(16), doi:10.1029/ 2012JD017483.

Dunkerton, T. J. (1997), The role of gravity waves in the quasi-biennial oscillation, *J.Geophys.Res.Atmos.*, *102*(D22), 26,053–26,076, doi:10.1029/96JD02999.

Eyring, V., M. P. Chipperfield, M. A. Giorgetta, D. E. Kinnison, E. Manzini, K. Matthes, P. A. Newman, S. Pawson, T. G. Shepherd, and D. W. Waugh (2008), Overview of the new CCMVal reference and sensitivity simulations in support of upcoming ozone and climate assessments and the planned SPARC CCMVal report, *SPARC newsletter*, *30*, 20–26.

Eyring, V., J.-F. Lamarque, P. Hess, F. Arfeuille, K. Bowman, M. P. Chipperfiel, B. Duncan, A. Fiore, A. Gettelman, and M. A. Giorgetta (2013), Overview of IGAC/SPARC chemistry-climate model initiative (CCMi) community simulations in support of upcoming ozone and climate assessments, *SPARC newsletter*, *40*(January), 48–66.

Fioletov, V. E., and T. G. Shepherd (2003), Seasonal persistence of midlatitude total ozone anomalies, *Geophys. Res. Lett.*, *30*, 1417, doi:10.1029/2002GL016739,7.

Fioletov, V. E., and T. G. Shepherd (2005), Summertime total ozone variations over middle and polar latitudes, *Geophys. Res. Lett.*, *32*, L04807, doi:10.1029/2004GL022080.

Frith, S. M., N. A. Kramarova, R. S. Stolarski, R. D. McPeters, P. K. Bhartia, and G. J. Labow (2014), Recent changes in total column ozone based on the SBUV version 8.6 merged ozone data set, *J.Geophys.Res.Atmos.*, *119*(16), 9735–9751, doi:10.1002/2014JD021889.

Fueglistaler, S., A. E. Dessler, T. J. Dunkerton, I. Folkins, Q. Fu, and P. W. Mote (2009), Tropical tropopause layer, *Rev.Geophys.*, *47*(1), RG1004, doi:10.1029/2008RG000267.

Funk, J. P., and G. L. Garnham (1962), Australian ozone observations and a suggested 24 month cycle, *Tellus*, *14*(4), 378–382, doi:10.1111/j.2153-3490.1962.tb01350.x.

Garcia, R. R., D. R. Marsh, D. E. Kinnison, B. A. Boville, and F. Sassi (2007), Simulation of secular trends in the middle atmosphere, 1950-2003, *J.Geophys.Res.Atmos.*, *112*(D9), D09,301, doi:10.1029/2006JD007485.

Garcia, R. R., A. K. Smith, D. E. Kinnison, A. de la Cámara, D. Murphy (2017), Modification of the gravity wave parameterization in the Whole Atmosphere Community Climate Model: Motivation and results, *J.Atmos.Sci.*, *74*(1), 275–291, doi:10.1175/JAS-D-16-0104.1

Garfinkel, C. I., M. M. Hurwitz, L. D. Oman, and D. W. Waugh (2013), Contrasting effects of central pacific and eastern pacific El Niño on stratospheric water vapor, *Geophys.Res.Lett.*, *40*(15), 4115–4120, doi:10.1002/grl.50677.

Garny, H., G. E. Bodeker, and M. Dameris (2007), Trends and variability in stratospheric mixing: 1979-2005, *Atmos.Chem.Phys.*, *7*(21), 5611–5624, doi:10.5194/acp-7-5611-2007.

Garny, H., M. Dameris, and A. Stenke (2009), Impact of prescribed SSTs on climatologies and long-term trends in CCM simulations, *Atmos.Chem.Phys.*, *9*(16), 6017–6031, doi:10.5194/acp-9-6017-2009.

Gelaro, R., and co-authors (2017),The Modern-Era Retrospective Analysis for Research and Applications, Version 2 (MERRA-2), *J. Clim.*, 30, 5419-5454, https://doi.org/10.1175/JCLI-D-16-0758.1

Gray, L. J., and M. P. Chipperfield (1990), On the interannual variability of trace gases in the middle atmosphere, *Geophys.Res.Lett.*, *17*(7), 933–936, doi:10.1029/GL017i007p00933.

Gray, L. J., and J. A. Pyle (1989), A two-dimensional model of the quasi-biennial oscillation of ozone, *J.Atmos.Sci.*, *46*(2), 203–220.

Gray, L. J., and S. Ruth (1993), The modeled latitudinal distribution of the ozone quasi-biennial oscillation using observed equatorial winds, *J.Atmos.Sci.*, *50*(8), 1033–1046.

Haynes, P., and E. Shuckburgh (2000), Effective diffusivity as a diagnostic of atmospheric transport: 1. stratosphere, *J.Geophys.Res.Atmos.*, *105*(D18), 22,777–22,794, doi:10.1029/2000JD900093.

Holton, J. R., and R. S. Lindzen (1972), An updated theory for the quasi-biennial cycle of the tropical stratosphere, *J.Atmos.Sci.*, *29*(6), 1076–1080.

Hu, D., W. Tian, Z. Guan, Y. Guo, and S. Dhomse (2016), Longitudinal asymmetric trends of tropical cold-point tropopause temperature and their link to strengthened walker circulation, *J.Clim.*, *29*(21), 7755–7771, doi:10.1175/JCLI-D-15-0851.1.

Jian, R., and R. Rong-Cai (2014), Atmospheric and oceanic science letters statistical characteristics of ENSO events in CMIP5 models statistical characteristics of ENSO events in CMIP5 models, *Ocean.Sci.Lett*, *76*(710), 546–552, doi:10.3878/AOSL20140055.

Jockel, and co-authors (2006), The atmospheric chemistry general circulation model echam5/messy1: consistent simulation of ozone from the surface to the mesosphere, *Atmos.Chem.Phys.*, *6*(12), 5067–5104, doi:10.5194/acp-6-5067-2006.

Jourdain, L., S. Bekki, F. Lott, and F. Lefévre (2008), The coupled chemistry-climate model LMDz-reprobus: description and evaluation of a transient simulation of the period 1980-1999, *Annales Geophysicae*, *26*(6), 1391–1413, doi:10.5194/angeo-26-1391-2008.

Ju, J., and J. Slingo (1995), The Asian summer monsoon and ENSO, *Q.J.R.Meteorol.Soc.*, *121*(525), 1133–1168.

Kim, S. T., and J. Yu (2012), The two types of ENSO in CMIP5 models, *Geophys.Res.Lett.*, *39*(11).

Kinnersley, J. S., and K.-K. Tung (1998), Modeling the global interannual variability of ozone due to the equatorial QBO and to extratropical planetary wave variability, *J.Atmos.Sci.*, *55*(8), 1417–1428.

Konopka, P., J. Grooß F. Plöger, and R. Müller (2009), Annual cycle of horizontal in-mixing into the lower tropical stratosphere, *J.Geophys.Res.Atmos.*, *114*(D19),111, doi: 10.1029/2009JD011955

Konopka, P., J.-U. Grooß, Günther, F. Ploeger, R. Pommrich, R. Müller, and N. Livesey (2010), Annual cycle of ozone at and above the tropical tropopause: observations versus simulations with the Chemical Lagrangian Model of the Stratosphere (CLaMS), *Atmos.Chem.Phys.*, *10*(1), 121–132, doi:10.5194/acp-10-121-2010.

Kramarova, N. A., E. R. Nash, P. A. Newman, P. K. Bhartia, R. D. McPeters, D. F. Rault, C. J. Seftor, P. Q. Xu, and G. J. Labow (2014), Measuring the antarctic ozone hole with the new Ozone Mapping and Profiler Suite, *Atmos.Chem.Phys.*, *14*(5), 2353–2361, doi:10.5194/acp-14-2353-2014.

Lamarque, J.-F., D. E. Kinnison, P. G. Hess, and F. M. Vitt (2008), Simulated lower stratospheric trends between 1970 and 2005: Identifying the role of climate and composition changes, *J.Geophys.Res.Atmos.*, *113*(D12), D12,301, doi:10.1029/2007JD009277.

Lau, N.-C., and M. J. Nath (2000), Impact of ENSO on the variability of the Asian-Australian monsoons as simulated in GCM experiments, *J.Clim.*, *13*(24), 4287–4309.

Lau, N.-C., and M. J. Nath (2012), A model study of the air-sea interaction associated with the climatological aspects and interannual variability of the south Asian summer monsoon development, *J.Clim.*, *25*(3), 839–857, doi:10.1175/JCLI-D-11-00035.1.

Liess, S., and M. A. Geller (2012), On the relationship between QBO and distribution of tropical deep convection, *J.Geophys.Res.Atmos.*, *117*(D3), n/a, doi:10.1029/2011JD016317.

Lindzen, R. S., and J. R. Holton (1968), A theory of the quasi-biennial oscillation, *J.Atmos.Sci.*, *25*(6), 1095–1107.

Ling, X.-D., and J. London (1986), The quasi-biennial oscillation of ozone in the tropical middle stratosphere: A one-dimensional model, *J.Atmos.Sci.*, *43*(24), 3122–3137.

Livesey, N. J., M. J. Filipiak, L. Froidevaux, W. G. Read, A. Lambert, M. L. Santee, J. H. Jiang, H. C. Pumphrey, J. W. Waters, and R. E. Cofield (2008), Validation of Aura Microwave Limb Sounder O_3 and CO observations in the upper troposphere and lower stratosphere, *J.Geophys.Res.Atmos.*, *113*(D15).

Livesey, N. J., W. G. Read, P. A. Wagner, L. Froidevaux, A. Lambert, G. L. Manney, L. F. MillÃČÂąn-Valle, H. C. Pumphrey, M. L. Santee, M. J. Schwartz, S. Wang, R. A. Fuller, R. F. Jarnot, B. W. Knosp, and E. Martinez (2015), Version 4.2x level 2 data quality and description document, *tech. rep. JPL D-33509 rev. B*, Jet Propulsion Laboratory, available at http://mls.jpl.nasa.gov.

Marsh, D.R., M.J. Mills, D.E. Kinnison, J. Lamarque, N. Calvo, and L.M. Polvani (2013), Climate Change from 1850 to 2005 Simulated in CESM1(WACCM), *J. Clim.*, *26*, 7372–7391, doi:10.1175/JCLI-D-12-00558.1

Ming, A., P. Hitchcock, and P. Haynes (2016a), The response of the lower stratosphere to zonally symmetric thermal and mechanical forcing, *J.Atmos.Sci.*, *73*(5), 1903–1922, doi:10.1175/JAS-D-15-0294.1.

Ming, A., A. C. Maycock, P. Hitchcock, and P. Haynes (2016b), The radiative role of ozone and water vapour in the temperature annual cycle in the tropical tropopause layer, *Atmos.Chem.Phys.Discus.*, pp. 1–39, doi:10.5194/acp-2016-951.

Morgenstern, O., P. Braesicke, F. M. O'Connor, A. C. Bushell, C. E. Johnson, S. M. Osprey, and J. A. Pyle (2009), Evaluation of the new UKCA climate-composition model - part 1: The stratosphere, *Geoscientific Model Development*, *2*(1), 43–57, doi:10.5194/gmd-2-43-2009.

Morgenstern, and co-authors (2010), Review of the formulation of present-generation stratospheric chemistry-climate models and associated external forcings, *J.Geophys.Res.Atmos.*, *115*, doi:10.1029/2009JD013728, doi: 10.1029/2009JD013728; 09.

Newman, P. A., and R. McKenzie (2011), UV impacts avoided by the Montreal protocol, *Photochem.Photobiol.Sci.*, *10*(7), 1152–1160.

Newman, P. A., L. Coy, S. Pawson, and L. R. Lait (2016), The anomalous change in the QBO in 2015-2016, *Geophys.Res.Lett.*, *43*(16), 8791–8797, doi:10.1002/2016GL070373.

Oman, L. D., and A. R. Douglass (2014), Improvements in total-column ozone in GEOSCCM and comparisons with a new ozone-depleting substances scenario, *J.Geophys.Res.Atmos.*, *119*(9), 5613–5624, doi:10.1002/2014JD021590.

Oman, L. D., A. R. Douglass, J. R. Ziemke, J. M. Rodriguez, D. W. Waugh, and J. E. Nielsen (2013), The ozone response to ENSO in Aura satellite measurements and a chemistry-climate simulation, *J.Geophys.Res.Atmos.*, *118*(2), 965–976, doi:10.1029/2012JD018546.

Osprey, S. M., N. Butchart, J. R. Knight, A. A. Scaife, K. Hamilton, J. A. Anstey, V. Schenzinger, and C. Zhang (2016), An unexpected disruption of the atmospheric quasi-biennial oscillation, *Science*, *353*(6306), 1424–1427, doi:10.1126/science.aah4156.

Pan, L. L., S. B. Honomichl, D. E. Kinnison, M. Abalos, W. J. Randel, J. W. Bergman, and J. Bian (2016), Transport of chemical tracers from the boundary layer to stratosphere associated with the dynamics of the Asian summer monsoon, *J.Geophys.Res.Atmos.*, *121*(23), 14,174, doi:10.1002/2016JD025616.

Park, M., W. J. Randel, A. Gettelman, S. T. Massie, and J. H. Jiang (2007), Transport above the Asian summer monsoon anticyclone inferred from Aura Microwave Limb Sounder tracers, *J.Geophys.Res.Atmos.*, *112*(D16), D16,309, doi:10.1029/2006JD008294.

Pawson, S., R. S. Stolarski, A. R. Douglass, P. A. Newman, J. E. Nielsen, S. M. Frith, and M. L. Gupta (2008), Goddard earth observing system chemistry-climate model simulations of stratospheric ozone-temperature coupling between 1950 and 2005, *J.Geophys.Res.Atmos.*, *113*(D12).

Pitari, G., E. Mancini, V. Rizi, and D. T. Shindell (2002), Impact of future climate and emission changes on stratospheric aerosols and ozone, *J.Atmos.Sci.*, *59*(3), 414–440.

Ploeger, F., P. Konopka, R. Müller, S. Fueglistaler, T. Schmidt, J. Manners, J. Grooß, G. Günther, P. Forster, and M. Riese (2012), Horizontal transport affecting trace gas seasonality in the Tropical Tropopause Layer (TTL), *J.Geophys.Res.Atmos.*, *117*(D9).

Plumb, R. A. (1996), A "tropical pipe" model of stratospheric transport, *J.Geophys.Res.Atmos.*, *101*, 3957, doi:10.1029/95JD03002.

Plumb, R. A. (2002), Stratospheric Transport, *J.Meteorol.Soc.Japan.Ser.II*, *80*, 793-809, doi: 10.2151/jmsj.80.793

Ramanathan, K. R. (1963), Bi-annual variation of atmospheric ozone over the tropics, *Quarterly Journal of the Royal Meteorological Society*, *89*(382), 540–542, doi:10.1002/qj.49708938209.

Randel, W. J., and E. J. Jensen (2013), Physical processes in the tropical tropopause layer and their roles in a changing climate, *Nature Geoscience*, *6*(3), 169, doi:10.1038/ngeo1733.

Randel, W. J., and F. Wu (1996), Isolation of the ozone QBO in SAGE II data by singular-value decomposition, *J.Atmos.Sci.*, *53*(17), 2546–2559.

Randel, W. J., M. Park, F. Wu, and N. Livesey (2007), A large annual cycle in ozone above the tropical tropopause linked to the Brewer-Dobson circulation, *J.Atmos.Sci.*, *64*(12), 4479–4488, doi:10.1175/2007JAS2409.1.

Randel, W. J., R. R. Garcia, N. Calvo, and D. Marsh (2009), ENSO influence on zonal mean temperature and ozone in the tropical lower stratosphere, *Geophys.Res.Lett.*, *36*(15), 1–5, doi:10.1029/2009GL039343.

Randel, W. J., M. Park, L. Emmons, D. Kinnison, P. Bernath, K. A. Walker, C. Boone, and H. Pumphrey (2010), Asian monsoon transport of pollution to the stratosphere, *Science*, *328*(5978), 611–613, doi:10.1126/science.1182274.

Rayner, N. A., D. E. Parker, E. B. Horton, C. K. Folland, L. V. Alexander, D. P. Rowell, E. C. Kent, and A. Kaplan (2003), Global analyses of sea surface temperature, sea ice, and night marine air temperature since the late nineteenth century, *J.Geophys.Res.Atmos.*, *108*(D14), 4407, doi:10.1029/2002JD002670

Ribera, P., C. Peña-Ortiz, R. Garcia-Herrera, D. Gallego, L. Gimeno, and E. Hernańdez (2004), Detection of the secondary meridional circulation associated with the quasi-biennial oscillation, *J.Geophys.Res.Atmos.*, *109*(D18), D18,112, doi:10.1029/2003JD004363.

Riese, M., F. Ploeger, A. Rap, B. Vogel, P. Konopka, M. Dameris, and P. Forster (2012), Impact of uncertainties in atmospheric mixing on simulated UTLS composition and related radiative effects, *J.Geophys.Res.Atmos.*, *117*(16), doi:10.1029/2012JD017751.

Scaife, A. A., R. Comer, N. Dunstone, D. Fereday, C. Folland, E. Good, M. Gordon, L. Hermanson, S. Ineson, A. Karpechko, J. Knight, C. MacLachlan, A. Maidens, K. A. Peterson, D. Smith, J. Slingo, and B. Walker (2017), Predictability of European winter 2015/2016, *Atmos.Sci.Lett.*, *18*, 38-44, doi:10.1002/asl.721.

Schoeberl, M. R., A. R. Douglass, P. A. Newman, L. R. Lait, D. Lary, J. Waters, N. Livesey, L. Froidevaux, A. Lambert, W. Read, M. J. Filipiak, and H. C. Pumphrey (2008), QBO and annual cycle variations in tropical lower stratosphere trace gases from HALOE and Aura MLS observations, *J.Geophys.Res.Atmos.*, *113*(D5), doi:10.1029/2007JD008678.

Schraner, M., E. Rozanov, C. S. Poberaj, P. Kenzelmann, A. M. Fischer, V. Zubov, B. P. Luo, C. R. Hoyle, T. Egorova, and S. Fueglistaler (2008), Technical note: Chemistry-climate model SOCOL: version 2.0 with improved transport and chemistry/microphysics schemes, *Atmos.Chem.Phys.*, *8*(19), 5957–5974.

Scinocca, J. F., N. A. McFarlane, M. Lazare, J. Li, and D. Plummer (2008), Technical note: The CCCMA third generation AGCM and its extension into the middle atmosphere, *Atmos.Chem.Phys.*, *8*(23), 7055–7074.

Scott, R. K., E. F. Shuckburgh, J.-P. Cammas, and B. Legras (2003), Stretching rates and equivalent length near the tropopause, *J.Geophys.Res.Atmos.*, *108*, 4394, doi:10.1029/2002JD002988.

Shibata, K., and M. Deushi (2008), Long-term variations and trends in the simulation of the middle atmosphere 1980-2004 by the chemistry-climate model of the meteorological research institute, *Annales Geophysicae*, *26*(5), 1299–1326, doi:10.5194/angeo-26-1299-2008.

Song, Q., G. A. Vecchi, and A. J. Rosati (2007), Indian ocean variability in the GFDL coupled climate model, *J.Clim.*, *20*(13), 2895–2916, doi:10.1175/JCLI4159.1.

Stolarski, R. S., P. Bloomfield, R. D. McPeters, and J. R. Herman (1991), Total ozone trends deduced from Nimbus 7 TOMS data, *Geophys.Res.Lett.*, *18*(6), 1015–1018.

Stolarski, R. S., D. W. Waugh, L. Wang, L. D. Oman, A. R. Douglass, and P. A. Newman (2014), Seasonal variation of ozone in the tropical lower stratosphere: Southern tropics are different from northern tropics, *J.Geophys.Res.Atmos.*, *119*(10), 6196–6206, doi:10.1002/2013JD021294.

Strahan, S. E., A. R. Douglass, R. S. Stolarski, H. Akiyoshi, S. Bekki, P. Braesicke, N. Butchart, M. P. Chipperfield, D. Cugnet, and S. Dhomse (2011), Using transport diagnostics to understand chemistry climate model ozone simulations, *J.Geophys.Res.Atmos.*, *116*(D17).

Strahan, S. E., L. D. Oman, A. R. Douglass, and L. Coy (2015), Modulation of antarctic vortex composition by the quasi-biennial oscillation, *Geophys.Res.Lett.*, *42*(10), 4216–4223, doi:10.1002/2015GL063759.

Strahan, S. E., A. R. Douglass, and S. D. Steenrod (2016), Chemical and dynamical impacts of stratospheric sudden warmings on arctic ozone variability, *J.Geophys.Res.Atmos.*, *121*(19), 11,851, doi:10.1002/2016JD025128.

Tevini, M. (1993), UV-B radiation and ozone depletion: effects on humans, animals, plants, microorganisms, and materials, Lewis Publishers Boca Raton, FL

Teyssudre, H., M. Michou, H. Clark, B. Josse, F. Karcher, D. Olivi, V.-H. Peuch, D. Saint-Martin, D. Cariolle, and J.-L. Atti (2007), A new tropospheric and stratospheric chemistry and transport model mocage-climat for multi-year studies: evaluation of the present-day climatology and sensitivity to surface processes, *Atmos.Chem.Phys.*, *7*(22), 5860.

Tian, W., and M. P. Chipperfield (2005), A new coupled chemistry-climate model for the stratosphere: The importance of coupling for future O_3-climate predictions, *Q.J.R.Meteorol.Soc.*, *131*(605), 281–303.

Tweedy, O. V., D. W. Waugh, R. S. Stolarski, L. D. Oman, W. J. Randel, and M. Abalos (2017a), Hemispheric differences in the annual cycle of tropical lower stratosphere transport and tracers, *J.Geophys.Res.Atmos.*, *122*(13), 7183–7199, doi:10.1002/2017JD026482.

Tweedy, O. V., N. A. Kramarova, S. E. Strahan, P. A. Newman, L. Coy, W. J. Randel, M. Park, D. W. Waugh, S. M. Frith (2017b), Response of trace gases to the disrupted 2015–2016 quasi-biennial oscillation, *Atmos.Chem.Phys.*,17, 6813-6823, doi:10.5194/acp-17-6813-2017.

Tweedy, O. V., D. W. Waugh, W. J. Randel, M. Abalos, L. D. Oman, D. Kinnison, The impact of boreal summer ENSO events on tropical lower stratospheric ozone, submitted to *J.Geophys.Res.Atmos.* in May 2018

Udelhofen, P. M., P. Gies, C. Roy, and W. J. Randel (1999), Surface UV radiation over Australia, 1979-1992: effects of ozone and cloud cover changes on variations of UV radiation, *J.Geophys.Res.Atmos.*, *104*(D16), 19,135–19,159.

Wallace, J. M., R. L. Panetta, and J. Estberg (1993), Representation of the equatorial stratospheric quasi-biennial oscillation in eof phase space, *J.Atmos.Sci.*, *50*(12), 1751–1762

Wang, H. J., D. M. Cunnold, L. W. Thomason, J. M. Zawodny, and G. E. Bodeker (2002), Assessment of SAGE version 6.1 ozone data quality, *J.Geophys.Res.Atmos.*, *107*(D23).

Waugh, D. W., and L. M. Polvani (2000), Climatology of intrusions into the tropical upper troposphere, *Geophys.Res.Lett.*, *27*(23), 3857–3860.

Webster, P. J., and S. Yang (1992), Monsoon and ENSO: Selectively interactive systems, *Q.J.R.Meteorol.Soc.*, *118*(507), 877–926, doi:10.1002/qj.49711850705.

Yan, X., P. Konopka, F. Ploeger, M. Tao, R. Müller, J. Bian, and M. Riese (2018), El Niño Southern Oscillation influence on the Asian summer monsoon anticyclone, *Atmos.Chem.Phys.Discuss.*, (January 2018), 1–25.

Yang, C., and B. S. Giese (2013), El Niño Southern Oscillation in an ensemble ocean reanalysis and coupled climate models, *J.Geophys.Res.Ocean.*, *118*(9), 4052–4071, doi: 10.1002/jgrc.20284.

Zawodny, J. M., and M. P. McCormick (1991), Stratospheric Aerosol and Gas Experiment II measurements of the quasi-biennial oscillations in ozone and nitrogen dioxide, *J.Geophys.Res.Atmos.*, *96*(D5), 9371–9377.

Olga Tweedy

CONTACT INFORMATION

Address	Department of Earth and Planetary Sciences Johns Hopkins University 3400 N. Charles Street, Baltimore, MD, USA, 21218
Mobile	(443) 803-0442
E-Mail	otweedy1@jhu.edu
Webpage	pages.jh.edu/ otweedy1/

RESEARCH INTERESTS

Transport of chemical trace gases in the Middle Atmosphere and Upper-Troposphere Lower-Stratosphere, stratosphere-troposphere coupling, seasonality and interannual variability of stratospheric trace gases, climate variability and change.

EDUCATION

Ph.D. Atmospheric Sciences 2013-May, 2018
Johns Hopkins University
Morton K. Blaustein Department of Earth and Planetary Sciences
Advisor: Dr. Darryn Waugh

B.S Marine Sciences 2010-2013
Coastal Carolina University, Conway, SC
Minor in Applied Mathematics
Magma cum Laude
Advisor: Dr. Varavut Limpasuvan

PROFESSIONAL EXPERIENCE

NSF Graduate Student Research Fellow 2013-present
Johns Hopkins University, EPS, Baltimore, MD
Supervisor: Dr. Darryn Waugh

NASA Student Research Collaborator 2014-present
NASA's Goddard Space Flight Center, Greenbelt, MD
Supervisors: Drs. Luke Oman and Paul Newman

NCAR ASP Graduate Student Visitor Program June -September, 2017
National Center for Atmospheric Research, ACOM
Supervisor: Dr. William Randel

Undergraduate Student Research Assistant 2011-2013
Coastal Carolina University, Department of Chemistry and Physics,Conway, SC
Supervisor: Dr. Varavut Limpasuvan

FELLOWSHIPS AND AWARDS

National Science Foundation Graduate Research Fellowship (NSF GRFP) 2013-2018
Atmospheric Chemistry and Dynamics

NCAR Advance Study Program (ASP) Graduate Student Visitor Program Fellowship 2017

Best Student Presentation Award for the 19th Conference on Middle Atmosphere June 2017
American Meteorological Society (AMS)
Title: Response of Trace Gases to the Disrupted 2015 - 2016 Quasi-Biennial Oscillation

Journal Club Student Presentation Award May 2017
Department of Earth and Planetary Science, Johns Hopkins University
Title: Analysis of Trace Gases Response to the Anomalous Change in the QBO in 2015 −2016

College of Science Award for Outstanding Achievements in Undergraduate Research 2013
Coastal Carolina University

TECHNICAL SKILLS

IDL, Python, Bash, NASA Goddard and NCAR (Yellowstone) HPC environments, LATEX
Analysis of Chemistry- Climate Models (GEOSCCM and WACCM) and satellite observations (MLS, SAGE-II, OMPS, SABER)

PUBLICATIONS

1. A. K. Smith, Espy, P. J., Lopez-Puertas, M., **Tweedy, O.V**., Spatial and temporal structure of the tertiary ozone maximum in the polar winter mesosphere, *Journal of Geophysical Research: Atmospheres*, accepted

2. **O. V. Tweedy**, Kramarova, N. A., Strahan, S. E., Newman, P. A., Coy, L., Randel, W. J., Park, M., Waugh, D. W., and Frith, S. M. (2017). Response of trace gases to the disrupted 2015−2016 quasi-biennial oscillation. *Atmos. Chem. Phys.*,17(11):6813−6823.

3. **O. V. Tweedy**, Waugh, D., Stolarski, R., Oman, L., Randel, W., and Abalos, M. (2017). Hemispheric differences in the annual cycle of tropical lower stratosphere transport and tracers. *Journal of Geophysical Research: Atmospheres*, 122, doi:10.1002/2017JD026482.

4. Weber, M., Steinbrecht, W., Frith, S. M., **O. V. Tweedy**, Coldewey-Egbers, M., Davis, S.,Degenstein, D., Fioletov, Y. E., Froidevaux, L., de Laat, J., Long, C. S., Loyola, D., Roth, C., , and Wild., J. D. (2017). Stratospheric ozone [in state of the climate in 2016]. *Bull. Amer. Meteor. Soc.*

5. **O. V. Tweedy**, Limpasuvan, V., Orsolini, Y. J., Smith, A. K., Garcia, R. R., Kinnison, D., Randall, C. E., Kvissel, O., Stordal, F., and Harvey, V. L. (2013). Nighttime secondary ozone layer during major stratospheric sudden warmings in specified dynamics WACCM. *Journal of Geophysical Research: Atmospheres*, 118(15):83468358.

SELECTED CONFERENCE PRESENTATIONS

ENSO Influence on Trace Gases in the Tropical Lower Stratosphere, AGU Fall Meeting New Orleans, LA, USA. 2017, oral

Response of Trace Gases to the Disrupted 2015-2016 Quasi-Biennial Oscillation, 19th Conference on the Middle Atmosphere and 21st Conference on Atmospheric and Oceanic Fluid Dynamics, Portland, OR, 26-30 June 2017, oral

Hemispheric Differences in Tropical Lower Stratospheric Transport and Tracers Annual Cycle, AGU Fall Meeting San Francisco, CA, USA. 2016, oral

Analysis of Trace Gases Response on the Anomalous Change in the QBO in 2015-2016, AGU Fall Meeting San Francisco, CA, USA. 2016, oral

Hemispheric Asymmetries in the Annual Cycle of Tropical Lower Stratospheric Ozone: Implications for Transport, Quadrennial Ozone Symposium, Edinburgh, UK. 2016, poster

Impact of Stratospheric Ozone Zonal Asymmetries on the Tropospheric Circulation, AMS Annual Meeting, 18th Conference on Middle Atmosphere, Phoenix, AZ, 48 January 2015, poster

Impact of Antarctic ozone asymmetries on tropospheric climate, the Latsis Symposium on Atmospheric and Climate Dynamics, Zürich, Switzerland, 18-21 June 2014, poster

The Response of Polar Mesosphere-Low Thermospheric (MLT) Ozone to Stratospheric Sudden Warming, AGU Fall Meeting San Francisco, CA, USA. 2012, poster

Wintertime Polar Ozone Evolution during Stratospheric Vortex Break-Down, AGU Fall Meeting San Francisco, CA, USA. 2011, poster